View Article Online / Journal Homepage / Table of Contents for this issue

Nanoparticles functionalised with reversible molecular and supramolecular switches

Rafal Klajn,†[a] J. Fraser Stoddart[b] and Bartosz A. Grzybowski*[ab]

Received 30th September 2009
First published as an Advance Article on the web 21st April 2010
DOI: 10.1039/b920377j

Published on 21 April 2010. Downloaded by Pennsylvania State University on 06/03/2016 20:02:52.

Nanoparticles (NPs) and molecular/supramolecular switches have attracted considerable interest during the past decade on account of their unique properties and prominent roles in the fields of organic chemistry and materials science. Materials derived from the combination of these two components are now emerging in the literature. This *critical review* evaluates materials which comprise NPs functionalised with well-defined self-assembled monolayers of molecular and supramolecular switches. We draw attention to the fact that immobilisation of switches on NPs does not, in general, hamper their switching ability, although it can impart new properties on the supporting particles. This premise leads us to the discussion of systems in which switching on the surfaces of NPs can be used to modulate reversibly a range of NP properties—optical, fluorescent, electrical, magnetic—as well as the controlled release of small molecules. Finally, we discuss examples in which molecular switches direct reversible self-assembly of NPs (308 references).

1. Introduction

The marriage of organic and materials chemistry can lead to the birth of novel hybrid materials, which combine the beneficial characteristics and properties of both components. The past decade has witnessed an explosion of interest in nanoparticles (NPs)[1–4] on account of their unique and size-dependent optical,[5–7] electronic,[8,9] and catalytic[10,11] properties, to name but a few. On the other hand, molecular and supramolecular switches are amongst some of the most appealing chemical compounds, since their structures, superstructures, and properties can be controlled by external stimuli. While excellent reviews on both molecular and supramolecular switching on *planar* surfaces[12–17] and in solution[18–21] abound, those focusing on *nanoparticles* decorated with switchable molecules are lacking. It is the goal of this review to fill this gap by presenting materials which comprise nanoparticles functionalised with well-defined self-assembled monolayers (SAMs) of molecular and supramolecular switches. We have tried to catalogue all such hybrid systems reported in the literature to date and to emphasise the singular features of switches when confined to NP surfaces.

We define a reversible switch as a molecular, supramolecular, or mechanically interlocked entity capable of changing its shape in response to an external stimulus. Although systems

[a] *Department of Chemical and Biological Engineering, Northwestern University, 2145 Sheridan Rd., Evanston, IL 60208, USA. E-mail: grzybor@northwestern.edu*
[b] *Department of Chemistry, Northwestern University, 2145 Sheridan Rd., Evanston, IL 60208, USA*
† Current address: Department of Organic Chemistry, Weizmann Institute of Science, 76100 Rehovot, Israel.

Rafal Klajn

From 2004 to 2009, Rafal Klajn was a PhD student working with Prof. Bartosz Grzybowski in the Department of Chemical and Biological Engineering at Northwestern University, USA. He is now a research group leader in the Department of Organic Chemistry at the Weizmann Institute of Science, Israel. His research interests include nanocrystals, nanofabrication, and supramolecular chemistry.

Bartosz A. Grzybowski

Bartosz A. Grzybowski graduated summa cum laude *and* Honoris in Chimia *from Yale University in 1995. In 2000, he obtained his PhD in Physical Chemistry from Harvard University in 2000 (with G. M. Whitesides). In 2003 he joined the faculty of Northwestern University where he is now Burgess Professor of Physical Chemistry and Chemical Systems Engineering. Grzybowski pioneered research on dynamic self-assembly. His other scientific interests include chemistries in non-equilibrium/dynamic systems, complex chemical networks, nanostructured materials, and nanobiology.*

View Article Online

Published on 21 April 2010. Downloaded by Pennsylvania State University on 06/03/2016 20:02:52.

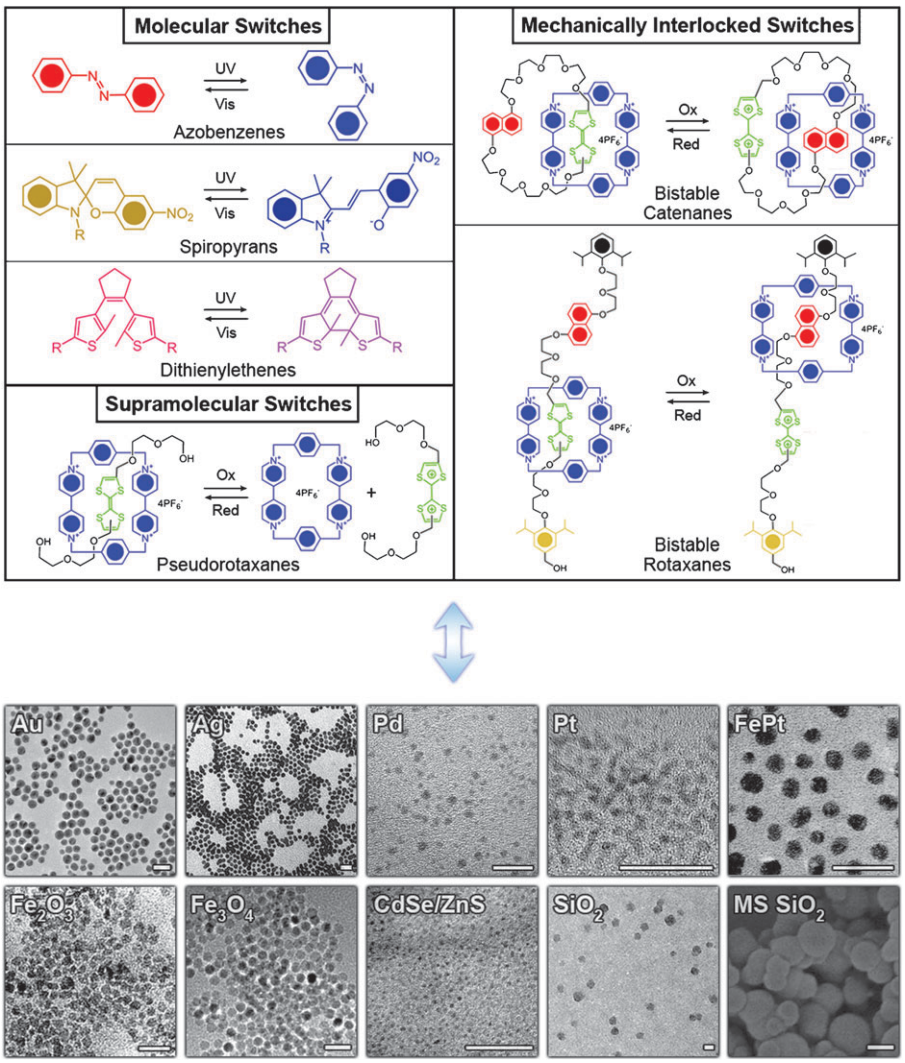

Fig. 1 Integrating switches with NPs. Top panel: examples of molecular, supramolecular, and mechanically interlocked switches. Bottom panel: examples of nanoparticles that have been functionalised with molecular, supramolecular, or mechanically interlocked switches (from left to right, top to bottom): Au,[68] Ag,[272] Pd,[69] Pt,[69] FePt,[214] Fe_2O_3,[211] CdSe–ZnS,[308] Fe_3O_4,[43] SiO_2,[107] and mesoporous (MS) SiO_2.[250] Scalebars correspond to 20 nm except for MS SiO_2 (500 nm). Reproduced with permission from ref. 43 (Copyright 2008 Royal Society of Chemistry), ref. 69 (Copyright 2009 American Chemical Society), ref. 107 (Copyright 2008 Royal Society of Chemistry), ref. 211 (Copyright 2004 Wiley-VCH Verlag GmbH & Co. KgaA), ref. 214 (Copyright 2007 American Chemical Society), ref. 250 (Copyright 2006 American Chemical Society), ref. 272 (Copyright 2000 American Chemical Society), ref. 308 (Copyright 2005 Royal Society of Chemistry).

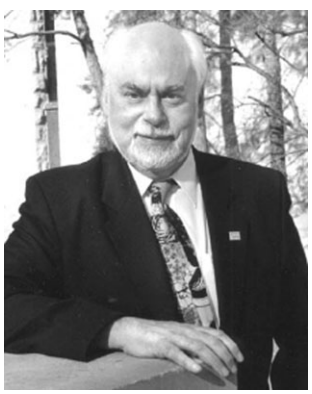

J. Fraser Stoddart

Sir Fraser Stoddart received all (BSc, PhD, DSc) of his degrees from the University of Edinburgh, UK. Presently, he holds a Board of Trustees Professorship in the Department of Chemistry at Northwestern University. His research has opened up a new materials world of mechanically interlocked molecular compounds and, in doing so, has produced a blueprint for the subsequent growth of functional molecular nanotechnology.

in which these components are addressed by light have attracted most of the attention, we also discuss systems in which redox potential, as well as pH change, are used. Importantly, geometrical changes occur *reversibly* and so the altered molecule can return to its original geometry when the stimulus is removed, or upon the application of another stimulus. Fig. 1 summarises the main types of switches we will be considering in this review, and which can be divided into three groups: molecular, supramolecular, and mechanically interlocked. In the first category, isomerisation occurs within individual molecules. Here, light-responsive switches have been investigated in most detail and used most broadly because they can be controlled "remotely" and can be actuated rapidly (typically, milliseconds) throughout the bulk of the sample. Among these switches, one can further distinguish

 This journal is © The Royal Society of Chemistry 2010

View Article Online

Published on 21 April 2010. Downloaded by Pennsylvania State University on 06/03/2016 20:02:52.

systems in which both isomers are thermally stable and can be interconverted by different wavelengths of light (*e.g.*, dithienylethenes,[22–25] DTEs; Fig. 1), and systems in which one of the forms is metastable[26] and can exist only as long as a source of energy (*i.e.*, light of an appropriate wavelength) is continuously provided (*e.g.*, azobenzenes,[27,28] AB, and spiropyrans,[29,30] SPs, in Fig. 1). Supramolecular switches comprise two components interacting with one another through non-covalent bonding interactions. An external stimulus can be used to disturb these interactions, so that the two components dissociate from one another. Pseudorotaxanes[31–35] are one of the most versatile of such supramolecular switches and can be dissociated and re-assembled using a variety of stimuli—such as light,[36,37] redox potential,[38,39] or pH gradients.[40,41] Finally, mechanically interlocked switches (*e.g.*, bistable catenanes and rotaxanes, Fig. 1) denote molecular entities composed of components whose dissociation is prohibited even in the absence of any attractive interactions. Switching is achieved by the components of these molecules sliding or rotating with respect to one another upon changes in their mutual interactions.

Essential for the ensuing discussion is that all of the above types of molecules have been immobilised onto a range of nanoparticles. While some of the surface-ligation schemes are seasoned (gold–thiolate or silane–silica binding), other types of attachments have been demonstrated only recently—examples include immobilisation by networks of hydrogen bonds[42] or the use of polymer chains[43] as a ''glue'' between the NPs and individual switchable molecules. Once on the nanoparticles, the switches can endow these NPs a rich variety of behaviours which we are now going to narrate in detail. We will begin by discussing the effects of NP immobilisation on the properties of switches: their isomerisation kinetics, equilibrium between the two isomers, and, in the case of redox-controlled switches, their redox potentials. With the understanding of (or at least intuition for) these effects, we then devote Sections 3–9 to the discussion of systems in which the presence of switches affects the optical, electrical, magnetic, fluorescent, controlled release, and aggregation properties of the NPs onto which the switches are immobilised.

2. Does immobilisation on NPs affect switching performance?

Molecules that switch effectively in solution might not necessarily retain these characteristics after attachment onto NP surfaces. Steric and electronic effects can pose significant challenges in that (i) molecular switches assembled as tightly packed monolayers might lose the free volume needed for the isomerisation to take place, and (ii) in the case of photoisomerisation on noble metal NPs, excited states of the molecules can be quenched by the NPs' surface plasmon resonance (SPR). These challenges can in principle be met by, respectively, (i) the formation of *mixed* self-assembled monolayers (*m*SAMs) on NPs, and (ii) extending the distance between the switch and the NP core.

2.1 Attachment strategies: overcoming steric hindrance

Isomerisation processes in molecular switches are often accompanied (Fig. 1) by large changes in internal geometry/shape. While this issue is not a problem for molecules or complexes moving around freely in solution, it can hamper isomerisation severely within SAMs on planar substrates or NPs. These effects have predominantly been studied in monolayers of azobenzenes (ABs). Specifically, it has been shown[44–46] that AB-terminated thiols completely lose the ability to photoisomerise when adsorbed as densely packed monolayers on planar gold (Fig. 2a, left). Fortunately, attachment to nanoparticle surfaces creates[47] additional free volume accessible to the ligands by virtue of the curvature effect (Fig. 2a, centre). The smaller and more curved the NP, the more pronounced is this effect. For example, Shin and Shin reported that 2 nm Au NPs functionalised with 4-(7-mercaptoheptanoxy)azobenzene exhibit efficient photoisomerisation, with both *trans–cis* and *cis–trans* isomerisations following first-order kinetics, indicative[48] of no steric hindrance during the process. Interestingly, both these reactions are *faster* on NPs than in solution, with the reaction rates larger by a factor of 2.9 for *trans–cis* and 2.3 for *cis–trans* isomerisations. Although the authors do not provide any explanation of this intriguing effect, it seems

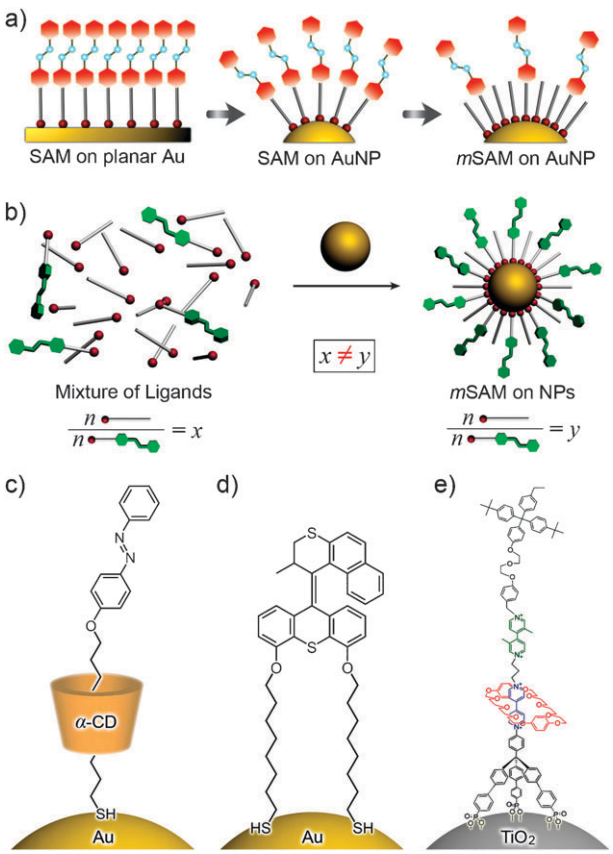

Fig. 2 Strategies used to increase the free volume required for efficient isomerisation of molecular switches immobilised on surfaces: (a) the curvature effect (centre), formation of mixed self-assembled monolayer (right). (b) A word of caution: the ratio of the switches and background ligands in solution used for NP functionalisation does not necessarily reflect the ratio of these molecules forming a *m*SAM on a nanoparticle. (c–e) Other strategies used to increase the free volume required for efficient isomerisation: increasing bulkiness of a ligand by the formation of an inclusion complex (c), equipping switches with multiple points of attachment (d and e).

View Article Online

Published on 21 April 2010. Downloaded by Pennsylvania State University on 06/03/2016 20:02:52.

reasonable to assume that it derives from the π–π stacking interactions between the azobenzene groups in the SAM. Since these interactions are maximised when the interacting molecules are in the same (*cis* or *trans*) geometries, UV-induced *trans–cis* isomerisation of one AB group should make the isomerisation of the neighbouring groups easier (a cooperative effect). Likewise, Vis-induced *cis–trans* reisomerisation of a given *cis*-AB group should occur faster if this group is surrounded by already-isomerised *trans*-AB moieties.

For larger NPs, AB isomerisation becomes completely inhibited—in one recent example, our group verified[49] such inhibition within monocomponent AB SAMs on 5.5 nm Au NPs. A solution to this problem is the preparation of mixed SAMs (*m*SAMs), a strategy which has been applied widely with planar substrates.[46,50–55] These *m*SAMs comprise the functional ligands, as well as shorter, ''background'' ligands, which provide (Fig. 2a, right) additional free volume for isomerisation. The strategy based on *m*SAMs has attracted most interest and examples of it are abundant in the literature and throughout this review. The problem with *m*SAMs, however, is that it can sometimes be difficult to control their composition—that is, the ratio of the switches and background ligands in solution used for NP functionalisation does not necessarily reflect the ratio of these molecules immobilised onto the NPs (Fig. 2b).[56–59] This discrepancy can sometimes be very pronounced,[57] and is due to either attractive or repulsive interactions between the two types of molecules within the SAM,[56] or due to different degrees of their solvation.[58] While in planar *m*SAM systems monolayer composition can be inferred from, for instance, the wetting properties (*via* the Young equation),[60–62] this method of analysis cannot be extended to *m*SAMs on the NPs. Instead, I_2-induced decomposition of the Au NPs followed by NMR analysis of the liberated ligands[58] is routinely used. More recently, Kalsin *et al.* have proposed an alternative, non-destructive method to study the composition of *m*SAMs provided one of the ligands comprising the *m*SAM is charged.[56] This method is based on ''titration''[63] of NPs covered with *m*SAM containing an unknown percentage of charged ligands with NPs functionalised with a single-component SAM of oppositely charged ligands. At the point of electroneutrality where the NP charges are compensated, the NPs precipitate from solution, and the volume of the titrant can be used to calculate the composition of the *m*SAM of the titrated species.

Several research groups have considered alternative strategies to engineer free volume sufficient for isomerisation without the need to prepare *m*SAMs. One way is to use bulky ''spacers'' around the switches. For example, Sortino *et al.*[64] reported a supramolecular inclusion complex between an α-cyclodextrin (CD) host and an AB-terminated alkyl thiol guest (Fig. 2c). These complexes are prepared prior to the adsorption of the complex onto Au NPs. On account of their bulkiness, the α-CD rings increase the distance between the AB switches and thus enable their effective photoisomerisation. As anticipated, the absence of π–π stacking was verified by UV-Vis spectroscopy, and the AB switching rates were identical to those of the free molecules in solution. In addition, the presence of α-CD rendered the NPs soluble in polar solvents, such as DMF.

Another way to ''dilute'' switches on the NPs is the use of ligands terminated in more than one surface ''anchor''. For sulfur-based ligands and noble metal NPs, one can use asymmetrical/mixed disulfides[65] or dithiolanes, which reduce the surface coverage by 50% compared to SAMs prepared from the corresponding thiol. Tamada *et al.*[66] prepared AB-coated 5.2 nm Au NPs using 4-hexyl-4′-(12-(dodecyldithio)-dodecyloxy)azobenzene (C6-AB-C12-SS-C12), and demonstrated excellent switching performance on these NPs, with the reaction kinetics identical to that in the solution phase. Moreover, no deviations from the first-order kinetics for both UV- and Vis-induced isomerisations were observed. It must be

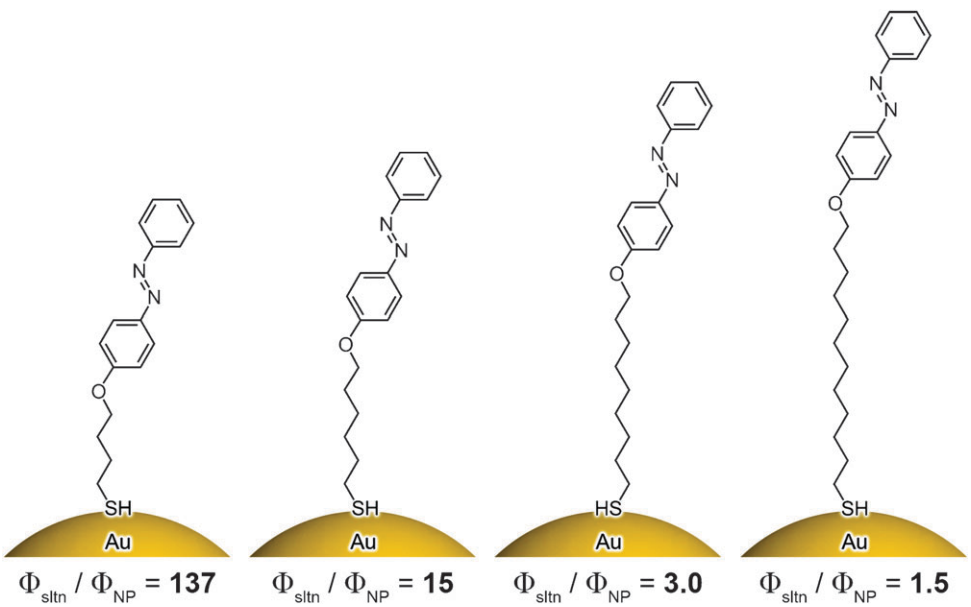

Fig. 3 Effect of the spacer length on the relative yield of AB isomerisation on the surface of Au NPs. The relative yields, Φ_{sltn}/Φ_{NP}, have been defined as isomerisation quantum yield of free thiol to the thiol immobilised on the gold surface.

 This journal is © The Royal Society of Chemistry 2010

View Article Online

Published on 21 April 2010. Downloaded by Pennsylvania State University on 06/03/2016 20:02:52.

noted, however, that mixed disulfides are prone to slow phase separation[67] which, in time, decreases isomerisation rates; this complication is absent[68–70] in dithiolane SAMs.

An elegant, albeit probably less general strategy for SAM dilution has been demonstrated by Feringa and co-workers, who tethered stilbene-based molecular "rotors"[71,72] onto 2 nm Au NPs *via* two alkane thiol "legs" (Fig. 2d).[73,74] The primary rationale behind the use of two anchor points was to prevent thermal rotation of the switch with respect to the NP surface. Long alkyl chains were used to limit electronic interactions between the gold core and excited states of the chromophore (see also Section 2.2). With these precautions, the rotor's performance on NPs was virtually identical to that in solution. Another multivalent linker has been designed by Fitzmaurice *et al.*[75,76] with the aim of orienting redox-switchable pseudorotaxanes and [2]rotaxanes normal to the NP surface and, at the same time, to ensure that these switches do not interact with one another. Specifically, they functionalised $\sim$5.5 nm TiO_2 NPs with tripodal, phosphonate-terminated,[77–79] viologen-incorporating threads encircled by crown ether rings (Fig. 2e). Introducing sufficient separation between the viologen units was necessary to avoid pimerisation[80–82] of the viologen groups in their radical cation forms.[83] The loose packing of the tripodal linkers was confirmed by the fact that only 12 rotaxanes (see Fig. 2e) and 13 pseudorotaxanes could be accommodated on the surfaces of $\sim$5.5 nm TiO_2 NPs. In addition, restricted motion of the ligand due to the three-point attachment was confirmed by NMR spectroscopy.

2.2 Inhibition of switching by surface plasmon resonance

It is well-known that noble metal nanoparticles can quench the electronic excited states of organic molecules harboured on their surfaces,[84,85] leading to the reduced performance of molecular switches.[86] In general, the extent of quenching is determined by the overlap between the chromophore absorption and the NP SPR bands.[87] The quenching process is attributed to resonance energy transfer (see also Section 4), and its effectiveness decreases with increasing length of the linker between the chromophore and the underlying NP surface. It follows that efficient switching is expected in systems in which the two units—the photoswitch and the NP core—are separated by a long spacer.[88]

These effects are well exemplified by research of Whitesell *et al.*,[88] who investigated the efficiency of AB photoisomerisation on 2.5 nm Au NPs as a function of the linker chain length. Specifically, the AB groups were attached to the NP surfaces through linkers containing n = 4, 6, 9, and 12 methylene groups (Fig. 3). Relative yields, defined as the ratio of the AB isomerisation quantum yield in solution and on NP surfaces, were 137, 15, 3.0 and 1.5 for n = 4, 6, 9, and 12, respectively. In other words, increasing the distance between the AB unit and the gold surface from $\sim$0.54 nm (for n = 4) to $\sim$1.25 nm (for n = 12) results in a $\sim$100-fold increase in isomerisation quantum yield.

Matsuda *et al.* studied[89,90] the photoisomerisation of dithienylethene (DTE) attached to the surfaces of differently-sized Au and Ag NPs through a pentamethylene spacer (Fig. 4a). Cyclisation and cycloreversion reactions were performed

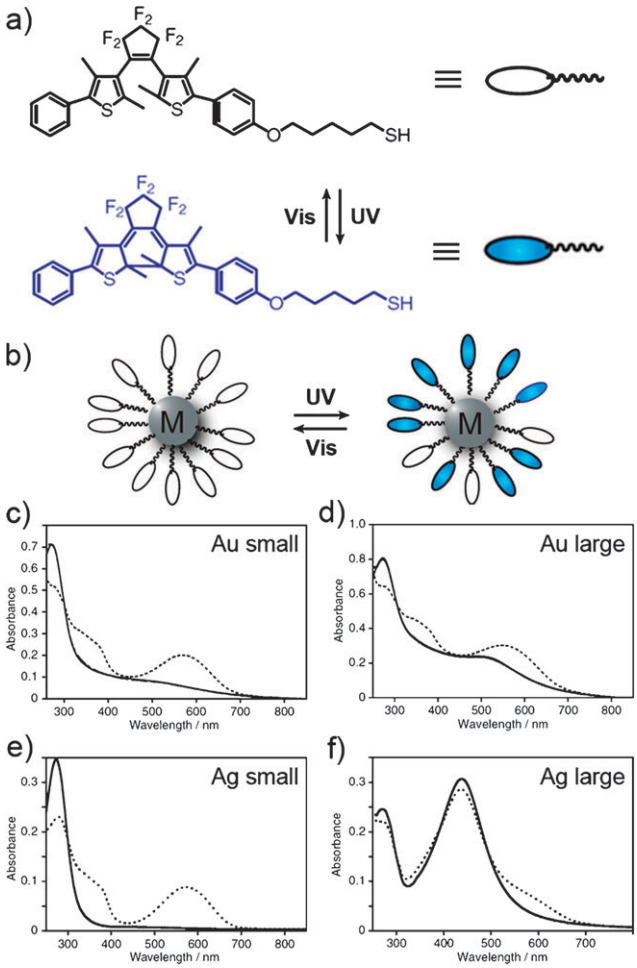

Fig. 4 (a) Structural formulae of the open (top) and closed (bottom) forms of a thiol-functionalised dithienylethene (DTE). (b) Isomerisation on the surface of NPs. (c–f) UV-Vis spectra of DTE-coated NPs of different sizes and compositions before (solid lines) and after (dashed lines) irradiation with λ = 313 nm light. Average diameters: Au small: 2.2 nm; Au large: 3.2 nm; Ag small: 1.2 nm; Ag large: 6.7 nm. Adapted with permission from ref. 90 (Copyright 2006 Chemical Society of Japan).

under irradiation with UV (313 nm) and visible (578 nm) light, respectively. Despite its attachment to NPs (Fig. 4b), DTE photoisomerisation was observed, although with a somewhat (no quantitative data are available) decreased efficiency (Fig. 4c–f). As expected, an increase in the NP size led to quenching, which is a consequence of the higher SPR absorption values for NP of larger diameters. The fact that DTE retains its switching ability is attributed[91] to the very fast cyclisation within less than 10 ps (that is, much faster than the rate of quenching by the NP SPR). In a more detailed investigation,[87] the same group presented quantum yield analysis of DTE-functionalised Ag NPs and demonstrated that cyclisation was effectively quenched by the NP SPR—conversion decreased from 81% in solution to 16% on NPs—while cycloreversion was scarcely affected.

Inhibition of photocyclisation—induced by λ = 313 nm UV light—by NPs was also studied[92] in low-polydispersity DTE polymers. Thiol-terminated polymers of varying chain lengths

View Article Online

Published on 21 April 2010. Downloaded by Pennsylvania State University on 06/03/2016 20:02:52.

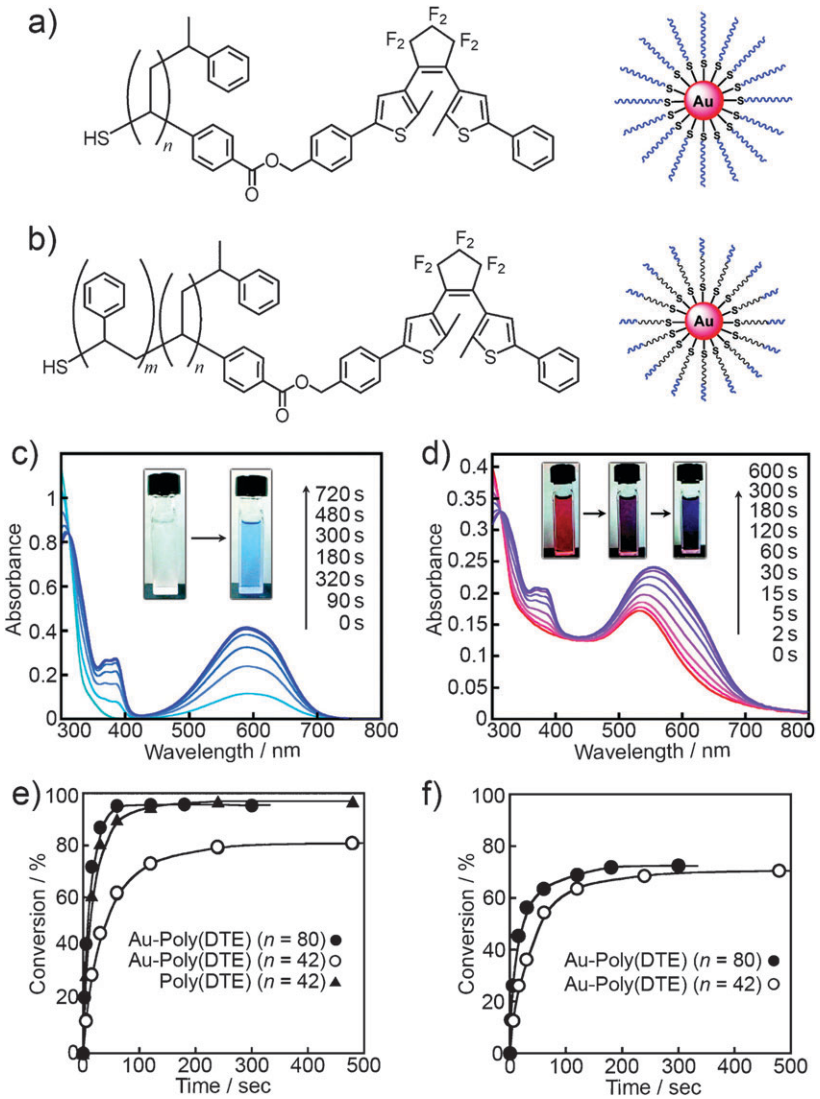

Fig. 5 (a and b) Structural formulae of thiol-terminated (a) DTE polymer and (b) DTE–styrene block copolymer. (c) UV-Vis spectra accompanying UV irradiation (λ = 313 nm) of DTE polymer (n = 80) in toluene. (d) UV-Vis spectra accompanying UV irradiation (λ = 313 nm) of DTE-polymer-coated Au NPs in toluene. (e) Kinetics of DTE cyclisation within DTE polymers present free in solution and on Au NP surfaces. (f) Kinetics of the same reaction performed on a surface of a quartz glass slide. Decreased conversion efficiencies are caused by quenching of the excited states of DTE by NPs in densely packed nanoparticle layers. Adapted with permission from ref. 92 (Copyright 2008 American Chemical Society).

(n = 42 and 80 units, corresponding to ~11 nm and ~20 nm lengths, respectively; Fig. 5a) were prepared *via* the reversible addition–fragmentation chain transfer (RAFT) polymerisation,[93] and showed excellent photoresponsive properties in solution, with an almost quantitative photocyclisation conversion—97% for both polymers (Fig. 5c and e). When adsorbed onto the surface of Au NPs (Fig. 5d), however, the two polymers exhibited (Fig. 5e) markedly different behaviours. While the photoreactivity in the long-chain polymer remained virtually unchanged (96% conversion), NPs reduced photoconversion of the short-chain polymer to 81%. Furthermore, a copolymer comprising non-reactive polystyrene segments (m = 46 units, total length 12 nm) closer to gold surface and DTEs groups (n = 25 units, length 6.3 nm) further away from the surface was synthesised (Fig. 5b). In this case, photoconversion yield remained high at 94%. These results suggest that the photocyclisation reactivity of DTEs decreases with the decreasing distance between the chromophore molecules and the gold surface. In an elegant experiment designed to test this hypothesis, isomerisation was conducted within densely packed monolayers of polymer-covered NPs on a quartz glass substrate. In this case, the yields for the n = 42 and n = 80 polymers (m = 0) were, respectively, 70% and 72% (Fig. 5f). The fact that the conversion dropped significantly for *both* polymer chain lengths indicates that the DTE moieties in their excited state were quenched by not only their parent NP, but also by the adjacent NPs in the monolayer. Importantly, this decrease was caused by quenching of the excited states by SPR, and not by decreased reactivity in the solid state—in fact, free polymers (*i.e.*, in the absence of the Au NPs) retained excellent (97%) photoisomerisation yields even in the solid state.

 This journal is © The Royal Society of Chemistry 2010

View Article Online

Published on 21 April 2010. Downloaded by Pennsylvania State University on 06/03/2016 20:02:52.

In contrast to the above study, in which the photochromic unit was deliberately isolated from the NP metal core by long alkyl chains, Feringa *et al.*[94,95] investigated the behaviour of DTEs attached to Au NPs directly through the aromatic system. DTE units were attached to gold NPs through either phenylene (**1** and **2** in Fig. 6a and b) or thiophene (**3** in Fig. 6c) rings. As might be expected on the basis of increased electronic "communication" between the NP and the chromophore, photoisomerisation efficiencies were further decreased. In the case of the phenylene linker, the quantum yields for the ring closure process were ~0.07 for both the *m*- and *p*-isomers (see Fig. 6a and b, centre)—these values were significantly lower than ~0.40 measured[96] for the same molecules present freely in solution. DTE with the thiophene linker represented an even more extreme case—here, no changes in the UV-Vis spectra were observed upon UV irradiation (Fig. 6c, centre) and the measured quantum yield was less than 0.01 demonstrating that the excited state of the open-ring isomer was effectively quenched by the metal. Ring-opening induced by visible light was also studied on NPs prepared using the closed-ring DTE isomers. In this case, the process was slowed down as well, but all three linkers gave the same results (Fig. 6a–c, bottom). The efficient energy transfer from the excited open-ring isomer of thiophene–DTE (**3**o in Fig. 6) to gold was attributed to a greater overlap between the highest occupied molecular orbital of **3**o and the metal density band of states near the Au Fermi level[97]—indeed, this supposition was later corroborated[98] by computational studies. In sum, demonstration of spacer-dependent uni- and bi-directional switching emphasises the importance of the spacer connecting the switching units to the nanoparticle.

2.3 NP-induced inverse photochromism

In certain microenvironments—for example, on nanoparticle surfaces—equilibrium between the two isomers of a switchable molecule can be shifted. An extreme case of this situation is called negative photochromism,[99–101] wherein the normally unstable isomer is stabilised to the extent that it becomes the dominating species. The spiropyran–merocyanine (SP–MC) system is the most recognised example of this behaviour, with the SP and MC isomers prevailing in, respectively, non-polar and polar solvents (solvatochromism).[102–104] Several investigators[105–108] have reported that these stabilities can be reversed ("inverse photochromism") when the switch is immobilised onto a nanoparticle. Although the molecule can still be photoswitched, the thermally stable isomer becomes metastable (and *vice versa*). This effect was first reported by Ueda *et al.*,[106,108] who tethered SP on 150 nm SiO_2 NPs immersed in ethylene glycol. Although this polar solvent stabilises the MC form in solution, the switches on nanoparticles are predominantly in the SP form, even for short linkers (C2 and C10 chains were studied) connecting the switch to the NP surface. A plausible explanation for this behaviour is that the SP moiety on the nanoparticle surface is not directly exposed to ethylene glycol, but, instead, is surrounded by a non-polar environment due to other molecules in the monolayer; in other words, the monolayer masks the interactions with the solvent and thus disfavours SP-to-MC isomerisation.

The same NPs dispersed in hydrophobic solvents (*e.g.*, CCl_4, cyclohexane) displayed normal photochromism, with the SP form being thermally stable both in solution and on the particles. Interestingly, adsorption of SP onto these SiO_2 NPs avoided formation of intramolecular complexes. Specifically, UV-induced ring-opening of SP present freely in CCl_4 or cyclohexane was accompanied by the formation of intermolecular SP–MC complexes[109,110] of various stoichiometries (*e.g.*, 1:1, 2:1, 3:1),[111] as evidenced by the appearance of new, red-shifted bands in the UV-Vis spectra. In contrast, UV-Vis spectra of SP harboured on NPs dispersed in the same solvents showed only one band following UV irradiation.

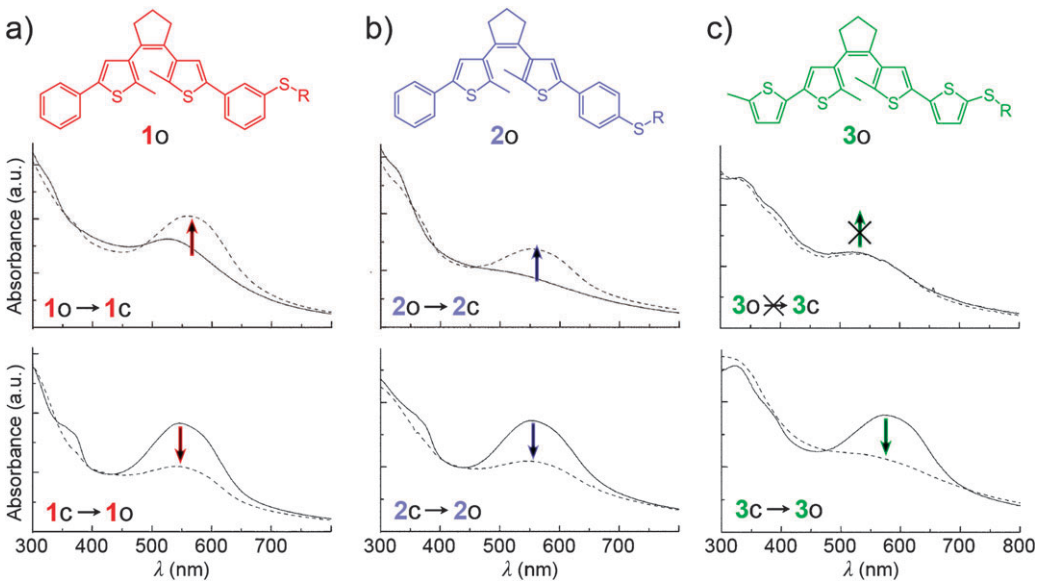

Fig. 6 Structural formulae (top panel) and UV-Vis spectra accompanying cyclisation (middle panel) and ring-opening (bottom panel) of various DTEs attached to Au NPs. Substitution pattern of the DTE moiety has a pronounced effect on isomerisation efficiency. "o" and "c" indicate the open and the closed isomers of DTE. Adapted with permission from ref. 94 (Copyright 2006 Royal Society of Chemistry).

View Article Online

Published on 21 April 2010. Downloaded by Pennsylvania State University on 06/03/2016 20:02:52.

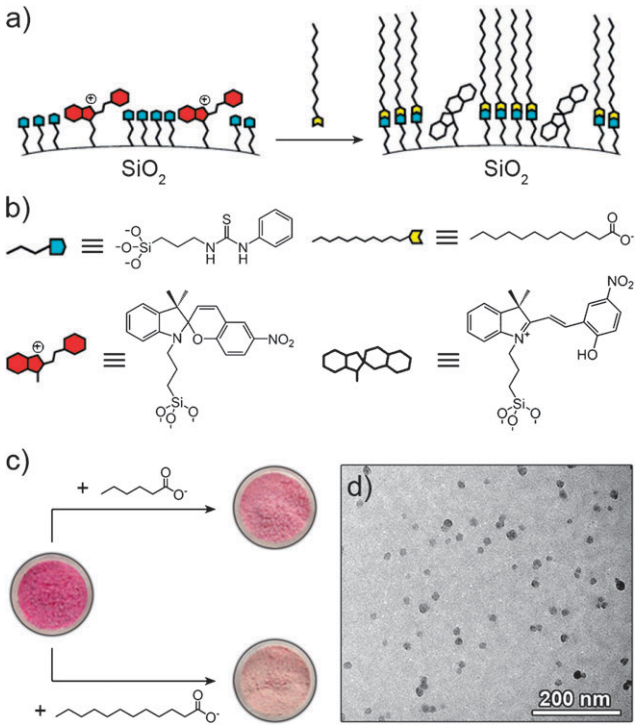

Fig. 7 (a) Schematic of a sensor based on SiO_2 NPs functionalised with SP switches. Binding of carboxylates to thiourea (blue) induces transformation from the coloured MC to the colourless SP isomers. (b) Structural formulae of the components. (c) Visual changes accompanying binding of carboxylates (here, hexanoate (top) and dodecanoate (bottom)) to SiO_2 NPs. (d) TEM image of 20 nm SiO_2 NPs. Adapted with permission from ref. 107 (Copyright 2008 Royal Society of Chemistry).

This band corresponded to the open-ring MC isomer and indicated the absence of the complex mixture of SP–MC oligomers—likely, because of relatively large ($\sim$1.3 nm) and *fixed* spacings between the individual SP units on the NP surface.

Recently, the delicate balance between the coloured MC and colourless SP forms has been used[107] as a basis of NP-based chemical sensor (Fig. 7). Here, SiO_2 NPs, 20 nm in diameter (Fig. 7d), were functionalised with a mixed monolayer of SP and phenylthiourea, with the latter ligand used in excess (Fig. 7a and b). On account of the hydrophilic nature of thiourea, the SP switches exist in the open, MC form. At the same time, thiourea groups act as recognition sites for anions such as carboxylates. While the addition of simple inorganic anions does not result in any visual changes, the addition of long alkyl chain carboxylates renders the silica NP surface effectively hydrophobic, thus shifting the SP–MC equilibrium towards the closed, SP isomer. As a result, the colour intensity of the NP solution decreases. Importantly, the system could be calibrated to sense carboxylates of different chain lengths. For example, Fig. 7c shows the response of the thiourea-functionalised silica NPs (left) to hexanoate (top right) and dodecanoate (bottom right). As the length of the alkyl chain increases, the SP form of the switch is stabilised to a greater extent, and a gradual colour change from red to light pink is observed. It is worth emphasising that the sensing application was possible on account of both the spiropyran's photochromism and the optical transparency (*e.g.*, absence of absorption due to SPR) of the silica NPs.

In another intriguing piece of research, Raymo *et al.*[105] discovered that SP adsorbed onto CdSe quantum dots (QDs) can display either normal or inverse photochromism, depending on the method of preparation of the NPs. In the first method (QD-1), NPs were prepared from $Cd(OAc)_2$ and elemental sulfur in the presence of tri-*n*-octylphosphine as the surfactant. The second route (QD-2) relied on the use of $Cd(ClO_4)_2$ and Na_2SO_3, with sodium dioctylsulfosuccinate as the surfactant. In both bases, the NPs were coated with decanethiol, followed by ligand exchange to a spiropyran dithiolane.[105] As expected on the basis of the non-polar nature of the SAM coating the particles, NPs obtained by the QD-1 route displayed normal photochromism (*i.e.*, SP favoured over MC form), although the kinetics of the thermal ring closure were somewhat inhibited. When the NPs were prepared by the QD-2 method, however, MC was the stable form and SP became the metastable isomer which was not observed unless the NPs were continuously irradiated with visible light. The authors suggested that the particles prepared by the QD-2 protocol have charged defects on their surfaces, which manifest[105] themselves (i) in broadened bands in the emission spectra, and (ii) by the fact that these NPs encourage adsorption of negatively charged species, such as heteropolyacids[112] (similar electrostatic interactions are thought to stabilise the charged form of SP). Although the structural origin of the charged defects remains obscure, they likely result from the excess of Cd^{2+} cations on the NP surfaces stabilised by the anionic surfactant used in this synthetic method. In sum, this study demonstrates that subtle differences in surface properties of NPs can drastically alter the isomerisation behaviour of molecular switches.

2.4 NP-induced modulation of redox potentials

The finite size and curvature of NPs can have pronounced effects on the switches that comprise changed or ionisable groups. We have recently demonstrated[69] that the attachment of supramolecular and mechanically interlocked switches to NP surfaces (Fig. 8a and b) affects their redox potentials. Specifically, oxidation potentials of dithiolane-terminated tetrathiafulvalene (TTF) ligands (**2** in Fig. 8b) were found to be higher after their immobilisation than in solution, and these shifts could be controlled by the surface concentrations, χ, of the switch, a parameter that is adjusted easily by varying the ratio of **2** to the background ligand **1** in the *m*SAMs. The observed gradual increase of the oxidation potentials with increasing χ (Fig. 8c, left) was attributed to the accumulation of positive charge on the surfaces of NPs. Oxidation of **2** on a NP increases the electric potential around that NP, making it more difficult to oxidise other TTF ligands on the same particle. Dithiolane-terminated bistable [2]rotaxane $\mathbf{3}^{4+}$ showed an analogous behaviour, with the cyclobisparaquat-*p*-phenylene ($CBPQT^{4+}$) ring reduction potentials shifted to more positive values (Fig. 8c, right).[113] These shifts indicate that as the surface concentration of $CBPQT^{4+}$ increases (and the positive charge accumulates), it becomes gradually easier to reduce these groups, and therefore to decrease the unfavourable electrostatic potential energy of the system.

 This journal is © The Royal Society of Chemistry 2010

View Article Online

Published on 21 April 2010. Downloaded by Pennsylvania State University on 06/03/2016 20:02:52.

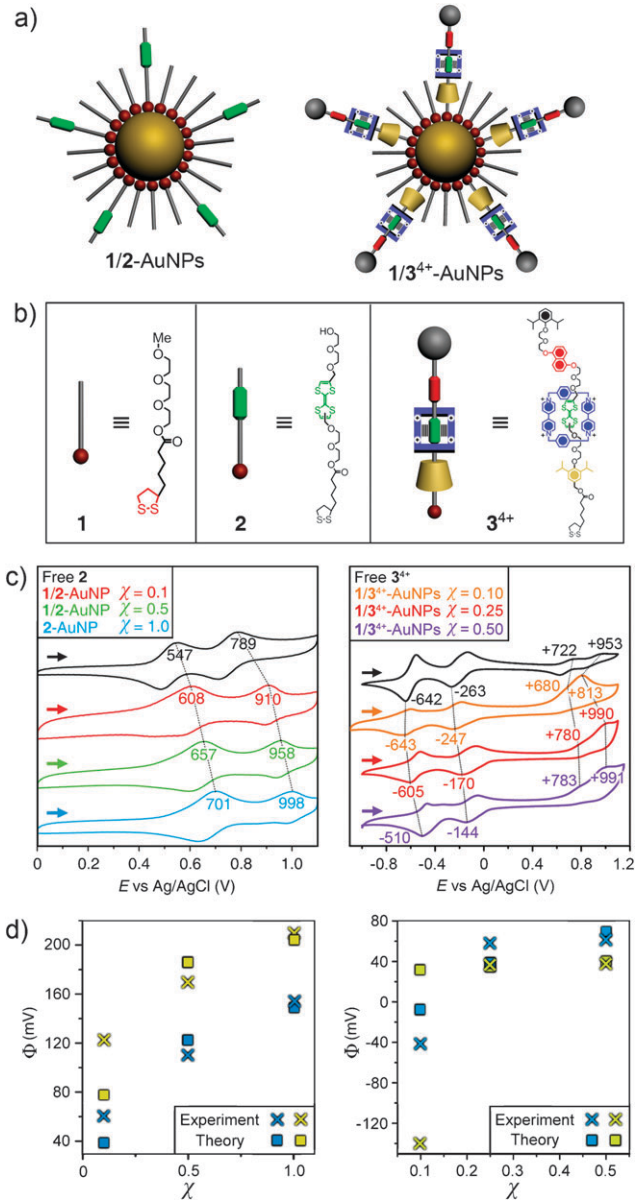

Fig. 8 (a) Schematic of Au NPs functionalised with electron-rich TTF stalks (left) and bistable [2]rotaxanes (right). (b) Structural formulae of the ligands. (c) Cyclic voltammograms of ligands **2** (left) and $\mathbf{3}^{4+}$ (right) present free in solution and adsorbed on Au NPs at various surface concentrations. (d) Experimental (×) and calculated (□) shifts in the redox potential, Φ, of TTF in **1**/**2**-Au NPs (left) and $\mathbf{1}/\mathbf{3}^{4+}$-Au NPs (right) as a function of the surface coverage, χ. Blue and yellow traces correspond to the first and second oxidation potentials of TTF, respectively. More details will be published in an upcoming publication.[113] Adapted with permission from ref. 69 (Copyright 2009 American Chemical Society).

An important extension of these studies is that the experimental results can be fully rationalised by an electrostatic model which relates the shifts in redox potential, E, to the changes in the electrostatic potential around the particles, Φ. Two observations are relevant here: (i) that the oxidation of switches X adsorbed on NP surfaces causes Φ around the particle to increase and (ii) that the more of the oxidised species are already present on the surface, the more difficult it is to oxidise more of these groups and introduce additional charge onto the particle (negative electrostatic cooperativity). Based on these premises, it can be expected that the oxidation potential of adsorbed X is related to Φ: to the first approximation, one can write $E^x = E^0 + \Phi$, where E^x is the observed oxidation potential at the particle's surface (metal core plus SAM) and E^0 is the oxidation potential of the switch X in a dilute solution. In other words, the shift in the oxidation potential $E^x - E^0$ is equal to the electrostatic potential due to the immobilised switches, Φ. The value of the latter is found readily by solving the Poisson–Boltzmann equation, $\nabla^2\psi = \kappa^2 \sinh(\psi)$, where κ^{-1} is the Debye screening length, $\psi = e\Phi/k_BT$ is the dimensionless potential, e is the charge of an electron, k_B is Boltzmann's constant, and T is the temperature. Importantly, the dependence of the potential on the surface concentration of the switches, χ, and the curvature/radius of the nanoparticle, a, influences the solution to the problem *via* the boundary condition of the form $\frac{\partial\Phi}{\partial r}\Big|_a = -\frac{\sigma(X,\chi)}{\varepsilon_0\varepsilon}$, where σ stands for the surface charge density on the NP. While other mathematical details can be found in ref. 69 and 113, the important point is that this relatively straightforward model predicts accurately—to within less than 5%—the changes in redox potentials for NPs of different sizes and functionalised with various pseudorotaxanes and bistable [2]rotaxanes (Fig. 8d). Lastly, the model is generic in the sense that it can be easily adapted to other types of charged switches.

Although not all phenomena discussed in this section can yet be described as accurately as can the redox properties of the switches, a general understanding of these phenomena appears sufficient to at least begin to design systems of switchable NPs in rational ways. One direction of this research is to design systems in which the switches control various nanoparticle properties—we are now in a position to discuss several such examples.

3. Molecular switches control optical properties of NPs

Widespread interest in noble metal NPs comes from their size-dependent properties, and optical properties are arguably the most vivid manifestation of this dependence. Metal NPs exhibit a strong absorption band in the visible, which is not present in the spectrum of the bulk metal. This band, called the surface plasmon resonance (SPR) band, appears when the frequency of incident photons is resonant with the collective oscillations of the conduction electrons (or surface plasmons) of the NPs.[114] It is well-established that the wavelength of the SPR band is very sensitive to NP size,[3,115] shape,[116,117] proximity to other particles,[5,49,63] as well as dielectric properties[118–120] of the surrounding medium. Molecular switches adsorbed on the surfaces of NPs can modify their optical properties in two ways. First, isomerisation of a switch entails change in its electronic properties, thereby modifying the dielectric constant in close proximity to the NP surface. Second, and often more pronounced, molecular switches can control the optical properties of NPs "indirectly" by way of changing the distances between the NPs and/or mediating NP aggregation. One strategy to decouple the electronic and the aggregation-dependent effects and to study only the former is by immobilising

View Article Online

Published on 21 April 2010. Downloaded by Pennsylvania State University on 06/03/2016 20:02:52.

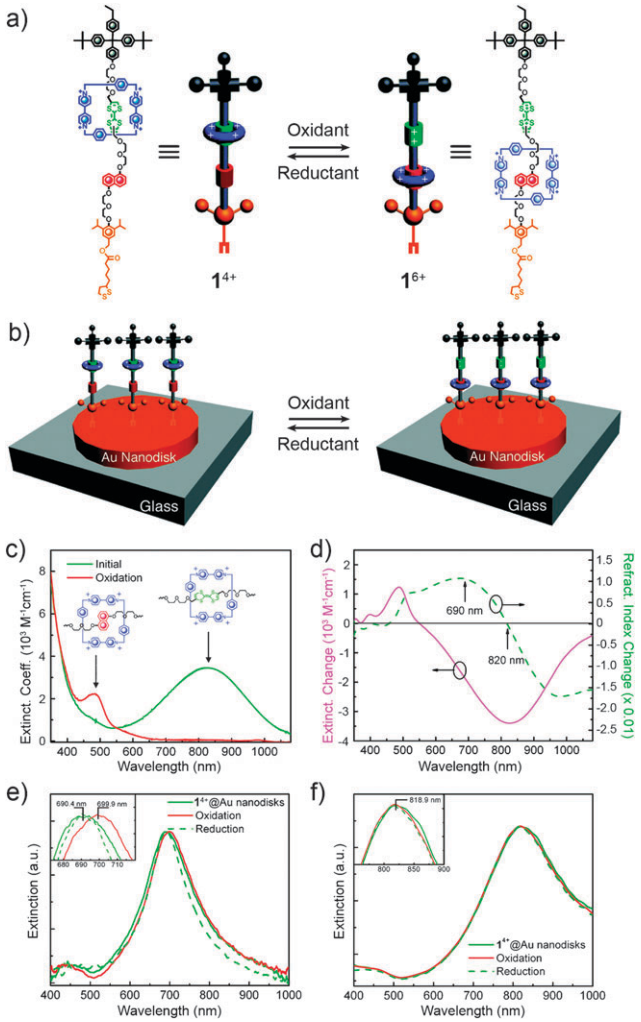

Fig. 9 (a) Structures and redox-induced switching of a dithiolane-terminated bistable [2]rotaxane. (b) Schematic illustration of molecular mechanical switching at the surface of a gold nanodisk. (c) Extinction spectra of $\mathbf{1}^{4+}$ before (green line) and after (red line) oxidation of the TTF station with $Fe(ClO_4)_3$. (d) Differential extinction spectrum derived from the data in (c) (pink line) and the corresponding wavelength-dependent refractive index change calculated using the Kramers–Kronig equation. (e and f) Redox-induced extinction spectra changes for $\mathbf{1}^{4+}$-coated gold nanodisks with their SPR bands tuned to ~690 nm (e) and ~820 nm (f). Adapted with permission from ref. 126 (Copyright 2009 American Chemical Society).

the switch-decorated NPs on a solid support. A number of such systems have been reported,[121–123] but they usually displayed a one-way, irreversible change in SPR. Recently, however, (i) arrays of Au nanodisks[124,125] (NDs) covered with bistable [2]rotaxanes,[126] and (ii) hexagonally close-packed monolayers of Au NPs functionalised with DTEs,[127] both capable of undergoing reversible structural changes, were prepared and their optical properties were investigated.

The first of these reports[126] is an elegant study in which the authors present a system rationally designed for a maximum change of SPR using a molecular switch, in this case, a bistable [2]rotaxane ($\mathbf{1}^{4+}$ in Fig. 9a). This mechanically interlocked molecule consists of a long, dithiolane-terminated thread incorporating two electron-rich recognition units—tetrathiafulvalene (TTF) and 1,5-dioxynaphthalene (DNP)—which is encircled by the electron-deficient macrocyclic ring, $CBPQT^{4+}$. In the ground state of $\mathbf{1}^{4+}$, the $CBPQT^{4+}$ ring has a higher affinity for and resides preferentially at the TTF station. Upon oxidation of the TTF station, however, the $CBPQT^{4+}$ ring loses its affinity for the now oxidised TTF^{2+} on account of the Coulombic repulsion, and moves (Fig. 9a, b) to the DNP station. The two co-conformations[128] have markedly different electronic properties and extinction spectra (Fig. 9c). Fig. 9d shows the differential extinction spectra of the two co-conformers and the corresponding changes in the refractive index as a function of the wavelength, calculated using the so-called Kramers–Kronig equation.[121] These results imply that the largest change in the refractive index before and after oxidation of $\mathbf{1}^{4+}$ occurs at ~690 nm, while at ~820 nm, the change is expected to be close to zero. To test these hypotheses, two types of nanodisk arrays (differing in disk diameters and heights) were prepared—one array exhibited SPR at 690.4 nm and the other at 818.9 nm.[126] Remarkably, the former sample showed a significant (~9.5 nm) and reversible shift in the SPR band maximum upon oxidation, whereas SPR of the latter remained insensitive to oxidation and reduction (Fig. 9e and f, respectively). To confirm that the reversible changes in the optical properties of the NDs derived from the mechanical motion within the molecular switches, two control experiments[126] were performed. In these experiments, optical responses of (i) bare (non-functionalised) Au NDs, and (ii) Au NDs coated with dithiolane analogous to $\mathbf{1}^{4+}$, but lacking the $CBPQT^{4+}$ ring, were investigated. As expected, the SPR band of these NDs was not affected by the addition of oxidants or reductants.

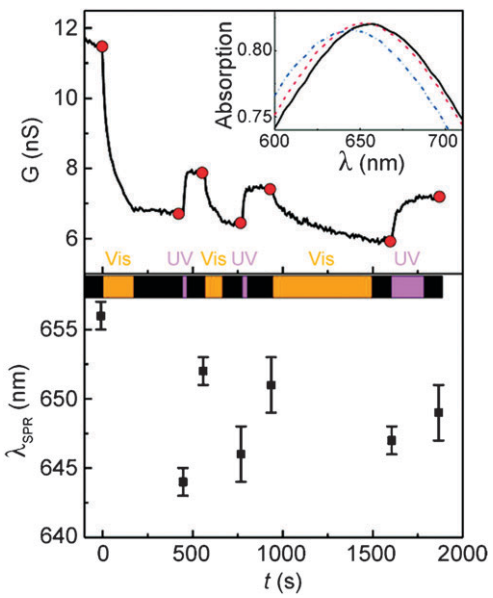

Fig. 10 Relation between the conductance of a hexagonally close-packed monolayer of Au NPs crosslinked by DTE-incorporating ligands on its optical properties. Coloured bars correspond to irradiation with visible (orange) or UV (purple) light for times indicated on the ordinate. See also Fig. 16. Adapted with permission from ref. 127 (Copyright 2009 American Chemical Society).

 This journal is © The Royal Society of Chemistry 2010

View Article Online

Published on 21 April 2010. Downloaded by Pennsylvania State University on 06/03/2016 20:02:52.

In another study whose primary focus was the modulation of electronic properties of NPs (see also Section 5), the optical response of spherical Au NPs arranged in a hexagonally closed-packed monolayer and crosslinked with a DTE dithiol was investigated (Fig. 10, bottom).[127] An initial sample—prepared from the closed-ring isomer—had the SPR band maximum at $\lambda_{max} \approx 656$ nm, which shifted to $\lambda_{max} \approx 644$ nm upon irradiation with visible light and concomitant isomerisation to the open-ring isomer. Consecutive irradiation cycles resulted in smaller SPR shifts (Fig. 10, bottom), most likely on account of an incomplete isomerisation and co-existence of the two isomers. Overall, average values of $\lambda_{max} \approx 652$ nm and $\lambda_{max} \approx 646$ nm were obtained for the closed and open isomers over three switching cycles. These results are in agreement with earlier experimental[129–131] and theoretical[132] studies which demonstrated that the refractive index of mixtures of the two DTE isomers increases linearly with the content of the closed isomer.

In the two examples, shifts in the SPR bands were relatively small, below ~10 nm. Much more pronounced changes in optical properties of NPs can be achieved by changing the distances between nearby NPs. Such effects have been studied[133] in aggregates of NPs covalently crosslinked with dithiols incorporating a photoswitchable AB group. For these experiments, azobenzene is the ligand of choice on account of the large-amplitude motions it undergoes during light-induced isomerisation. As a result of this molecular motion, the aggregates undergo[133] reversible switching between "breathe in" and "breathe out" states. The switching between these two states is accompanied by changes in the NPs' optical properties. In the original study, AB functionalised at the *para* positions with two cysteine residues was used and NP aggregation was induced by crosslinking the NPs with AB-containing dithiols that displaced part of the weak octadecylamine (ODA) or benzyldimethylstearylammonium chloride (BDSAC) surfactant stabilisers. The crosslinked aggregates that formed were subsequently irradiated with UV and visible light. Although the "breathing" motion was not apparent from the TEM images, UV-Vis spectroscopy confirmed reversible spectral changes due to electrodynamic coupling between nearby plasmons. For ODA-protected NPs, the wavelength of SPR maximum shifted between $\lambda_{max,\ trans} \approx 530$ nm (Vis irradiation) and $\lambda_{max,\ cis} \approx 550$ nm (UV irradiation). BDSAC-coated NPs showed a more pronounced response, with the SPR band maximum shifting from $\lambda_{max,\ trans} \approx 550$ nm to $\lambda_{max,\ cis} \approx 640$ nm, and then back to $\lambda_{max,\ trans'} \approx 560$ nm under visible light. The authors proposed[134] that this efficient isomerisation was facilitated by the lability of ammonium surfactants on the NPs. Unfortunately, "breathing" of the aggregates in this case was accompanied by a significant coalescence of NPs' metal cores, which presumably occurs when the aggregates are in their "collapsed" states. As a result, the number of "breaths" for a given sample was limited to three or four. Analogous results for silver NPs crosslinked with an azobenzene dithiol have been obtained.[135] More examples of distance-dependent electrodynamic coupling between metal NPs will be discussed in Section 9 which deals with reversible aggregation and crystallisation of NPs.

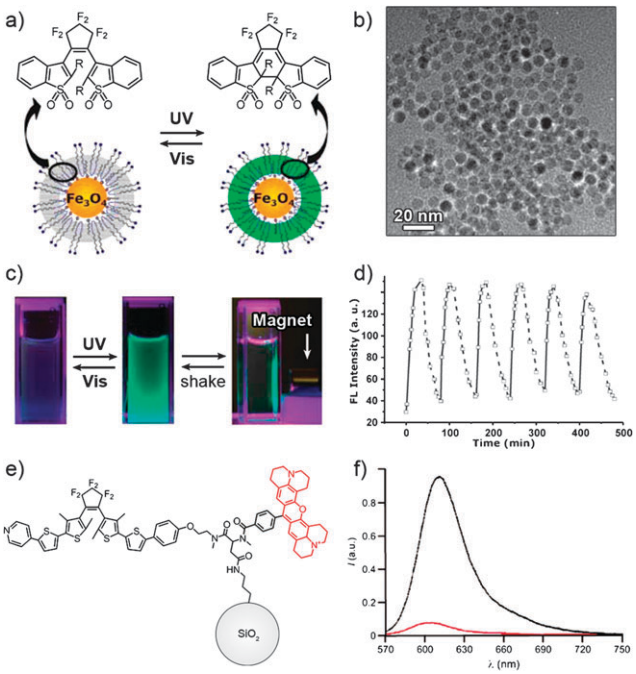

Fig. 11 (a) Photoisomerisation of dithienylethene on the surface of Fe_3O_4 NPs. R = Me or Pr^n. (b) TEM image of sulfur-oxidised DTE (oDTE) (R = Pr^n)-coated Fe_3O_4 NPs. (c) Visual changes accompanying photoinduced isomerisation of oDTE on Fe_3O_4 NPs and effect of a magnetic field (right) on the sample. (d) Modulation of the fluorescence signal upon alternating irradiation with UV (312 nm) and visible (420 nm) light. Adapted with permission ref. 43 (Copyright 2008 Royal Society of Chemistry). (e) Structural formula of a fluorescent DTE used to cover SiO_2 NPs. (f) Modulation of the fluorescence signal before (black) and after (red) UV irradiation. Adapted with permission from ref. 152 (Copyright 2008 Wiley-VCH Verlag GmbH & Co. KgaA).

4. Molecular switches control fluorescent properties of NPs

Fluorescent NPs are of interest[136–138] mainly as highly sensitive and fatigue-resistant labels for biological applications. Fluorescence in these materials can originate either from the NP core or from the protective ligand shell. Although fluorescence is usually much stronger when it is derived from the NP core, the combination of fluorescent ligands and NP cores exhibiting other types of material properties can lead to the development of multifunctional nanomaterials. For example, Lee *et al.*[43] prepared superparamagnetic 7 nm Fe_3O_4 NPs[139] decorated with a layer of photoresponsive sulfur-oxidised dithienylethene (oDTE; Fig. 11a and b). Since these molecules do not form organised SAMs on the NPs, ethylene oxide–propylene oxide block copolymer was used to mediate their attachment to the NPs; the polymer effectively acted as "glue" binding the chromophores to the surface of oleic acid-stabilised Fe_3O_4 NPs. Although it has proven difficult to estimate the thickness of the resulting organic layer, the number of photoactive units per NP was determined (by inductively-coupled plasma atomic emission spectroscopy, ICP-AES, and by elemental analysis) to be 200–300, depending on the solvent used during the dye immobilisation. The switching behaviour of these NPs is

View Article Online

Published on 21 April 2010. Downloaded by Pennsylvania State University on 06/03/2016 20:02:52.

illustrated in Fig. 11c and d. When exposed to UV light, the virtually colourless solution (Fig. 11c, left) changes its emission properties—its intense green fluorescence (monitored at 505 nm; Fig. 11c, centre) can be attributed[140–142] to the closed form of oDTE. Kinetics of the switching on NPs is significantly slower than for oDTE in solution and the photostationary state is reached only after ~30 minutes of continuous irradiation (*vs.* ~3 minutes in solution). Fluorescence quantum yields, however, are almost identical to the solution values (0.12 *vs.* 0.14), as Fe_3O_4 NPs do not absorb the emitted light. Irradiation with visible light reverts the switch to its original open form, and fluorescence values drop significantly. The process (Fig. 11d) is fully reversible and the isomerisation cycle can be repeated at least six times. Finally, because of the superparamagnetism of NP cores, the particles can be precipitated from solution under magnetic fields but then redispersed by vigorous shaking (Fig. 11c, right). Combination of this magnetic control with fluorescent properties can be of value in applications based on the combination of magnetic resonance and optical imaging techniques.[143–146]

The remaining examples in this section describe systems in which one form of the photoswitch quenches the emission of a nearby fluorescent component. The process occurs by fluorescent resonance energy transfer (FRET)[147–150] from the fluorescent moiety to the acceptor photoswitch. In this photochromic FRET, or pcFRET,[151] the fluorophore's emission maximum overlaps with the absorption maximum of one of the isomers of the switch, but there is no such overlap with the absorption spectrum of the other isomer. In general, the efficiency of FRET is determined by the extent of overlap between these emission and absorption bands. As a result, the excitation energy of the fluorophore can be absorbed by the proximal switch with an accompanying loss of the emission intensity.

For example, Bossi *et al.*[152] reported a system in which 30 nm silica NPs were chemically functionalised with ligands comprising both the fluorescent rhodamine (Rh) group and a DTE switch (Fig. 11e). It was found that Rh's fluorescence was quenched by up to 95% by the closed form of DTE (Fig. 11f, red trace). In this system, the NPs acted solely as a scaffold to immobilise multiple copies of the ligands. Because of the confinement of these ligands on the NPs, however, fluorescence quenching was much more efficient than in solution of free DTE–Rh dyads. For example, fluorescence of a solution of DTE–Rh in which 50% of the DTE groups were in their closed geometries was quenched by ~50% (because DTE ring closure conversion is linearly proportional to fluorescence quenching). In contrast, the same 1 : 1 mixture of open and closed isomers on NPs gave an almost complete fluorescence quenching. This observation was rationalised by the fact that even for the open form of an individual DTE–Rh dyad, the Rh's fluorescence can still be quenched by the neighbouring DTE groups, assuming they are present in their closed forms. Silica NPs of other sizes (120, 250, and 600 nm) were also investigated and exhibited behaviour analogous to that of the smaller particles.

Many more studies[105,151,153–161] have been performed with semiconducting ZnS–CdSe core–shell QDs functionalised with chromophores capable of reversibly switching the QDs' fluorescence. QDs[162–164] represent a unique group of fluorescent

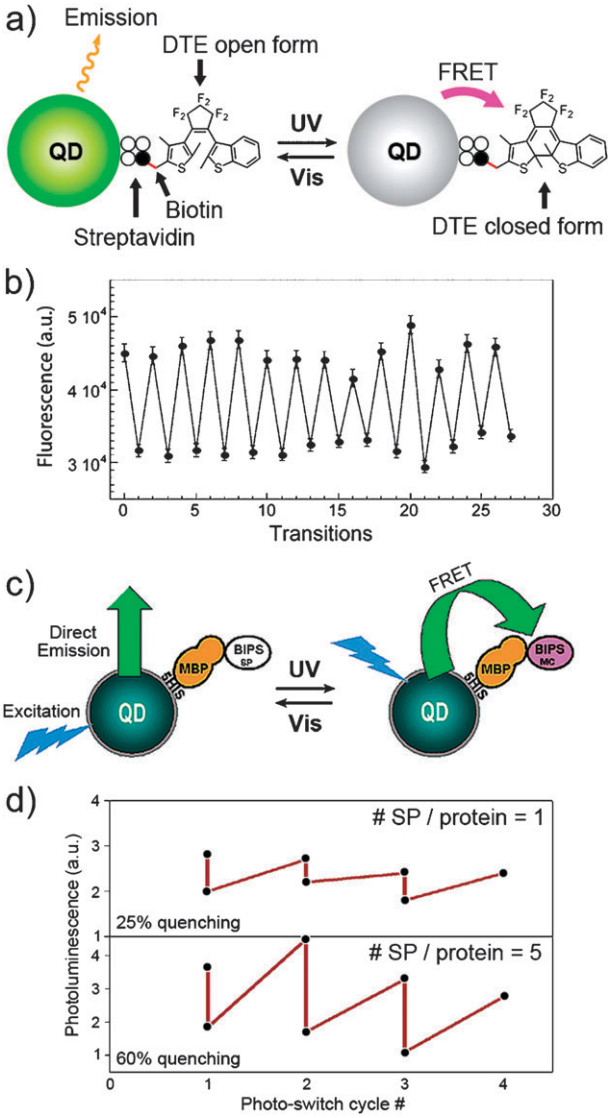

Fig. 12 Chromophore-induced modulation of QD fluorescence in QD–protein–DTE constructs. (a and b) Schematic representation and photoinduced fluorescence emission changes in constructs involving biotin–streptavidin binding. The closed isomer of DTE quenches fluorescence by FRET, whereas the open isomer does not. Adapted with permission from ref. 151 (Copyright 2005 Taylor & Francis Group). (c and d) Schematic representation and photoinduced fluorescence emission changes in maltose-binding protein-modified QDs to which SP units have been bound covalently. The open isomer of SP quenches fluorescence by FRET, whereas the closed isomer does not. Adapted with permission from ref. 155 (Copyright 2004 American Chemical Society).

materials with size-dependent, tunable absorption and emission properties, narrow emission spectra as well as excellent photobleaching resistances. Rational design of QD ligands for pcFRET could result in functional systems in which fluorescence can be activated and suppressed "on demand". Initial attempts to prepare such constructs incorporating QDs and photoswitches date back to 2004 and are based on the use of various proteins—such as streptavidin[151] or maltose-binding protein[155]—acting as linkers between the nanoparticles and the switches. In one of the first reported examples,[151]

 This journal is © The Royal Society of Chemistry 2010

View Article Online

Published on 21 April 2010. Downloaded by Pennsylvania State University on 06/03/2016 20:02:52.

commercial QD–streptavidin conjugates were reacted with molecules incorporating both biotin and DTE. When covered with the open form of the dye, the QDs remained fluorescent (Fig. 12a). Photocyclisation of the ligand, however, activated an energy transfer pathway from the particles to the coloured (closed) form of the chromophore and led to partial quenching of the emission (Fig. 12b). This rather low (34%) FRET efficiency could result[151] from the relatively large distance between the donor and the acceptor.

Another reported system[155] was based on the SP switch, whose metastable, open-ring MC isomer absorbed light in the visible region and caused fluorescence quenching. This construct incorporated the maltose-binding protein functionalised with the SP moieties *via* active ester chemistry (Fig. 12c). In addition, the protein was appended with a C-terminal polyhistidine tag through which it coordinated to QDs' shell zinc atoms.[155] Taking advantage of the multiple amino groups in the protein's stucture, a predetermined number of SP groups could be attached to a single protein molecule. As expected, increasing the number of SPs led to more pronounced (up to ~60%) FRET efficiencies (Fig. 12d).

More recent reports have focused on interactions between well-defined SAMs of chromophores and their parent fluorescent QD cores. One of the first studies employed thiol-terminated SP assembled on ZnS–CdSe QDs.[161] In its ground state, SP absorbs light in the UV region, therefore bands corresponding to the molecular switching and the fluorescence emission processes are well-separated. On the other hand, the open-ring MC isomer (Fig. 13a) absorbs mostly at λ_{max} = 588 nm, close to the band of the nanocrystal emitter. For a maximum overlap, NPs comprising a 2.6 nm CdSe core enclosed inside of a 1.7 nm ZnS shell and emitting maximally at λ_{max} = 578 nm were engineered. For smaller NPs, the efficiency of FRET progressively decreased. Fig. 13b illustrates the performance of these QDs. Overall, ~95% of the ground-state fluorescence intensity was quenched. This study is an elegant example of a rational design of a system to maximise fluorescence quenching.

In a related system, SP units were attached to ZnS–CdSe QDs *via* dithiolane, rather than thiol linkages.[154,157,159,160] Their FRET efficiencies, however, were limited[157] to ~45% likely because of an incomplete overlap between the inorganic component's emission (554 nm) and the organic ligand's absorption (592 nm) bands. A decreased number of quenchers per NP (a single dithiolane ligand takes about twice as much space on the NP surface compared to a thiol ligand) could also be a contributing factor. Finally, it is worth pointing out that the reversible, light-induced modulation of fluorescence quenching in SP-coated QDs has been used as evidence for a successful attachment of the ligands onto the QD surfaces in a new surface modification method.[153]

Also recently, Raymo *et al.* developed a new family of pH switches[165–167] based on the [1,3]oxazine ring (Fig. 14a). This molecular design is an interesting example of a system in which either acidic or basic conditions lead to a ring-opening isomerisation. Whereas the absorption band of the open-ring,

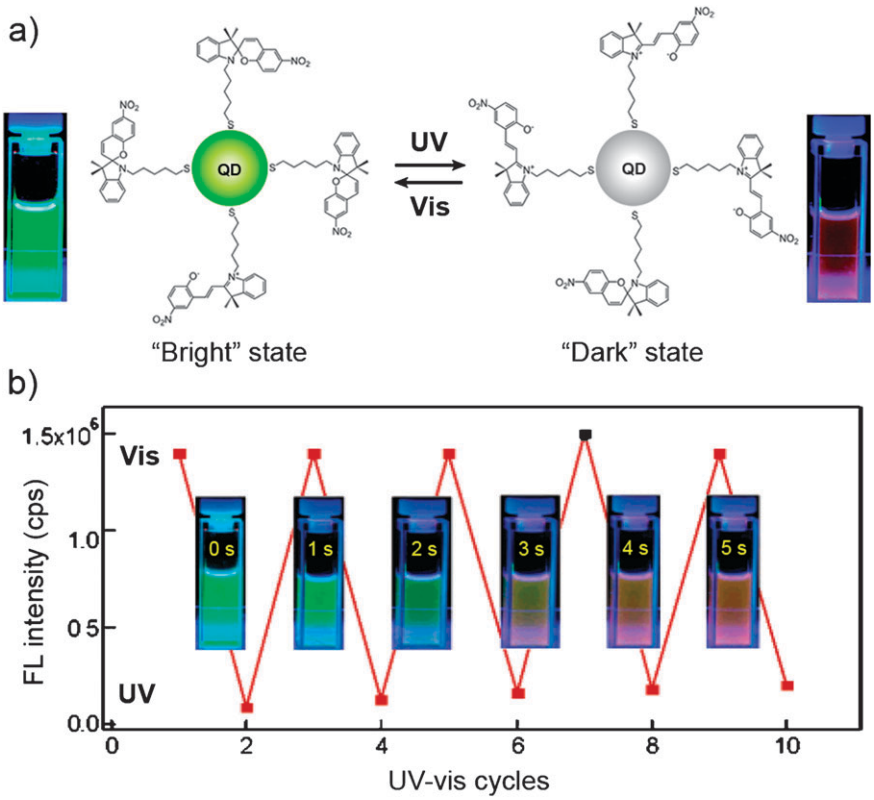

Fig. 13 Photoinduced fluorescence modulation in QDs functionalised with well-defined monolayers of SP switches. (a) Structural transformation and visual changes accompanying UV and visible light irradiation. (b) Modulation of fluorescence intensity with alternating UV and visible light irradiation. Adapted with permission from ref. 161 (Copyright 2005 American Chemical Society).

View Article Online

Published on 21 April 2010. Downloaded by Pennsylvania State University on 06/03/2016 20:02:52.

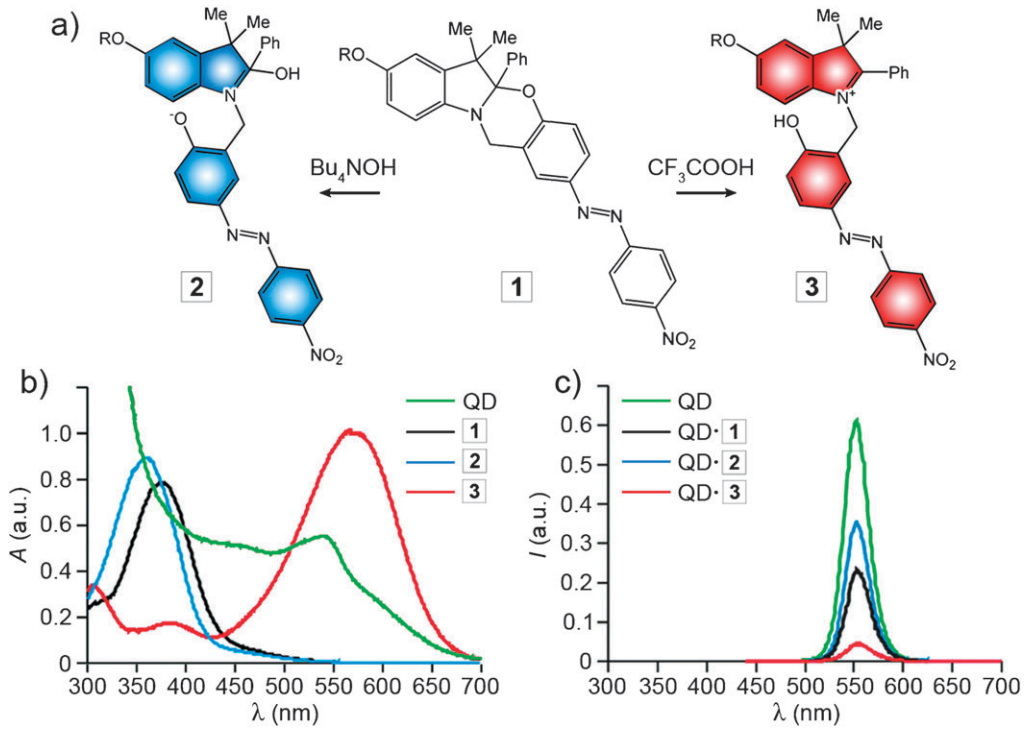

Fig. 14 (a) pH-induced structural transformations of [1,3]oxazine **1**. Under both basic (Bu_4NOH) and acidic (CF_3COOH) conditions, molecules undergo ring-opening reactions, resulting in **2** or **3**, respectively. R = Me or deprotonated thioctic acid. (b) These isomerisation reactions lead to either a minor hypsochromic shift (blue trace), or to a drastic bathochromic shift (red trace), respectively. The green trace shows absorption of the QD cores. (c) Changes in fluorescence emission of QDs (green trace) upon functionalisation with oxazine (black) and subsequent treatment with Bu_4NOH (blue) or CF_3COOH (red). Adapted with permission from ref. 156 (Copyright 2006 American Chemical Society).

deprotonated form (**2** in Fig. 14a) is slightly blue-shifted with respect to the parent structure **1**, the other open-ring form **3** absorbs strongly (Fig. 14b) in the visible region, and electron transfer from its indole group to the particles decreases the fluorescence intensity significantly (Fig. 14c). As in previously discussed examples, the extent of fluorescence quenching is governed by the overlap between the chromophore's absorption band and the QDs' emission band (Fig. 14b). Accordingly, FRET efficiency for the three forms of the dye follows the trend QD·**3** > QD·**1** > QD·**2**. It has been suggested that these oxazine-decorated QDs could be used as fluorescent chemosensors for OH^- ions, as well as for other analytes, after an appropriate modification of the ligand's structure.[158] Note that the [1,3]oxazines employed in this study also incorporate an azobenzene moiety. Although its role and switchability have not been investigated, an intriguing question would be whether the fluorescence of QD·**1** can be tuned "orthogonally", using both pH switching of the [1,3]oxazine moiety and light-based impulses causing azobenzene isomerisation.

5. Molecular switches control electrical properties of NPs

Electron transport through individual molecules lies at the heart of molecular electronics.[9,168,169] In order to investigate the conductive properties of single molecules, they need to be placed between two electrically conductive materials which act as electrodes. This goal is achieved (by now, routinely) by functionalising the molecule of interest with two thiol groups and using it as a linker between two gold electrodes.[170–174] Crosslinkers comprising light-addressable units have attracted considerable interest as potential components of future molecular optoelectronic switches and memories. To date, light-controlled conductance through AB[175] and DTE[176,177] groups has been demonstrated. A significant obstacle on the way to practical applications, however, is posed by technical difficulties associated with positioning individual molecules between two planar surfaces.[178,179] One way to overcome these difficulties and to study light-induced electrical properties is based on the self-assembly of thiolated molecules inside nanogaps formed in multisegmented nanowires by on-wire lithography (OWL).[180–182] A more traditional and currently more popular approach, however, is based on the use of metal nanoparticles, which can easily be prepared, handled, and crosslinked with single layers of molecules.[183–185] In order to encourage effective molecular switching, it is important that the structural changes accompanying the switching process are negligible; otherwise, isomerisation efficiencies in these confined environments would be greatly decreased. Photoisomerisation of DTEs (Fig. 15c) changes π-conjugation length, without significantly affecting the shape of the molecule—accordingly, DTEs have attracted most attention as model photoswitchable components in these architectures.[127,186–188]

Matsuda *et al.*[186–188] were the first to demonstrate reversible switching of conductance through NPs covered with molecular photoswitches. A typical experimental setup used in their conductance measurements consists of monolayers of NPs deposited on interdigitated nanogapped (5 μm gaps) electrodes

 This journal is © The Royal Society of Chemistry 2010

View Article Online

Published on 21 April 2010. Downloaded by Pennsylvania State University on 06/03/2016 20:02:52.

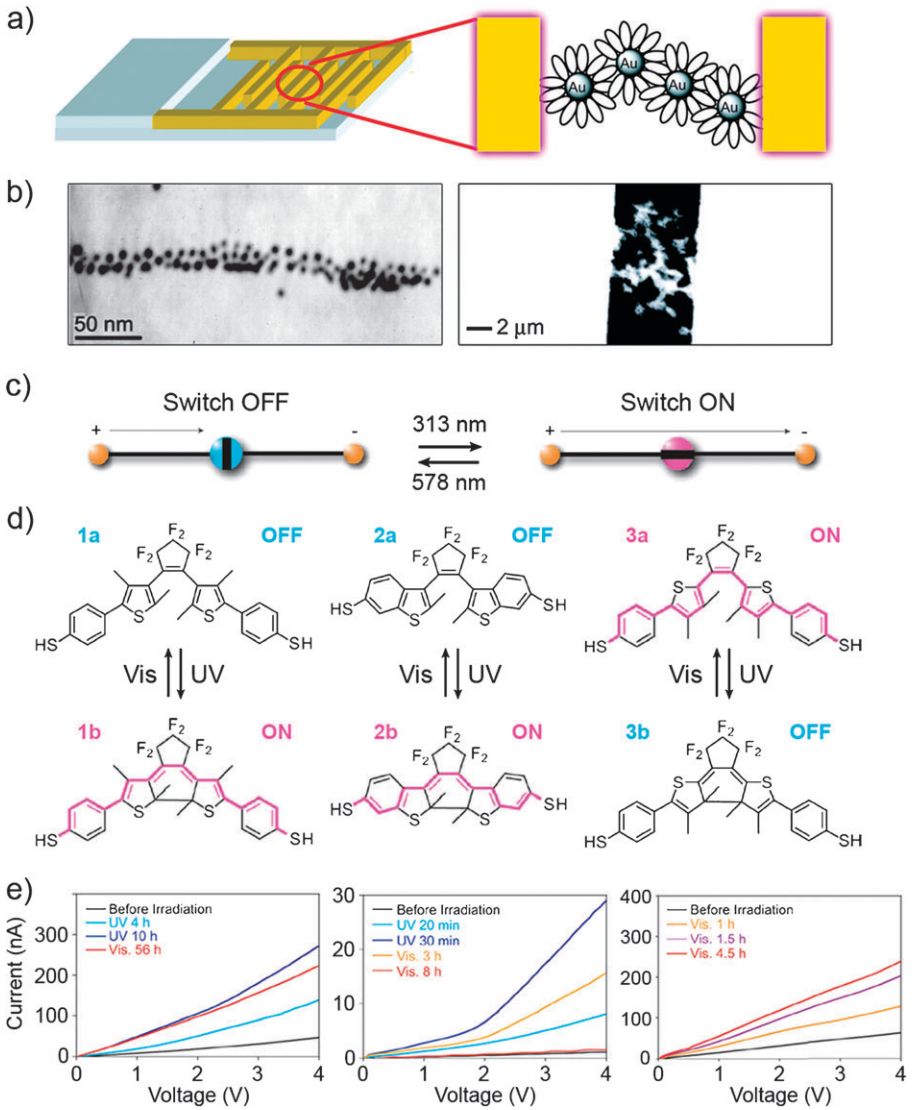

Fig. 15 (a) Scheme of the experimental setup. DTE-coated Au NPs bridge the gaps between interdigitated Au electrodes. (b) TEM (left) and SEM (right) images of a network of Au NPs-coated with ligand **2a**. In the SEM image, white parts represent Au electrodes and Au NP network connecting them. (c) Schematic illustration of the irradiation-induced change in the π-conjugation length. (d) Photoinduced isomerisation reactions in three different DTEs used in this study. Note that cyclisation in an inverse, 2-thienyl type switch disturbs the π-conjugated system. (e) UV and visible light-induced changes in the *I*–*V* curves in devices made using switches **1**–**3**. Adapted with permission from ref. 187 (Copyright 2008 American Chemical Society).

and crosslinked with DTE dithiols. The combination of the NPs and the ligands creates (Fig. 15a and b) a conducting path between the electrodes.[186] Note that in order to achieve higher conductance values, molecules employed in these experiments are fully conjugated and have the thiol groups attached directly[172,189] to the π-conjugated system (Fig. 15d). Five-hour, UV-induced isomerisation of crosslinker **1** (Fig. 15d) used in the original study led to a five-fold increase in conductance (as compared to the conductance before UV irradiation), but the conductance was only partially restored,[186] even after prolonged (56 h) illumination with visible light (Fig. 15e, left). Short (0.5 h) UV irradiation led to only a 1.2-fold increase in conductance. The system returned, however, to its original state when exposed to visible light for 16 h. These results confirm that the reversible molecular switching of DTE, as opposed to recently reported light-enhanced conductivity of NP films,[189,190] is the underlying reason for the conductance changes. This observation was further confirmed[186] by control experiments involving a structurally related, but non-photoswitchable, dithienylbenzene.

The poor reversibility of the system was most likely caused by the low yield of the cycloreversion reaction caused by a severe quenching of the excited state of the closed form of DTE by the NPs (see Section 2.2). To overcome this limitation, at least to some extent, Irie *et al.*[191,192] designed another photoswitch **2** (Fig. 15d, centre) characterised by an increased (by a factor of 23) cycloreversion quantum yield as compared to **1**, and found that both the response times and reversibility of the system (Fig. 15e, centre) were greatly improved.[187] Crosslinker **2** was used successfully to bring about a reversible,

View Article Online

Published on 21 April 2010. Downloaded by Pennsylvania State University on 06/03/2016 20:02:52.

25-fold—and 18-fold in an analogous device made of Ag NPs[188]—change in the conductance values. While this result is still much lower than the three orders of magnitude change in the conductance of individual DTE molecules,[95] it paves the way for molecular-scale circuitry controlled by light. Finally, an "inverse", 2-thienyl type[193] switch **3** was considered whereby the cyclisation reaction disturbs the π-conjugated system (Fig. 15d, right). As expected, the reverse switching was observed in that visible light irradiation resulted in a 4-fold *increase* in conductance.

More recently, Feringa *et al.*[127] described a similar system based on Au NPs crosslinked with DTEs. These researchers employed di(phenylthienyl)ethenes with the thiol groups attached[94,194] to the *meta* position of the phenyl rings (Fig. 16a). The response times and reversibility of the system (Fig. 16d) were significantly improved compared to the earlier studies. This improvement could be attributed to the hexagonally close-packed arrangement of the nanoparticles (Fig. 16c). As an unequivocal proof that the molecular switching of DTE is the origin of the observed conductance changes, UV-Vis spectroscopy was performed along with conductivity measurements, using an experimental setup illustrated in Fig. 16b. Since the on-state of DTE has a higher[127] dielectric permittivity, ε, the SPR peak of the NPs is expected to red-shift, along with the reversible conductance increase (Fig. 10). This elegant experiment showed a clear relationship between SPR absorption and conductance, thus confirming the mechanism of conductance switching.

In both[127,188] of the above systems, the dependence of sample conductivity on the fraction of molecules in the on-state was highly non-linear. Instead, conductance increased precipitously above a certain threshold value. A critical number of the on-state molecules was necessary to establish good electrical connections between the NPs and therefore the conducting path between the electrodes.[188] This percolation-type behaviour is well-known[195–197] and the theory behind it has been used to predict[127] the decrease of conductance upon consecutive irradiation with visible and UV light (Fig. 16e).

6. Molecular switches control magnetic properties of NPs

Interest in materials that exhibit photoinduced magnetisation derives from their potential applications in next-generation high-density information storage media and memory devices.[198–201] Although photomagnetic effects have been reported in various types of materials, the transition temperatures are usually very low,[202–210] thus limiting the potential practical applications of these materials. Einaga *et al.*[211–214] described two types of nanostructured materials in which magnetic properties can be

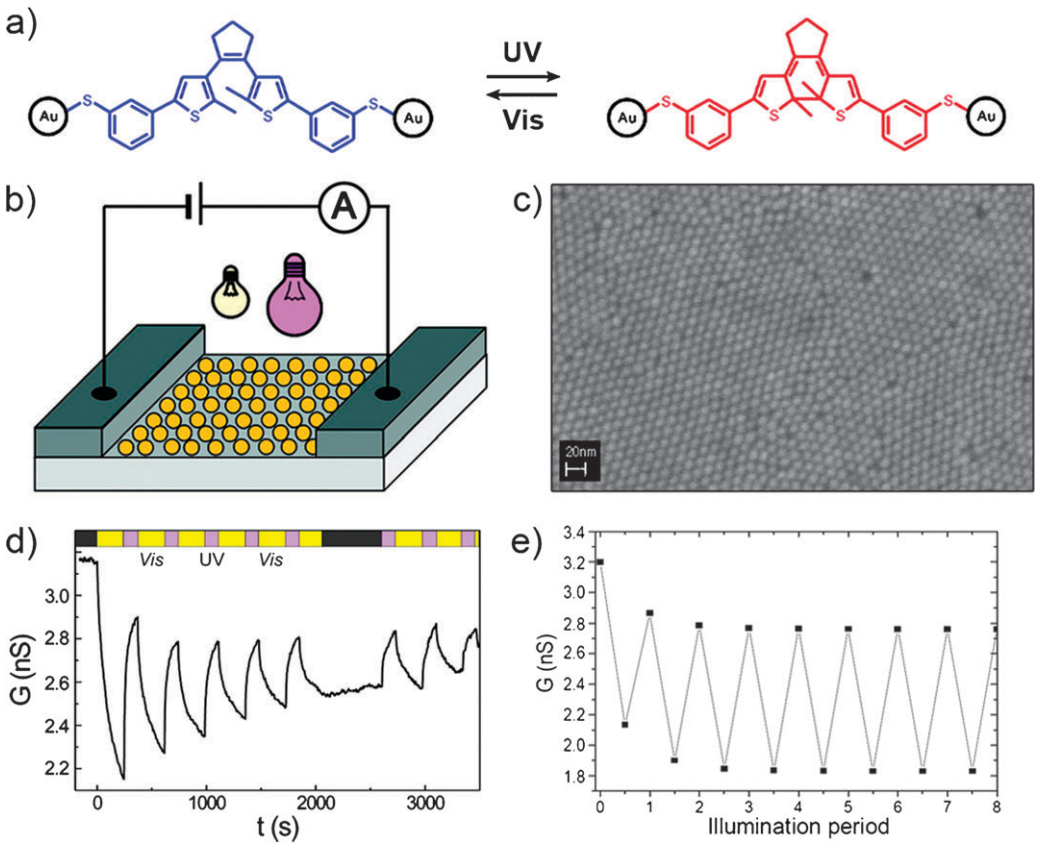

Fig. 16 (a) Photoinduced isomerisation of DTE-incorporating ligands crosslinking hexagonally close-packed monolayer of Au NPs. (b) Scheme of the experimental setup. UV-Vis spectra can be recorded during conductivity measurements (note that the intensity of light used to record the UV-Vis spectra was much lower than that used to photoisomerise the crosslinkers). (c) SEM image of the close-packed NP monolayer. (d and e) Experimental (d) and calculated (e) changes in conductance of the photoirradiated films. Adapted with permission from ref. 127 (Copyright 2009 American Chemical Society).

 This journal is © The Royal Society of Chemistry 2010

View Article Online

Published on 21 April 2010. Downloaded by Pennsylvania State University on 06/03/2016 20:02:52.

modulated by light. The first class are the magnetic (γ-Fe_2O_3, FePt) NPs decorated with a monolayer of AB. In the second one,[215,216] magnetic properties appear seemingly "out of nowhere" as a result of the combination of two diamagnetic components[217,218]—Au NPs and thiolate SAMs. We begin our discussion with the former, more "intuitive" class of materials.

Iron oxide (γ-Fe_2O_3) NPs decorated with AB were the first NPs whose light-induced magnetic properties were investigated in detail.[211–213] Taking advantage of the fact that the surface modification of magnetic NPs retains their magnetic properties,[219–221] these NPs were functionalised with a *m*SAM comprising an alcohol-terminated AB and *n*-octylamine, with the latter ligand "diluting" the AB SAM and providing free volume for AB isomerisation (see Section 2.1). The superparamagnetic properties of the functionalised NPs were then confirmed by means of superconducting quantum interference device (SQUID) measurements on solid samples prepared on quartz substrates. Although photoisomerisation of azobenzenes in these solid-state NP collections was significantly hampered, reversible magnetisation (M) was observed both at 5 K—that is, below the blocking temperature, $T_B \approx 15$ K of γ-Fe_2O_3 NPs (Fig. 17a and b)—and at room temperature (Fig. 17c and d, respectively). In both cases, UV irradiation resulted in a reversible increase in the magnetisation values by approximately 10%, although the M values were less reproducible—and, of course, much lower—at room temperature (Fig. 17d). While the mechanism by which AB switching affects the magnetisation values remains unclear, it has been suggested[213] that isomerisation-induced changes in either the electrostatic field around the NPs (due to *cis*-AB dipoles[49]) or in the ligand fields of the surface iron atoms could be responsible.

One important step in implementing magnetic-recording systems is the ability to fix the NPs' magnetic moments. To

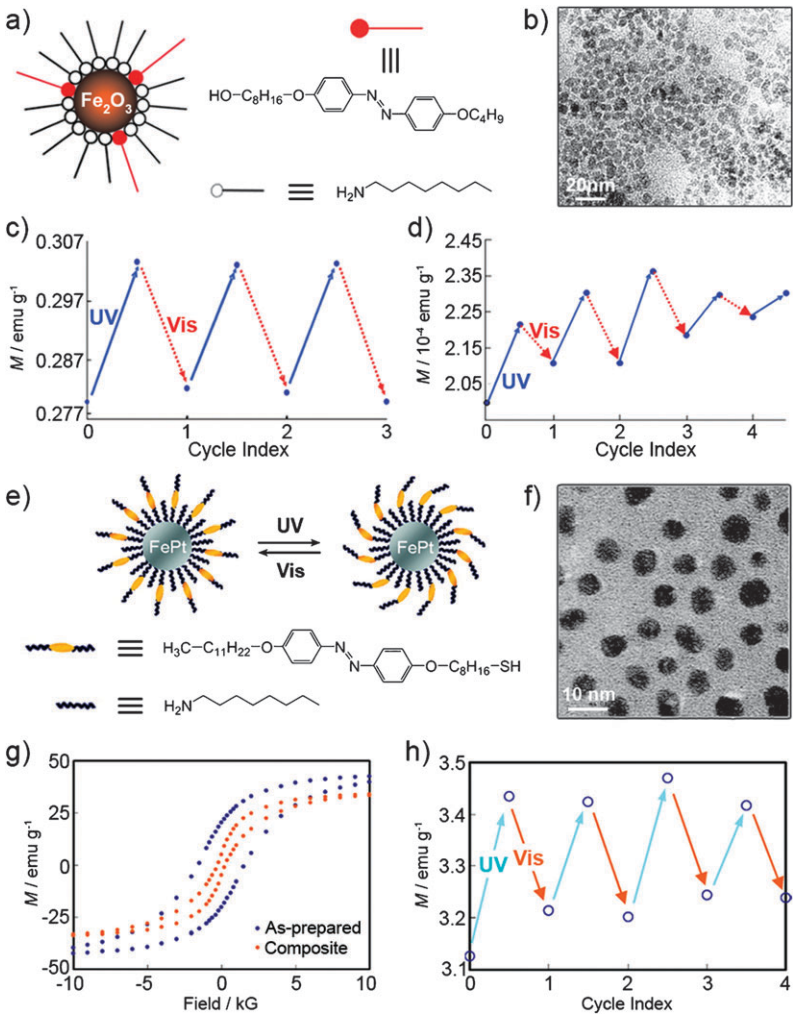

Fig. 17 (a) Scheme and (b) TEM image of γ-Fe_2O_3 NPs decorated with a *m*SAM of *n*-octylamine and 4-butoxy-4′-[(8-hydroxy)octyloxy]-azobenzene. (c and d) Photoinduced magnetisation changes in AB-functionalised γ-Fe_2O_3 NPs on a quartz glass slide at an external magnetic field of 10 G and temperature of (c) 5 K and (d) 300 K. Adapted with permission from ref. 211 (Copyright 2004 Wiley-VCH Verlag GmbH & Co. KgaA). (e) Scheme and (f) TEM image of FePt NPs decorated with a *m*SAM of *n*-octylamine and 4-dodecanoxy-4′-[(8-mercapto)octyloxy]-azobenzene. (g) Magnetisation curves of as-prepared (blue) and AB-functionalised (orange) FePt NPs recorded at $T = 300$ K. (h) Photoinduced magnetisation changes of AB-functionalised FePt NPs in the solid state at an external magnetic field of 10 G and temperature of 300 K. Adapted with permission from ref. 214 (Copyright 2007 American Chemical Society).

View Article Online

Published on 21 April 2010. Downloaded by Pennsylvania State University on 06/03/2016 20:02:52.

achieve this goal in light-switchable NP systems, the superparamagnetic Fe_2O_3 particles from the previous example were replaced (Fig. 17e and f) with the ferromagnetic FePt.[214] The advantage of the FePt alloy nanoparticles is that they can be protected by ligands with a wide variety of head groups,[222–224]—*i.e.*, both chemically "soft" and "hard". Accordingly, AB-terminated thiols, amines, as well as carboxylic acids have been successfully used as ligands for FePt NPs. As shown in Fig. 17g, surface-modified NPs retained typical magnetisation curves featuring hysteresis although values of coercivity (H_c) and remanence (M_r) were decreased by a factor of $\sim$8 and $\sim$4, respectively. AB switching proceeded readily in the solid state, with both isomerisation reactions reaching their photostationary states within one minute of irradiation. The high efficiency of the switching was attributed to the presence of the short octylamine background ligand which ensured free volume for AB isomerisation (Fig. 17e)—indeed, in NPs covered entirely with AB ligands, the yields of photoswitching were dramatically suppressed.[214] SQUID measurements on FePt NPs functionalised with the *m*SAMs showed that UV irradiation led to an increase in the M values (analogously to the Fe_2O_3 case), and the original values could be restored upon exposure to visible light (Fig. 17h). It is worth emphasising that the amplitude of room temperature magnetisation values was over one order of magnitude higher than in Fe_2O_3 NPs at $T = 5$ K. Also, as a control experiment, FePt NPs covered with non-photoswitchable ligands were prepared and their magnetisation was found not to be affected by light. In another important control experiment, magnetic properties of the photoswitchable FePt NPs were investigated in a highly diluted particle suspension in PMMA. Magnetisation changes observed in this case were identical to those observed in densely packed films of the NPs, thus confirming that the magnetisation changes originated from the electronic interactions between the AB ligands and the NP cores, and not from the magnetic interactions between different NPs.

The second class[217,218] of photoswitchable magnetic nanoparticles takes advantage of the recently discovered[225–228] ferromagnetic properties of thiolate-passivated, small ($d < 2$ nm) gold nanoparticles. This type of behaviour has been termed *ex nihilo*[215,216] ferromagnetism—since both components of the NPs (Au and thiols) are diamagnetic—and it originates at the gold–sulfur interface as a result of a gold-to-sulfur charge transfer. Consequently, localised holes in the 5d band of gold are formed and give rise to permanent magnetic moments.[225] The magnitude of the charge transfer is determined by the metal's work function, Φ_m, which in turn is known to depend on the molecular dipole of the molecules constituting SAM.[229,230] Since the two isomers of 4-alkoxyazobenzene have dipole moments pointing in opposite directions ("into" and "away" from the NP, see Fig. 18d), it was hypothesised that modulating the SAM's dipoles would influence Φ_m, and

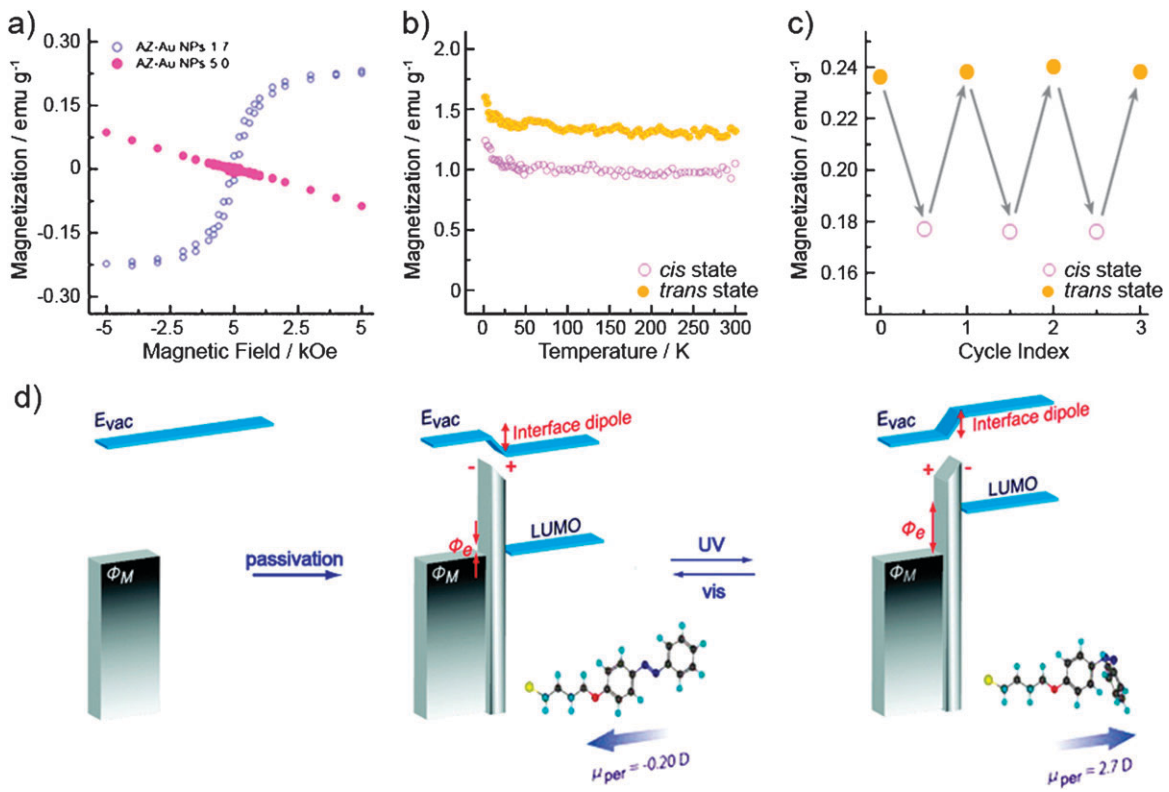

Fig. 18 (a) Size-dependent magnetic properties of Au NPs coated with 4-(4-mercaptobutanoxy)azobenzene. Average diameters of Au NPs are 1.7 nm (blue) and 5.0 nm (pink). The traces are indicative of diamagnetic (pink) and ferromagnetic (blue) properties of the NPs. (b) Temperature-dependent magnetisation of a UV (purple) and visible (orange) light-irradiated solid sample of 1.7 nm NPs in an external magnetic field of 5 T. (c) Reversible changes in magnetisation recorded on the same sample under an external magnetic field of 5 T at $T = 300$ K. (d) Schematic illustration of the changes in work function as a result of NP functionalisation and subsequent illumination with UV and visible light. Adapted with permission from ref. 217 (Copyright 2009 Elsevier Ltd.).

 This journal is © The Royal Society of Chemistry 2010

View Article Online

Published on 21 April 2010. Downloaded by Pennsylvania State University on 06/03/2016 20:02:52.

thus the magnetic properties of Au NPs.[217,218] Subsequent experiments confirmed this hypothesis.

In these experiments, the size of the NP core plays a key role in controlling the particles' magnetic properties. In their recent paper, Einaga *et al.*[217] compared Au NPs of two different sizes—1.7 and 5.0 nm, functionalised with identical SAMs, and found (Fig. 18a) that these two types of NPs exhibited markedly different magnetic characteristics. While the smaller NPs showed typical hysteresis loops with coercivity and remanence (blue traces), the bigger ones displayed purely diamagnetic properties (pink traces). At temperatures examined all the way up to room temperature, *cis–trans* isomerisation of the small NPs in the solid state resulted in ~30% increase in magnetisation (Fig. 18b), although the switching was to some degree suppressed, as evidenced[217,218] by the UV-Vis spectra. The changes in magnetisation were fully reversible (Fig. 18c), with the *cis–trans* reisomerisation taking place either rapidly upon visible light irradiation, or over the period of several hours as a result of thermal relaxation. Fig. 18d has a qualitative description of the changes in Φ_m resulting from light-induced switching in the magnitudes and the directions of surface dipoles. Kelvin probe analysis verified that *trans*-AB-coated NPs had $\Phi_m \approx 4.95$ eV, whereas in *trans*-AB NPs Φ_m was ~5.66 eV (compared with $\Phi_m \approx 5.0$ eV for bulk gold).[217] These elegant experiments confirm that the magnetic properties of NPs functionalised with molecular switches can be modulated reversibly using light, and, therefore, lay foundations for a rational design of materials exhibiting switchable magnetic properties.

7. Molecular switches control storage and release of molecular cargo

Nanoparticles described in this section—mesoporous silica (MS) NPs[231–233]—differ from those discussed above both in terms of their size as well as internal structure. Namely, MS NPs are considerably larger (~100–800 nm) and are not made of a bulk material, but instead contain ordered arrays of nanopores, which can be used to store guest molecules. Whereas MS NPs have been considered by several research groups as biocompatible vesicles for small molecule (in particular, drug) delivery,[234–238] the work of Zink *et al.* as well as our own work is most relevant in the context of this review as it demonstrates that controlled release of the cargo can be accomplished using surface-mounted molecular switches. Following a short paragraph about the synthesis and functionalisation of MS NPs, we describe two controlled release systems: (i) one[239–244] in which the AB groups installed inside the nanopores act as light-driven "nanoimpellers" and expulse the pore contents, and (ii) the other[245–256] in which "nanovalves"—supramolecular or mechanically interlocked entities attached to pore openings—can be engineered to open the "gates" reversibly, thus releasing the cargo molecules, in response to a variety of stimuli.

Fig. 19 shows representative TEM images of MS NPs. In a typical synthesis of these NPs, silica precursor (usually tetraethyl orthosilicate, TEOS) is added slowly to a warm (80 °C) aqueous solution of cetyltrimethylammonium bromide (CTAB) in the presence of a base. CTAB forms cylindrical micelles in water and templates the formation of 2 nm

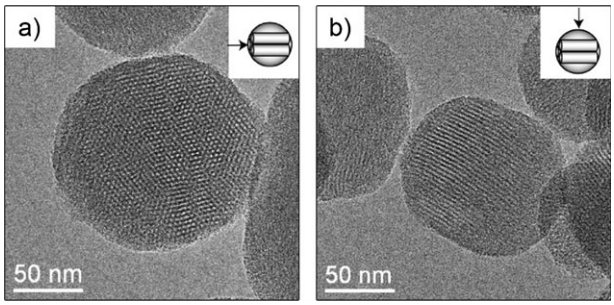

Fig. 19 TEM images of mesoporous silica nanoparticles taken from the direction (a) parallel and (b) perpendicular to the axis of the channels. Adapted with permission from ref. 237 (Copyright 2008 Elsevier Ltd.).

nanopores.[232] The template can then be removed from the NP pores either by calcination or by solvent extraction. Functional groups can be attached to MS NPs using two strategies. In a co-condensation method (CCM), a small amount of functional triethoxysilane is added during the particle synthesis and is allowed to co-condense into the silica framework. As a result, the functional groups are distributed uniformly inside the pores and on the NP outer surface. Alternatively, the post-synthesis modification method (PSMM) is based on the attachment of a triethoxysilane of interest to *pre-formed* silica spheres. If the ligand is bulky, it will only attach to the particle surfaces, *i.e.*, at the pore orifices. These two strategies have been employed (Fig. 20) to functionalise MS NPs with the AB groups, namely, triethoxysilane with pendant AB was attached in and on the NPs (Fig. 20b, left) in the CCM reaction, whereas an AB bearing a bulky G1 Fréchet dendron[239,257] was attached to the pore openings (Fig. 20c, left) *via* PSMM.

The "traditional" uses of molecular switches are based on the fact that two isomers have different properties and the aim is to increase the population of only one isomer to a maximum extent. In the case of photoswitches, this is achieved by irradiation with a wavelength at which only one isomer absorbs significantly. In the case of "nanoimpellers", however, the system is irradiated[241] with a wavelength at which both isomers have the same extinction coefficients, *i.e.*, at the isosbestic point—$\lambda \approx 413$ nm for AB. As a consequence, the pendant AB groups undergo a continual dynamic wagging (Fig. 20a), thus imparting motion upon the molecules trapped inside the nanopores, and eventually forcing their expulsion from the pores. Mesoporous silica is an ideal support for the AB switches since it is optically transparent.

Alternatively, bulky AB groups positioned at the pore entrances prevent release of the cargo, but their light-stimulated motion provides intermittent openings for the trapped molecules to escape. To demonstrate the proof-of-concept, NPs prepared by the PSSM and functionalised with the bulky AB dendron (Fig. 20b) were loaded with luminescent molecules, and the rate of expulsion of these probes was monitored using luminescence spectroscopy. There is no release (Fig. 20b) of the cargo in the dark. Illumination with $\lambda = 413$ nm, however, gives rise to a gradual increase in luminescence of the solution. It is worth pointing out that when the pore openings were functionalised with much smaller, unsubstituted AB groups,

View Article Online

Published on 21 April 2010. Downloaded by Pennsylvania State University on 06/03/2016 20:02:52.

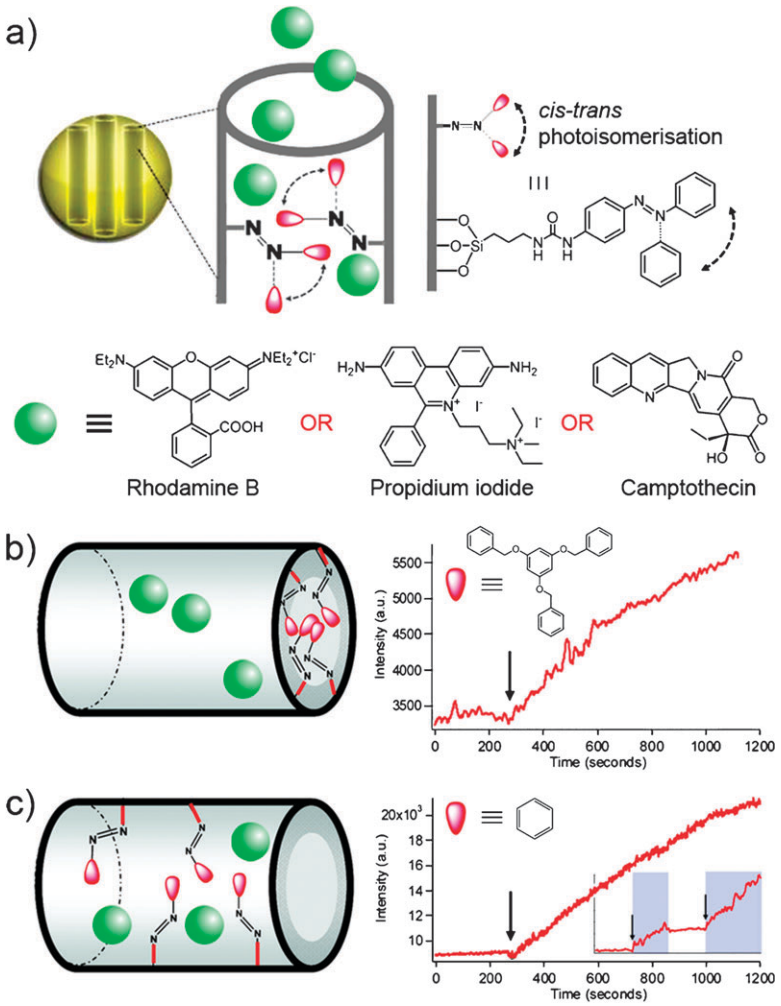

Fig. 20 (a) Schematic illustration of the "nanoimpeller's" action. Irradiation of AB with light of wavelength at which both isomers absorb results in a continuous "wagging" motion of the untethered terminus of the switch. When AB is attached to the interiors of the pores of the MS silica NPs, it stimulates expulsion of the guest molecules (such as dyes or drugs) filling the pores. Adapted with permission from ref. 241 (Copyright 2008 Wiley-VCH Verlag GmbH & Co. KgaA). (b) Release profile for MS silica NPs functionalised with bulky AB groups at the pore orifices. (c) Release profile for MS silica NPs functionalised with unsubstituted AB groups inside pore interiors. Adapted with permission from ref. 240 (Copyright 2007 American Chemical Society).

leakage was observed even in the absence of light irradiation. A much more pronounced response was achieved with NPs prepared (Fig. 20c) by the CCM method. Importantly, the cargo was released[240] only upon continual light irradiation with $\lambda = 413$ nm (irradiation with $\lambda = 647$ nm did not induce any release). Although no increase in luminescence was observed when irradiation was halted, release could be resumed when the light was switched back on (Fig. 20c, inset), thus confirming the dynamic nature of the system. These initial studies were followed by the successful realisation of a photoinduced drug delivery system,[241] in which an anticancer drug camptothecin was released inside and induced apoptosis of cancer cells.

The above discussion indicates that nanoimpellers need to be tethered to the *inner* pore walls of the MS NPs for the most effective results. In contrast, "nanovalves"—that is, operational entities in the second type of MS NPs-based release systems—are positioned at the pore openings. These "nanovalves" are either supramolecular or mechanically interlocked entities, in which a cyclic component can move with respect to a stationary stalk counterpart. This movement generates two states which, ideally, correspond to open and closed states of the pore entrance. A working principle of a reversible nanovalve is shown in Fig. 21. In their seminal paper, Zink *et al.*[252] tethered a bistable [2]rotaxane (Fig. 21a) to the nanopore openings on MS NPs. The rotaxane consists of a stalk containing two electron-rich stations (DNP and TTF) and encircled by an electron-deficient ring ($CBPQT^{4+}$). Because of the higher interaction energy, the ring preferentially resides on the TTF station, which is located (Fig. 21b, top left) further away from the pore entrance. In this co-conformation, the nanovalve is open and the NPs can be charged (Fig. 21b, top right) with cargo molecules. Upon oxidation with $Fe(ClO_4)_3$, however, the TTF station becomes positively charged, and the tetracationic $CBPQT^{4+}$ ring migrates to the DNP station. As a result, the valve "closes" (Fig. 21b, bottom right). The TTF^{2+} dication can then be reduced with ascorbic acid at which point it is encircled by the $CBPQT^{4+}$ ring, and the trapped molecules are released at will (Fig. 21b,

 This journal is © The Royal Society of Chemistry 2010

View Article Online

Published on 21 April 2010. Downloaded by Pennsylvania State University on 06/03/2016 20:02:52.

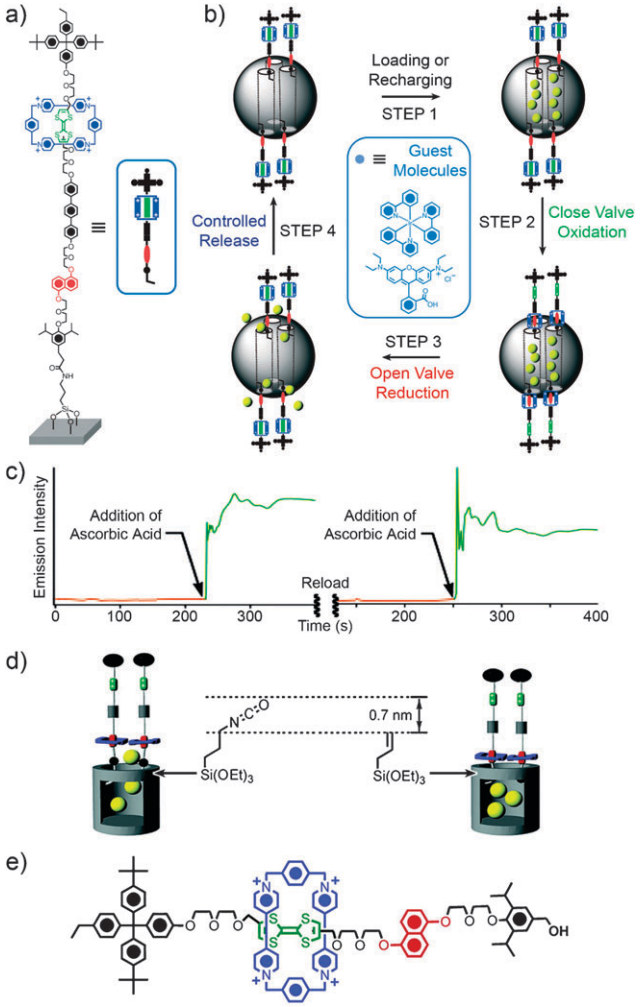

Fig. 21 Redox-controlled, bistable [2]rotaxane-based nanovalve. (a) Structural formula of a bistable [2]rotaxane employed in the initial design.[252] (b) Schematic illustration of the proposed mechanism for the operation of the nanovalve. (c) Release of guest molecules (in this case, rhodamine B) from the NPs upon "actuation" of the nanovalve with ascorbic acid. Note that the container can be refilled with the guest molecules and reused. Adapted with permission from ref. 252 (Copyright 2005 National Academy of Sciences USA). (d and e) Studies aimed at optimisation of the valve's performance have included, among others, modification of the linker connecting the nanovalve to the pores (d), and of the chemical structure of the nanovalve itself (e). Adapted with permission from ref. 251 (Copyright 2007 American Chemical Society).

bottom left). An example of a release profile is shown in Fig. 21c. The guest molecules (here, rhodamine B) are released instantaneously once ascorbic acid is added, as evidenced by a precipitous increase of luminescence of the solution. A similar release profile (Fig. 21c) is obtained once the nanocontainer is recharged and its contents expelled again—*i.e.*, the system is reusable.

Comprehensive mechanistic studies were undertaken[251] with the goal of optimising the performance of the [2]rotaxane-based nanovalves. The relative position of the two components—the movable elements and the supporting SiO_2 NP framework—is critical for an efficient operation of the nanovalves. Specifically, the distance between the $CBPQT^{4+}$ ring and the pore entrances determines whether the valve will "leak" or not. Varying this distance was achieved independently (or synergistically) by (i) attaching the gatekeepers selectively inside or outside the pores and (ii) by employing silane linkers of different lengths. With respect to the first issue, the movable components could be used to functionalise SiO_2 NPs either before or after template (CTAB) removal. In the first case, CTAB blocks access to the pores and the rotaxanes are attached exclusively to the outer surface of the particles. In contrast, post-extraction attachment resulted in the attachment to the interiors of the nanopores. In the latter case, only the part of the stalk encircled by the bulky ring—and further away from the attachment point—remain outside the pores. As expected, the switches attached to a location inside the pore gave virtually no leakage when the valve was closed—as opposed to the nanovalve attached to the outer surface—but the release was considerably slower when the valve was open. Likewise, modifying the length of the linker drastically influences valve performance. Two of the silane linkers are shown in Fig. 21d. Whereas valves incorporating the isocyanatopropyl linker were leaky, those based on the allyl linker (both linkers were attached inside the pores) showed an excellent performance. Also, the effect of the linker between the two recognition units in the bistable [2]rotaxane was investigated. Here, a release system based on a shorter molecule lacking the terphenyl linker (Fig. 21e) was prepared. As expected, altering this distance did not have a significant effect on the performance of the system.

Apart from the bistable [2]rotaxane-based nanovalve, whereby the cyclic component moves while being permanently associated with a stationary stalk, an elegant assortment of controlled release systems (Fig. 22) based on *pseudo*rotaxanes has also been developed. In this case, the ring can reversibly dissociate and associate with the stalk, thus opening and closing the valve. The original design[255] took advantage of the donor–acceptor interactions between 1,5-bis[2-(2-(2-hydroxyethoxy)-ethoxy)ethoxy]naphthalene (BHEEEN)-containing stalks attached to the silica surface, onto which $CBPQT^{4+}$ rings were threaded, thus preventing (Fig. 22, row 1) the nanopore contents from escaping. The valves could be open—and the cargo released—upon the addition of an external reducing agent ($NaBH_3CN$), which reduces the $CBPQT^{4+}$ rings, thus inducing their dissociation from the stalks. This system was later reconfigured (Fig. 22, row 2) for light activation.[256] To achieve this goal, photosensitisers—such as 9-anthracenecarboxylic acid and $Ru(bpy)_3$—were attached covalently to the pore orifices along with the gatekeeping pseudorotaxanes. In this case, light irradiation induced electron transfer from the excited photosensitiser to the $CBPQT^{4+}$ rings, reducing them and hence inducing their slippage off into solution. Unfortunately, release profiles (Fig. 22, row 2) for these photoactivated nanovalves were inferior to those which were reduced chemically.

Several pH-controlled nanovalves have also been reported. For example,[250] SiO_2 NPs functionalised with dibenzylammonium-containing stalks were encircled, and the entrances to the nanopores blocked, by dibenzo-24-crown-8. The ring interacted with the thread by virtue of strong hydrogen bonding interactions, and the complex could be dissociated by the

View Article Online

Published on 21 April 2010. Downloaded by Pennsylvania State University on 06/03/2016 20:02:52.

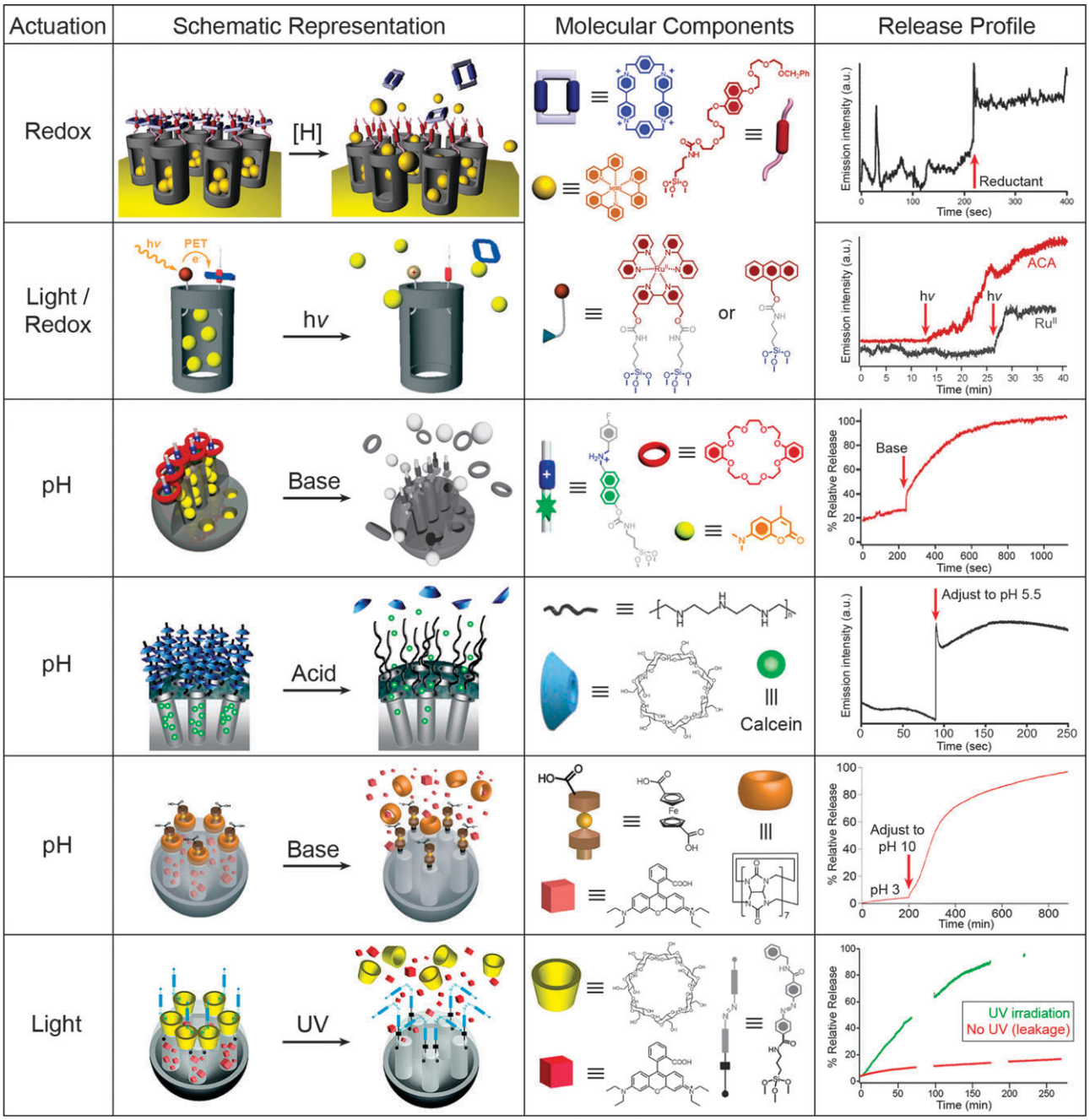

Fig. 22 Nanovalves based on pseudorotaxanes (please refer to the text for detailed discussion). Adapted with permission from ref. 247 (Copyright 2009 American Chemical Society), ref. 248 (Copyright 2009 Wiley-VCH Verlag GmbH & Co. KgaA), ref. 250 (Copyright 2006 American Chemical Society), ref. 253 (Copyright 2007 Wiley-VCH Verlag GmbH & Co. KgaA), ref. 255 (Copyright 2004 American Chemical Society), ref. 256 (Copyright 2007 Wiley-VCH Verlag GmbH & Co. KgaA).

addition of a base (Fig. 22, row 3). The rate of cargo release depended on and could be regulated by the size of the base molecule. Importantly, some of these supramolecular switches operate in water, which is an important prerequisite for interfacing nanovalves with biological systems. For example, Kim *et al.*[253] reported nanovalves which can be opened under acidic conditions. In their design, silica surface was modified with polyethyleneimine (PEI) stalks onto which cyclodextrins were threaded. In this case, the supramolecular binding (Fig. 22, row 4) was disrupted by the protonation of PEI's secondary amine groups. Different CDs were studied, and while β-CD did not bind to PEI, both α- and γ-CD could be used as effective "gates" by encircling an individual PEI chain, and two neighbouring PEI chains, respectively.[253] Also, a tight binding in aqueous solutions of cucurbit[6]uril (CB[6]) to bisammonium triazole[246] and ferrocene carboxylate[248] has been employed in the construction of base-activated release systems (Fig. 22, row 5). Interestingly, the nanovalve based on ferrocene could be activated[248] by electrochemical oxidation when it was closed with β-CD.

Remote activation of cargo release has been achieved[247] by constructing nanovalves based on photoactive AB stalks.

 This journal is © The Royal Society of Chemistry 2010

View Article Online

Published on 21 April 2010. Downloaded by Pennsylvania State University on 06/03/2016 20:02:52.

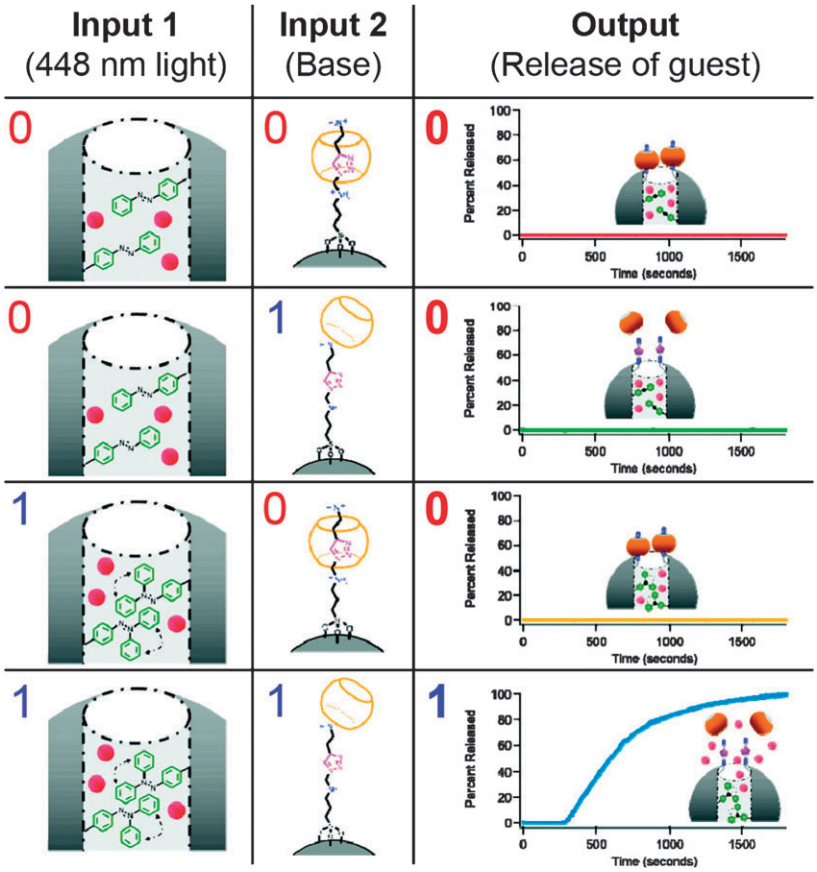

Fig. 23 $ClRe(CO)_3$–2,2′-bipyridine release profiles from MS SiO_2 NPs functionalised with (i) AB nanoimpellers inside the pore interiors, and (ii) pH-switchable pseudorotaxanes at the pore orifices. Input 1 = excitation with light of wavelength, λ = 448 nm; input 2 = addition of NaOH. Adapted with permission from ref. 245 (Copyright 2009 American Chemical Society).

This design took advantage of the high affinity of β-CD for *trans*-AB, which is significantly reduced when confronted with the *cis* isomer. As a result (Fig. 22, row 6), the β-CD rings dissociate, and the probe molecules are relatively quickly released, by irradiation with UV light.[247]

Finally, mesoporous silica NPs can be engineered to respond to various stimuli at the same time. In a state-of-the-art system reported[245] recently, the particles were functionalised with both impellers (inside the pores) and nanovalves (on the outer surface of the NPs) to give a dual-controlled release system which functioned as an AND logic gate. The valve component comprised a CB[6] ⊂ bisalkylammonium pseudorotaxane, which could be dissociated, and the valve opened, in response to high pH values. This input alone, however, did not result (Fig. 23, second row) in the release of the guest molecules. Likewise, the light-activated, dynamic motion of the AB impellers did not expel (Fig. 23, third row) the cargo when the valves were closed. Only when the two switches operate in tandem (Fig. 23, fourth row) can the guest molecules be released.

8. Molecular switches direct binding of small molecules to NP surfaces

In the previous section, we saw how mesoporous silica nanoparticles could be used to store guest molecules inside their pores, and release the "cargo" on demand. These NPs have been called "mechanised nanoparticles", as their key components—AB nanoimpellers and rotaxane/pseudorotaxane nanovalves—are nanoscale analogues of everyday devices. A simpler approach to capture and release small molecules by NPs can be accomplished using surface-immobilised molecular switches whose two forms differ in their interaction strengths with the small molecules. Spiropyran–merocyanine (SP–MC) switch is an ideal candidate for this type of application since the light-induced isomerisation is accompanied by a drastic change in the molecule's polarity.[258,259] It is also important that the solvent stabilises *both* forms of the switch—otherwise, the NPs would tend to aggregate before or after isomerisation (see Section 9). With these prerequisites in mind, SP-functionalised NPs in methanol were prepared and their interactions with amino acids were investigated.[260] In their ground state, SPs did not show any affinity to amino acids.[261] Upon photoisomerisation to the zwitterionic MC form, however, amino acids (which are zwitterions themselves) recognised and interacted strongly[262,263] with the "receptors" on the NP surfaces in a way similar to the binding of drugs to the receptor sites on the surface of a cell.[264] This was confirmed by both absorption and fluorescence spectroscopies, which showed that the MC isomer is greatly stabilised in the presence of amino acids, and the thermal ring closure does not occur unless the system is irradiated with visible light (at which point the bound amino acid molecules are liberated).[260] Although it has been suggested

View Article Online

Published on 21 April 2010. Downloaded by Pennsylvania State University on 06/03/2016 20:02:52.

that the SP-coated NPs could be used as vehicles for the delivery of amino acids, the system first needs to be reconfigured to work in an aqueous environment.

Likewise, Fitzmaurice *et al.* described Au NPs functionalised with thiols terminated with crown ethers (specifically, dibenzo-24-crown-8; see **2** in Fig. 24).[265] These moieties acted as hydrogen bond acceptors and selectively bound H-bond donors, such as dibenzoammonium cations (**4** in Fig. 24) *via* the formation of pseudorotaxane linkages in chloroform. The formation of pseudorotaxanes could be followed by NMR, whereby significant chemical shifts of the R–$^{+}$NH_2–R (and other) protons were observed, thus indicating threading of the linear guests through and their binding to the macrocyclic hosts. Quantitative analysis of the NMR spectra indicated that as much as 86% of the macrocyclic hosts densely packed on NPs could bind the ammonium guests. The binding event was accompanied by a slow precipitation of NPs from chloroform, but the pseudorotaxane-decorated NPs could be redispersed upon the addition of a small amount of acetonitrile.

We have recently reported an "inverse" system, in which the macrocyclic "receptors", in our case, electron-deficient CBPQT^{4+} rings, are present as free entities in solution, whereas electron-rich TTF ligands are tethered to NP (Au, Pd and Pt) surfaces. The binding of the rings to the NPs resulted from a combination[266] of donor–acceptor interactions and H-bonding and, again, led to the formation of pseudorotaxane linkages on the NP surfaces. We followed the formation of these complexes by means of ζ (zeta) potential measurements in DMF (Fig. 25).[69] In this context, we first note that the ζ potential on the NPs in the absence of the CBPQT^{4+} rings could reversibly be changed between the values of -0.5 ± 2.1 (close to 0) and $+21.9 \pm 1.9$ mV (strongly positive), depending on the TTF oxidation state. In their neutral states, TTF-NPs (**1** in Fig. 25a) interacted strongly with CBPQT^{4+}, as evidenced by further increase in the ζ potential (to $+29.2 \pm 0.7$ mV; **3** in Fig. 25a). Oxidation with $Fe(ClO_4)_3$, however, induced slippage of the CBPQT^{4+} rings on account of the Coulombic repulsion with the now positively charged TTF^{2+} ligands (**2** in Fig. 25a). At the same time, ζ potential of the NPs returned to its lower, $\sim$21.9 mV value. Of course, the system was reversible and the rings threaded back onto the stalks following reduction with ascorbic acid (Fig. 25a and b).

9. Molecular switches bring nanoparticles together

9.1 NP aggregation induced by pseudorotaxane formation

In all of the examples described in the previous section, nanoparticles, each decorated with multiple "guests", interacted reversibly with monomeric "hosts" (or *vice versa*). In a simple extension of this methodology, molecules bearing two or more host units can be used as "crosslinkers" mediating

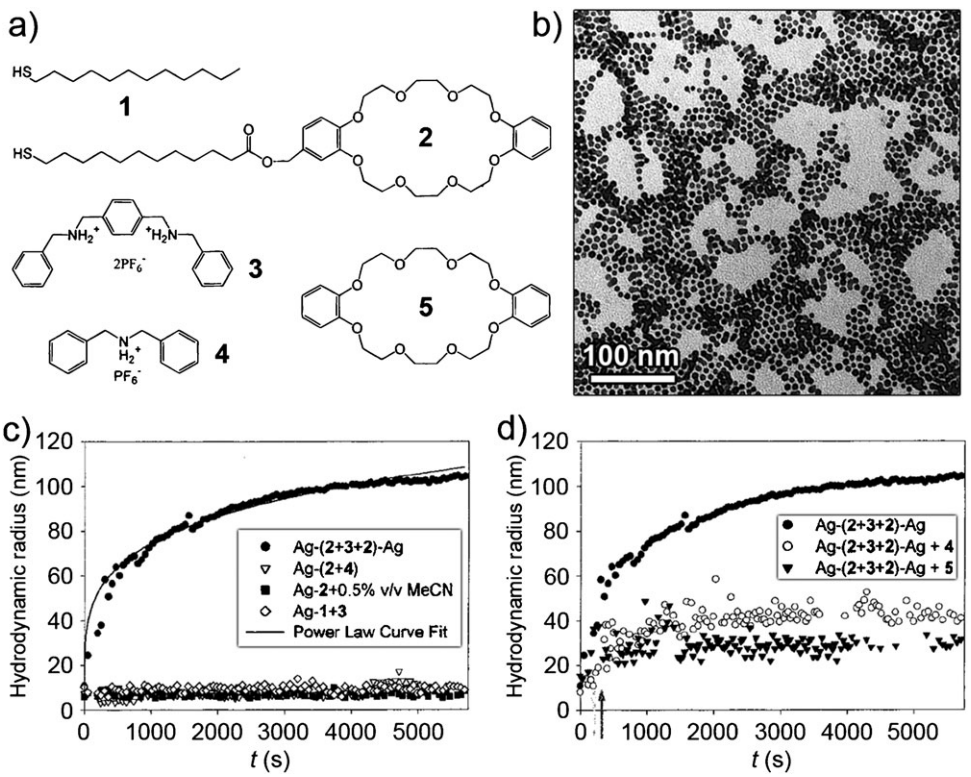

Fig. 24 (a) Structural formulae of the compounds used in the assembly of NPs mediated by the formation of pseudorotaxanes. (b) TEM image of Ag NPs functionalised with a *m*SAM of **1** and **2**. (c) Assembly of NPs followed by dynamic light scattering. The curves indicate that the presence of both **2** and **3** is essential to induce the assembly process. NPs lacking the receptor **2** on their surface do not assemble upon the addition of **3**. Likewise, **2**-coated NPs remain unaggregated upon the addition of compound **4** having only one recognition site and lacking the crosslinking ability. (d) Formation of these aggregates can be controlled by the addition (indicated by the arrow) of inhibitors **4** and **5**, as reflected by the flattening of the curves. Adapted with permission from ref. 272 (Copyright 2000 American Chemical Society).

 This journal is © The Royal Society of Chemistry 2010

View Article Online

Published on 21 April 2010. Downloaded by Pennsylvania State University on 06/03/2016 20:02:52.

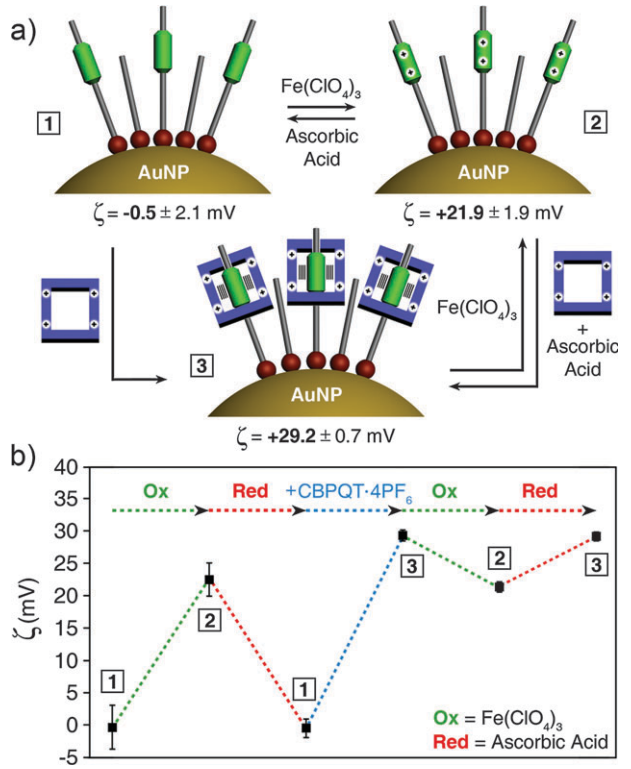

Fig. 25 (a) Scheme of redox-controlled binding of electron-deficient hosts ($CBPQT^{4+}$) to the surface of a NP modified with redox-switchable, electron-rich guests (in this case, TTF). (b) Reversible changes in ζ potential as a result of TTF oxidation/reduction and pseudorotaxane formation. Adapted with permission from ref. 69 (Copyright 2009 American Chemical Society).

reversible assembly of NPs into larger architectures. Recognition-mediated assembly of NPs has been pioneered by Rotello *et al.*[267,268] and attracted considerable interest as a route to new types of materials, but most of the systems described in the literature lack the reversibility potential.[269–271] One way to overcome this limitation is to use pH-switchable pseudorotaxane linkages and is a continuation of the work by Fitzmaurice *et al.* described above.[272] When the bis-dibenzylammonium cations (Fig. 24a, **3**) were added to a solution of silver NPs coated with a *m*SAM comprising dodecanethiol (Fig. 24a, **1**) and a crown ether-terminated thiol (Fig. 24a, **2**), NP aggregation commenced. Dynamic light scattering (DLS) was used to monitor the aggregation process and indicated that the average diameter (hydrodynamic radius) of the aggregates was ~100 nm after 100 min. This type of behaviour, in which rather small aggregates form in solution, and no precipitation is observed, is likely a result of the non-stoichiometric ratio of H-bond donors and acceptors used. Consequently, the majority component "envelops" and inhibits further growth of the aggregate. Nevertheless, it was demonstrated that aggregate sizes could be controlled by the addition of either free dibenzo-24-crown-8 (Fig. 24a, **5**) or dibenzylammonium cations (Fig. 24a, **4**). DLS showed that the average sizes of the resulting aggregates were ~25 nm and ~40 nm, respectively; unfortunately, no corresponding electron micrographs were provided. Control experiments have been performed and demonstrated that the addition of **3** to NPs covered only with **1**, or addition of a monodentate dibenzylammonium cation **4** to **1**/**2**-Ag NPs did not result in diameter change (see Fig. 24c).

More recently, we became interested in assembling NPs by means of switchable donor–acceptors interactions using TTF-decorated Au NPs and molecules incorporating multiple $CBPQT^{4+}$ rings (such as dimer $\mathbf{4}^{8+}$, trimer $\mathbf{5}^{12+}$, tetramer $\mathbf{6}^{16+}$ and polymer $\mathbf{7}^{4n+}$, where $n \approx 160$;[273] Fig. 26).[70] We hypothesised that the use of NPs bearing only one TTF functional ligand (for preparation of such NPs, see ref. 274) would lead to assemblies comprising well-defined numbers of particles. Indeed, such discrete duos and trios (Fig. 26c) were visualised by TEM, indicating that individual molecules were capable of bringing the NPs together. NPs could also be

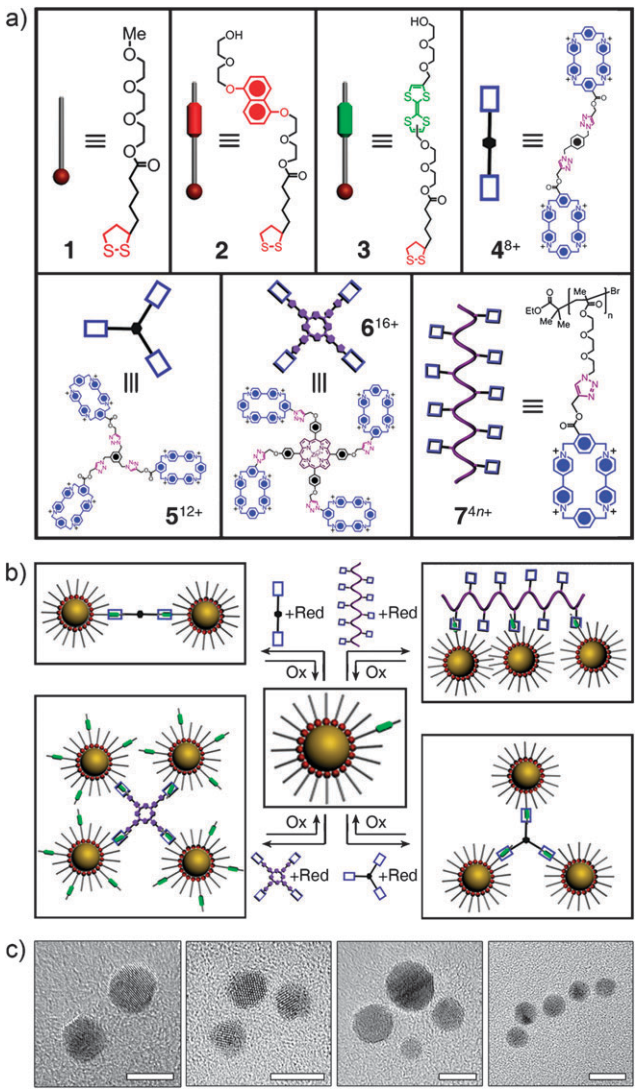

Fig. 26 (a) Structural formulae of a background ligand **1**, electron-rich ligands **2** and **3**, as well as electron-deficient templates $\mathbf{4}^{8+}$, $\mathbf{5}^{12+}$, $\mathbf{6}^{16+}$ and $\mathbf{7}^{4n+}$ used for redox-controlled assembly of NPs. (b) Schematic illustration of the pseudorotaxane formation-mediated self-assembly of NPs. (c) TEM images of Au NPs self-assembled into dimers, trimers, tetramers, as well as linear pentamers. Scalebars correspond to 5 nm for the NP dimer, trimer and tetramer, and 10 nm for the linear NP pentamer. Adapted with permission from ref. 70 (Copyright 2009 American Chemical Society).

View Article Online

Published on 21 April 2010. Downloaded by Pennsylvania State University on 06/03/2016 20:02:52.

assembled into quartets using a different strategy, in which NPs, each functionalised with ~11 TTF ligands, were mixed with an under-stoichiometric amount of $\mathbf{6}^{16+}$ tetramers (Fig. 26c). Most strikingly, perhaps, linear chains composed of several NPs were seen when the polymer $\mathbf{7}^{4n+}$ was used to mediate aggregation. TEM revealed that as much as 90% of the aggregates had either four or five NPs (Fig. 26c) and the total length of ~32 and ~40 nm, respectively—these lengths are in good agreement with a calculated length of a single $\mathbf{7}^{4n+}$ chain in its extended conformation (~38 nm).[68]

When the polymer $\mathbf{7}^{4n+}$ and the TTF-presenting nanoparticles were mixed in a stoichiometric ratio, orderless aggregates formed that precipitated from solution (Fig. 27a). These aggregates could be reverted into individual components under oxidising conditions (by the addition of an oxidising agent, such as $Fe(ClO_4)_3$, or electrochemically at +900 mV), and reformed again under reducing conditions (ascorbic acid or 0 V). This ability to reversibly address the oxidation state of the ligands and to form supramolecular complexes with the electron-deficient polymer led to the design of a system, in which the polymer acted as a selective "sponge" capturing and releasing different types of NPs selectively (Fig. 27b and c). In one example, silver NPs were coated with TTF, whereas gold NPs were functionalised with DNP ligands, which are also electron-rich and interact with $\mathbf{7}^{4n+}$, but lack the ability to undergo a reversible oxidation and reduction. In its unoxidised state, TTF binds to $\mathbf{7}^{4n+}$ stronger than DNP ($\Delta G^0_{298K,\ MeCN} = -6.49$ kcal mol^{-1} *vs.* $\Delta G^0_{298K,\ MeCN} = -5.33$ kcal mol^{-1}).[68] Therefore, when a mixture of DNP–Au NPs and TTF–Ag NPs was added to a solution of $\mathbf{7}^{4n+}$, the polymer interacted preferentially and formed an insoluble complex with the silver NPs (Fig. 27b, left). When, however, the TTF ligands were oxidised, Ag NPs lost its affinity to $\mathbf{7}^{4n+}$ and the binding preference was reversed (Fig. 27b, right)—that is, the DNP–Au NPs interacted and precipitated with the polymer. In other words, oxidation of TTF resulted in the release of Ag NPs to the solution and capture of Au NPs. Again, the process was reversible and the reduction of TTF^{2+}–Ag NPs was followed by a slow replacement of Au with Ag NPs in the precipitate. Indeed, electron-deficient polymer $\mathbf{7}^{4n+}$ acted as a selective "sponge" for controlled capture and release of NPs of different core compositions.

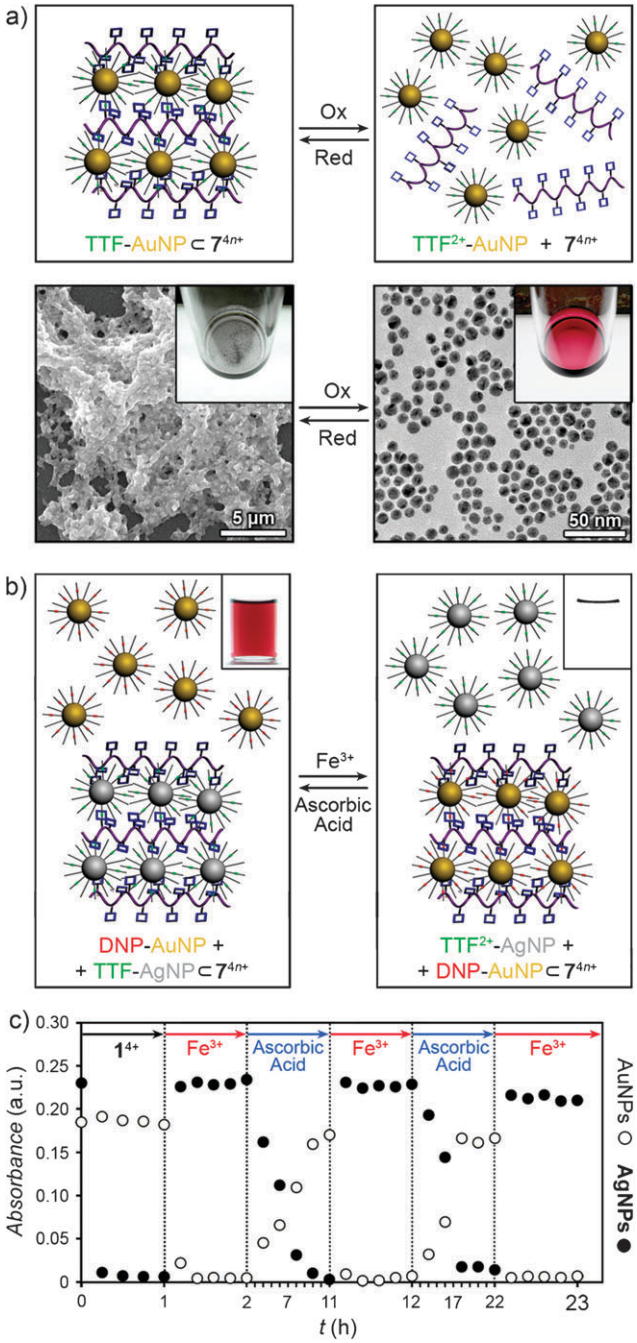

Fig. 27 (a) Top: schematic representation of the reversible binding of TTF-functionalised Au NPs to the polymer $\mathbf{7}^{4n+}$. Bottom left: SEM image of the TTF–Au NP ⊂ $\mathbf{7}^{4n+}$ complex. Bottom right: TEM image of TTF^{2+}-functionalised Au NPs. Insets show optical micrographs of the samples. (b) Illustration of the redox-controlled sorting of NPs. Left: $\mathbf{7}^{4n+}$ binds preferentially to and precipitates TTF–Ag NPs. Addition of $Fe(ClO_4)_3$ results in the oxidation of TTF–Ag NPs to TTF^{2+}–Ag NPs and an immediate release of Ag NPs, concomitant with the complexation of DNP–Au NPs. The reverse process can be induced by the addition of ascorbic acid. (c) Chemically driven release and capture of Au and Ag NPs followed by UV-Vis spectroscopy. Adapted with permission from ref. 68 (Copyright 2009 Nature Publishing Group).

9.2 NP aggregation induced by light-controlled molecular switches

We have so far considered assembly of NPs mediated by small molecules, which interacted with functionalised NP surface to form pseudorotaxanes. It is also possible to induce attractive interactions between NPs *directly*, *i.e.*, in the absence of any additional crosslinkers. This goal has been achieved for several systems comprising NPs functionalised with light-controlled molecular switches.[42,49,66,106,108,275–279] Light is an attractive form of "signal" with which to address nanoscopic objects remotely because it can be delivered instantaneously and into precise locations. In addition, using light of different wavelengths could lead to the development of non-equilibrium nanostructures, which "build themselves" and fall apart depending on light stimulus.[49,277] For a successful photocontrol of NP assembly, the two isomers of the molecular switch should differ substantially in their chemical and physical

 This journal is © The Royal Society of Chemistry 2010

View Article Online

Published on 21 April 2010. Downloaded by Pennsylvania State University on 06/03/2016 20:02:52.

properties. In principle, the solvent in which the NPs are dispersed should stabilise only one form of the switch, and be a "bad solvent" for the other. These conditions are met by some popular switches including azobenzenes and spiropyrans.

Interest in controlling aggregation and redispersion of colloidal NPs using monolayers of molecular switches dates back at least to 1994, when Ueda *et al.* first described 150 nm SiO_2 NPs decorated with SP switches (see also Section 2.3 for the discussion of this system in the context of negative photochromism).[106,108,275] Functionalisation of the NPs was achieved by DCC coupling between a SP carboxylate and aminopropylated silica NPs. An optical micrograph of a NP suspension in CCl_4 is shown in Fig. 28a (left). The solution is transparent due to refractive index matching between the solvent and the particles. UV irradiation induced a rapid SP–MC isomerisation, which was accompanied by a pronounced colour change, indicating formation of the open-ring isomer. At the same time, flocculation commenced (Fig. 28a, right). Samples collected before and after isomerisation were analysed by SEM and showed individual particles and NP clusters, respectively (Fig. 28a). It is important to point out that the aggregation of NPs took place on account of dipole–dipole interactions between the zwitterionic moieties on different NPs. Alternative mechanism based on the formation of SP–MC complexes[280,281] was ruled out based on the absence of the absorption bands characteristic for these complexes in the UV-Vis spectra.[106] CCl_4 was found to be an ideal solvent for an effective light-induced aggregation behaviour (Fig. 28a and b); in contrast, cyclohexane induced rapid flocculation of NPs coated with both forms of the switch,

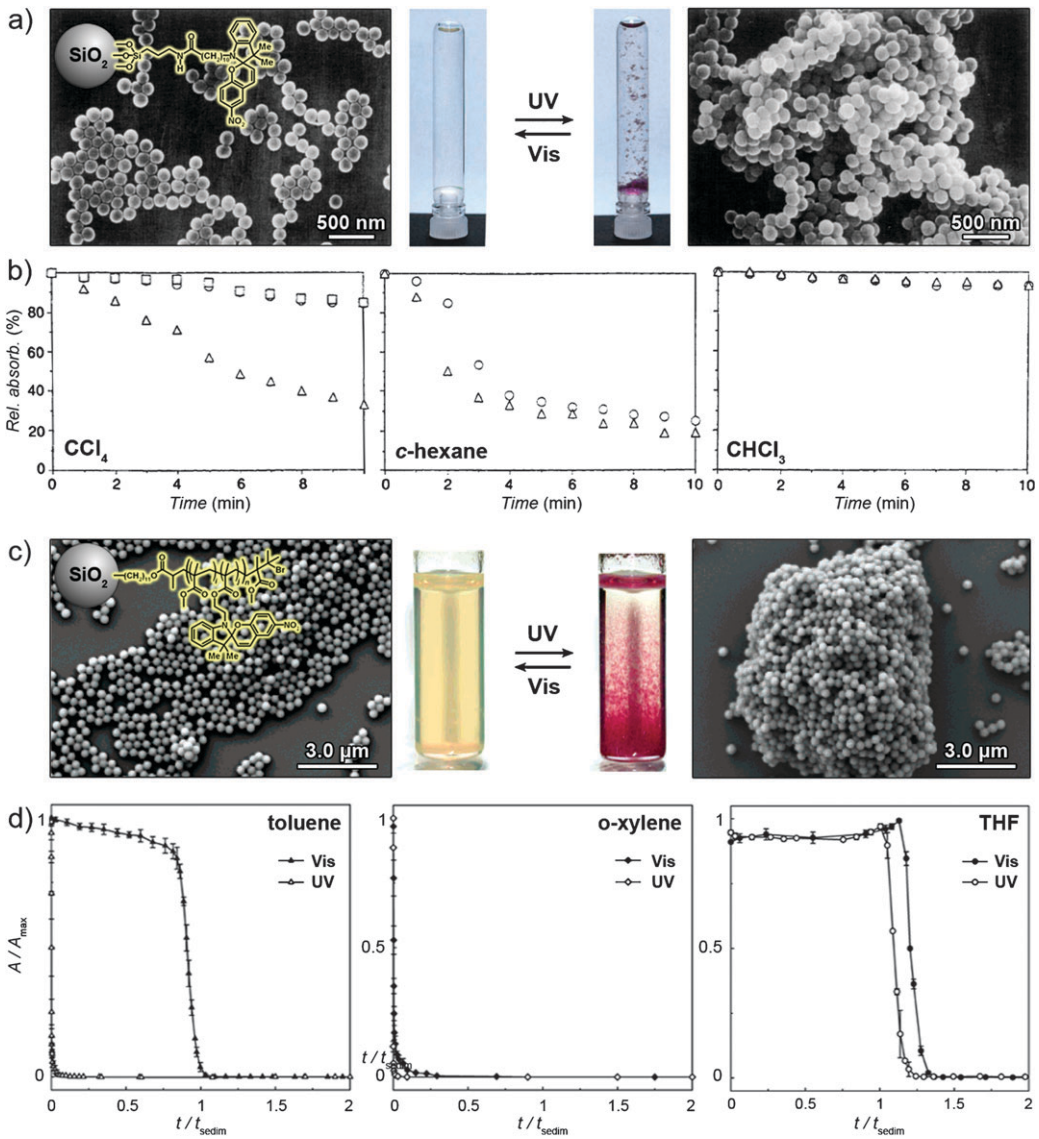

Fig. 28 SEM images, visual changes, and sedimentation behaviour accompanying photoinduced aggregation of SP-coated silica NPs. Note that in both cases, the behaviour is strongly solvent-dependent. (a and b) 150 nm SiO_2 NPs functionalised with SP-terminated silane monolayer. Adapted with permission from ref. 106 (Copyright 1994 Royal Society of Chemistry). (c and d) 927 nm SiO_2 NPs functionalised with methyl methacrylate polymer brushes containing pendant SP groups. Adapted with permission from ref. 279 (Copyright 2006 American Chemical Society).

View Article Online

Published on 21 April 2010. Downloaded by Pennsylvania State University on 06/03/2016 20:02:52.

whereas $CHCl_3$ suspensions were stable irrespective of the optical treatment (Fig. 28b).

A rigorous study of a related system has been presented by Bell and Piech.[279] In this case, silica NPs were derivatised (Fig. 28c) with grafted methyl methacrylate polymer brushes containing a varying number of pendant SP groups. Chromophores were immobilised to NP surfaces *via* atom transfer radical polymerisation[282] (using SiO_2 NPs functionalised with an active alkyl bromide[283]) to initiate the growth of the copolymer containing predetermined (1–80%) amounts of SP. The choice of the solvent (Fig. 28d) and the SP content in the copolymer were the two critical factors that affected light-modulated performance of the system. THF was a good solvent for NPs stabilised with both forms of the switch such that irradiation did not cause aggregation; in contrast, *o*-xylene caused both forms to precipitate readily (even in the absence of irradiation). Ultimately, only toluene provided sufficiently different stabilisation energies of the NPs before and after irradiation to allow for successful control of NP assembly using light (Fig. 28d). The second parameter which was investigated was the molar fraction of SP in the copolymer. When the content of SP was $<10\%$, the solvent (in this case, toluene) stabilised NPs covered with both forms of the switch. For $>40\%$ of SP, however, the particles precipitated under both UV and visible light irradiation. Reversible photoaggregation properties were optimal for NPs having $\sim 20\%$ of SP in their protective polymer shells. More recently, the same group developed elegant applications of their photoresponsive particles, in which local irradiation of the NPs was used to generate two-[284] and three-dimensional[285] structures.

Aggregation guided by light can also be achieved for NPs derivatised with AB ligands on account of the large differences in the dipole moments between their *cis* and *trans* isomers (~ 5 D and ~ 1 D, respectively, for 4-alkoxyazobenzenes[54]). Ueda *et al.* functionalised their 150 nm SiO_2 NPs with a calixarene bearing four AB moieties.[42] The calixarene ligands were not chemically attached to the silica surface, but the high stability of the monolayer was attributed to an extensive network of hydrogen bonds between the silica surface and the calixarene ligands (up to eight bonds per ligand). As expected, UV irradiation resulted in *trans–cis* isomerisation of AB and a rapid sedimentation of the particles in a hydrophobic solvent (cyclohexane). Visible light illumination "switched off" the dipoles and the particles returned to the solution. Analogous results were reported in 5 nm Au NPs discussed above (Section 2.1).[66] In this case, the AB-coated NPs formed a stable solution in toluene. Following UV irradiation, however, the hydrophobic solvent could not stabilise the more polar, *cis*-AB-coated NPs, and NP aggregation and precipitation commenced. These results indicate that the NPs are well-solvated by non-polar solvent molecules when protected with *trans*-, but not by *cis*-AB monolayer, and suggest that the use of a more polar solvent could result in an inverse effect whereby the *cis* isomer is solvated and the NP soluble. Interestingly, such a system has indeed been reported in a study which surveyed a variety of solvents.[278] In particular, a 1 : 3 chloroform–ethanol mixture was found to provide optimal conditions for an "inverse" light-induced aggregation of AB-coated NPs, whereby *trans*-AB NPs formed an insoluble precipitate but redispersed when the AB switches were isomerised to the *cis* form.

In all of the above studies, the precipitates that formed were internally disordered. In many applications, however, crystalline NP ordering is of value[286]—examples include greatly enhanced[287] electrical conductivities in superlattices composed of both PbTe and Ag_2Te NPs, magnetic percolation in superlattices of Co NPs,[288] and vibrational coherence in Ag NP supracrystals.[289] In order to guide the assembly of NPs into well-defined, three-dimensional supracrystals, we have designed a light-induced self-assembly (LISA) system,[49] in which the Au NPs were stabilised with a *m*SAM comprising 4,4′-bis(11-mercaptoundecanoxy)azobenzene (ADT; Fig. 29a) and dodecylamine (DDA). The NPs formed a stable solution in toluene when stabilised with an excess of didodecyldimethylammonium bromide (DDAB) surfactant. Upon UV irradiation, however, a rapid AB *trans–cis* isomerisation occurred and gave rise to a significant increase in the dipole moments of the AB[290] groups (0 to 4.4 D). Consequently, the NPs attracted one another (Fig. 29b, centre) and, once in close proximity, underwent covalent crosslinking by the free ends of the ADT dithiols (Fig. 29b, right). The nature of the resulting assemblies depended critically on the amount of ADT crosslinkers per NP, and on the solvent used for LISA (Fig. 29c). When the number of ADT groups was below ~ 20 or above ~ 300 ADTs per NP, the NPs did not assemble even upon UV irradiation. In the first case, the dipole–dipole interactions were not strong enough to overcome the thermal motion of NPs. In the second case, ABs did not have enough free volume to undergo isomerisation, in agreement with earlier observations.[66] Between these two extreme values, ADTs photoisomerised and the NPs assembled. When the process was conducted in toluene, the NPs presenting the polar *cis*-azobenzenes assembled into spherical aggregates (supraspheres,[276,291–293] SS in Fig. 29c) minimising the interfacial area contact with the hydrophobic solvent. A more polar medium (toluene–methanol mixtures) stabilised the *cis*-AB NPs, and the particles had more time to equilibrate, and self-assembled into covalently crosslinked, three-dimensional crystals that were stable after UV irradiation ceased (hence, "irreversible" crystals, IC, in Fig. 29c). Interestingly, the growth of these crystals could be halted and then resumed when the light was turned, respectively, on and off; in this way, it was possible to control the sizes of the NP crystals (Fig. 29d).[49] Equally ordered but *dynamic* structures were obtained when the solvent was moderately polar and the ADT coverage on the NPs was just above the aggregation threshold (*ca.* 20 ADT ligands per NP). Under these conditions metastable/"reversible" crystals (RC in Fig. 29c) were formed that could be assembled upon UV exposure and disassembled in the dark (slowly) or upon irradiation with visible light (rapidly). The key feature of these structures was that the energies of particle–particle attractions due to AB dipoles were commensurate with the thermal energies, $3/2\,kT$. When the *cis* isomers reverted to *trans* and the dipoles disappeared, the thermal noise was enough to disrupt the crystals.

The idea of preparing metastable materials that remain assembled only as long as energy (here, light) is delivered to them inspired development of another system in which photoactive NPs store graphical/textual information for prescribed

 This journal is © The Royal Society of Chemistry 2010

View Article Online

Published on 21 April 2010. Downloaded by Pennsylvania State University on 06/03/2016 20:02:52.

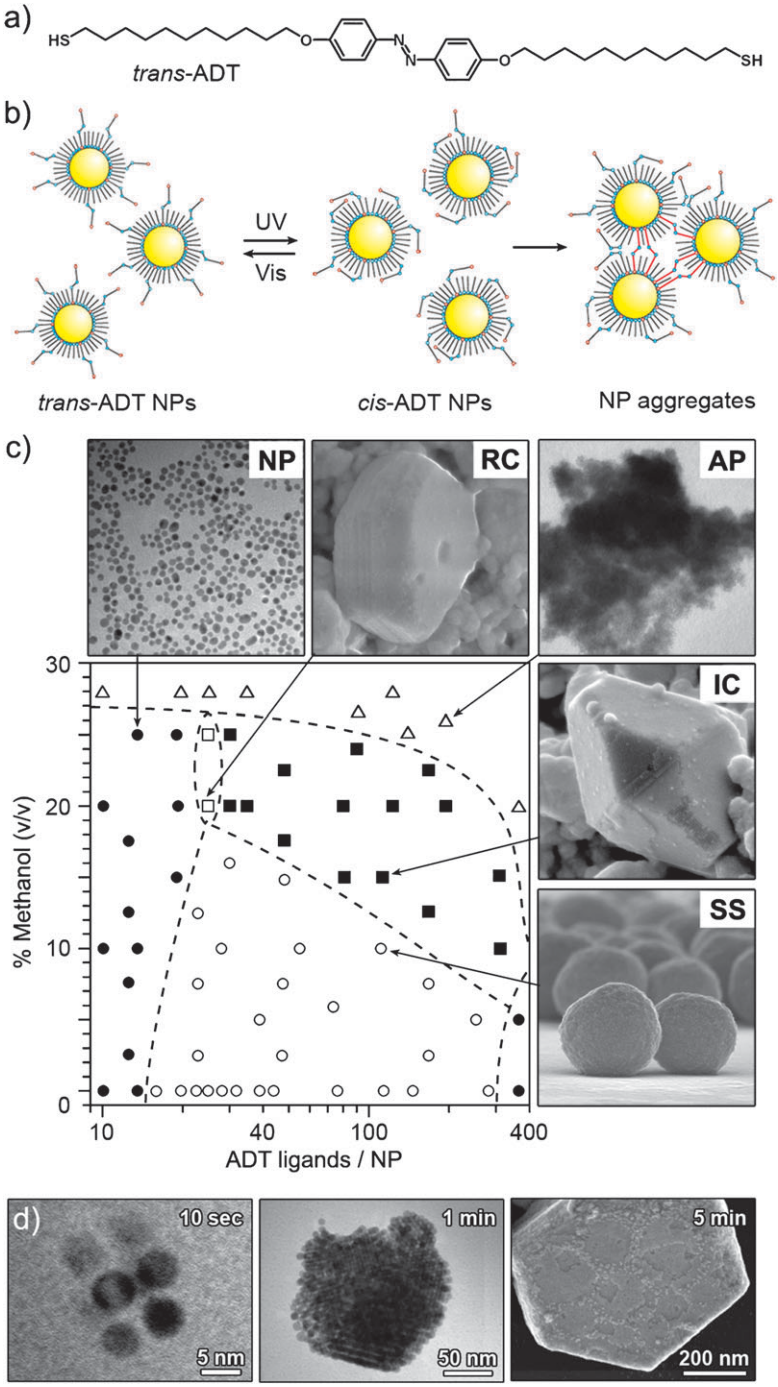

Fig. 29 (a) Structural formula of *trans*-(4,4′-bis(11-mercaptoundecanoxy)azobenzene) (*trans*-ADT). (b) Light-induced self-assembly of NPs. UV-irradiation of a stable solution of *trans*-ADT-coated NPs induces AB isomerisation and attractive interactions between NPs. When in close proximity, covalent crosslinks between the NPs form. (c) Phase diagram of NP suprastructures. Morphology of the resulting aggregate is dictated by the ADT surface concentration and the polarity of the solvent. NP = nanoparticles; RC = reversible crystals; AP = amorphous precipitate; IC = irreversible crystals; SS = supraspheres. (d) In the case of the irreversible crystals, sizes of the aggregates can be controlled by UV irradiation time. Adapted with permission from ref. 49 (Copyright 2007 National Academy of Sciences USA).

periods of time.[277] Here, the NPs acted as a smart and *self-erasable* "ink" whose colour changed when the NPs assembled and disassembled upon irradiation (Fig. 30). Au or Ag NPs were covered with AB-terminated thiols and were dispersed in semi-permeable syndiotactic PMMA "paper". Initially, the colour of the films was red for Au and yellow for Ag NP inks. When, however, the film was irradiated with UV (by a light pen or through a transparency mask, Fig. 30c), the NPs in the irradiated regions formed metastable aggregates. Importantly, due to electrodynamic coupling, NP aggregation translated into pronounced colour changes. Specifically, short irradiation of the red gold NP films turned them purple, and

View Article Online

Published on 21 April 2010. Downloaded by Pennsylvania State University on 06/03/2016 20:02:52.

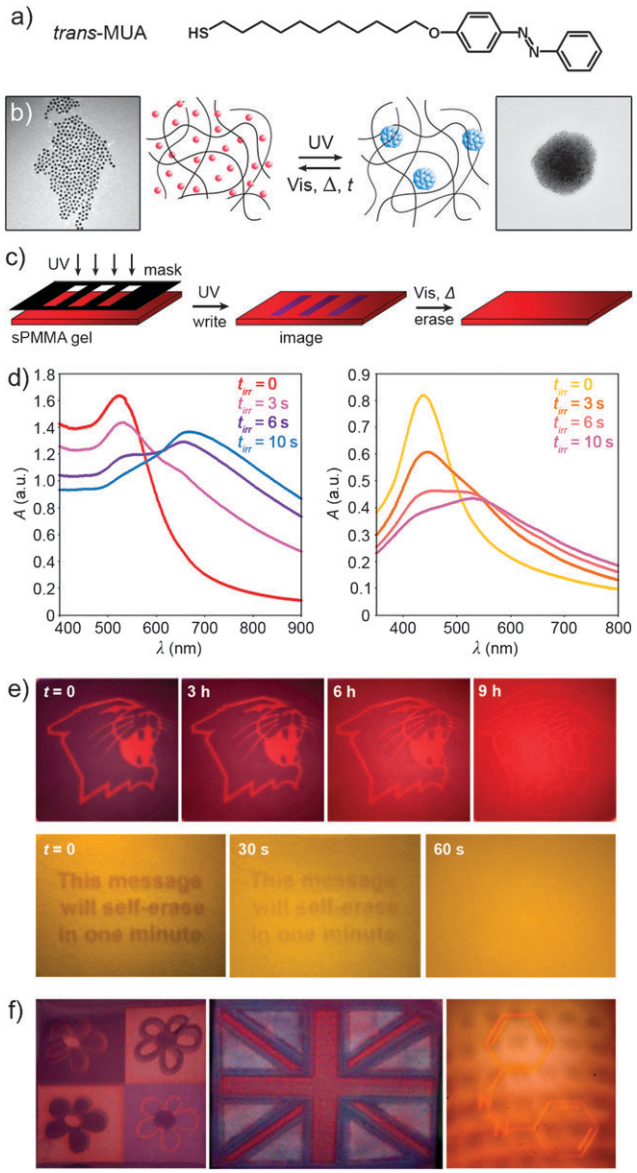

Fig. 30 (a) Structural formula of *trans*-azobenzene-terminated thiol (*trans*-MUA). (b) Schematic illustration of the light-induced NP self-assembly in a polymer gel. TEM images show dispersed NPs before (left) and aggregated NPs after (right) UV irradiation. (c) Local irradiation of the sample (here, through a transparency mask) can be used to record and store graphical information. (d) Aggregate size (and colour of the film) depends on the duration of UV irradiation. Colours of films based on Au NPs can be tuned from red to purple to blue (left), while colours of those based on Ag NPs can be tuned from yellow to orange to red to purple (right). (e) Examples of images/messages written in Au (top) and Ag (bottom) NP-based films and their self-erasure (slow in the dark, top; rapid upon intense visible light irradiation, bottom). (f) Examples of multicolour images written into Au NP (left, centre) and Ag NP (right) films. In the "flowers" picture, the purple regions were irradiated shorter than the bluish ones. In the Union Jack, the whitish-blue regions were irradiated longest (SPR shifted to near IR). In the picture on the right, the entire film was first exposed to UV light causing yellow-to-pale red colour change. The film was then bent and the pattern of squares was "written in" (pale red-to-purple transition). Finally, the film was flattened and an image of a *cis*-azobenzene molecule was created by exposure to visible light, which caused disassembly of the supraspheres in the irradiated region and return to the original light-orange hue. Adapted with permission from ref. 277 (Copyright 2009 Wiley-VCH Verlag GmbH & Co. KgaA).

when irradiated longer, the aggregates grew and the films became blue (Fig. 30d, left). Likewise, irradiation of films based on silver NPs changed their colour from yellow to red to purple (Fig. 30d, right). Because the aggregates persisted only as long as the dipole–dipole forces between the AB switches were operative, the aggregates slowly fell apart and the images self-erased. Remarkably, by adjusting the number, n, of AB switches per NP, it was possible to control the erasure times—from seconds for smaller values of n ($\sim$105), to minutes when n was large ($\sim$145). In addition, the erasure times could be accelerated by the intensity of visible light (Fig. 30e). Of course, the assembly process was fully reversible and at least hundreds of write–erase cycles could be performed without photobleaching or any noticeable damage to the materials. Since their recent publication, these NP-based self-erasing recording media have already attracted considerable industrial interest in the context of secure/timed information storage.

10. Conclusions

The last example illustrates well what we believe is the major promise of switchable NPs—namely, that they can constitute building blocks for materials and systems that function in the non-equilibrium regime. Unlike equilibrium structures, such dynamic materials could change their internal ordering and adapt to external stimuli; they can be, at least in the minimalistic sense, "smart". The field of dynamic self-assembly[26,294–298] is one in which the switches-on-NPs can make a real difference for they offer a new level of design flexibility not achievable with other "dynamic" components.[299,300] Of course, there are other potential avenues for future research on switchable particles. In principle, molecular and supramolecular switches assembled on the NP surfaces could be used to control a range of material properties of the NPs (*e.g.*, piezo-[301] or thermoelectric[302–304] characteristics) either by a direct "communication" between the switches and the NP cores, or by the switch-induced structural reorganisation of the NP assemblies. In the latter context, an appealing area of application could be in catalysis, where switch-mediated assembly-disassembly of catalytic NPs[305–307] would change the effective surface area and hence, catalytic activity. To summarise, we believe that the combination of NPs and switches can pave the way towards many classes of novel and useful materials.

Abbreviations used:

AB	Azobenzene
ADT	4,4′-Bis-(11-mercaptoundecanoxy)azobenzene
BDSAC	Benzyldimethylstearylammonium chloride
BHEEEN	1,5-Bis[2-(2-(2-hydroxyethoxy)ethoxy)ethoxy]naphthalene
bpy	2,2′-Bipyridine
CB[6]	Cucurbit[6]uril
$CBPQT^{4+}$	Cyclobisparaquat-*p*-phenylene
CCM	Co-condensation method
CD	Cyclodextrin
CTAB	Cetyltrimethylammonium bromide

 This journal is © The Royal Society of Chemistry 2010

View Article Online

Published on 21 April 2010. Downloaded by Pennsylvania State University on 06/03/2016 20:02:52.

DDA	Dodecylamine
DDAB	Didodecyldimethylammonium bromide
DLS	Dynamic light scattering
DTE	Dithienylethene
DNP	1,8-Dioxynaphthalene
FRET	Fluorescent resonance energy transfer
LISA	Light-induced self-assembly
MC	Merocyanine
MS	Mesoporous silica
*m*SAM	Mixed self-assembled monolayer
MUA	4-(11-Mercaptoundecanoxy)azobenzene
ND	Nanodisk
NP	Nanoparticle
ODA	Octadecylamine
PEI	Polyethyleneimine
PSMM	Post-synthesis modification method
QD	Quantum dot
Rh	Rhodamine
SAM	Self-assembled monolayer
SEM	Scanning electron microscopy
SP	Spiropyran
SPR	Surface plasmon resonance
TEM	Transmission electron microscopy
TEOS	Tetraethyl orthosilicate
TTF	Tetrathiafulvalene
UV	Ultraviolet
Vis	Visible

References

1 A. N. Shipway, E. Katz and I. Willner, *ChemPhysChem*, 2000, **1**, 18.
2 A. C. Templeton, M. P. Wuelfing and R. W. Murray, *Acc. Chem. Res.*, 2000, **33**, 27.
3 M. C. Daniel and D. Astruc, *Chem. Rev.*, 2004, **104**, 293.
4 C. Burda, X. B. Chen, R. Narayanan and M. A. El-Sayed, *Chem. Rev.*, 2005, **105**, 1025.
5 R. Elghanian, J. J. Storhoff, R. C. Mucic, R. L. Letsinger and C. A. Mirkin, *Science*, 1997, **277**, 1078.
6 J. J. Storhoff, A. A. Lazarides, R. C. Mucic, C. A. Mirkin, R. L. Letsinger and G. C. Schatz, *J. Am. Chem. Soc.*, 2000, **122**, 4640.
7 K. L. Kelly, E. Coronado, L. L. Zhao and G. C. Schatz, *J. Phys. Chem. B*, 2003, **107**, 668.
8 W. P. McConnell, J. P. Novak, L. C. Brousseau, R. R. Fuierer, R. C. Tenent and D. L. Feldheim, *J. Phys. Chem. B*, 2000, **104**, 8925.
9 A. Nitzan and M. A. Ratner, *Science*, 2003, **300**, 1384.
10 N. Tian, Z. Y. Zhou, S. G. Sun, Y. Ding and Z. L. Wang, *Science*, 2007, **316**, 732.
11 J. Y. Park, Y. Zhang, M. Grass, T. Zhang and G. A. Somorjai, *Nano Lett.*, 2008, **8**, 673.
12 N. Katsonis, M. Lubomska, M. M. Pollard, B. L. Feringa and P. Rudolf, *Prog. Surf. Sci.*, 2007, **82**, 407.
13 S. T. Wang, Y. L. Song and L. Jiang, *J. Photochem. Photobiol., C*, 2007, **8**, 18.
14 W. R. Browne and B. L. Feringa, *Annu. Rev. Phys. Chem.*, 2009, **60**, 407.
15 V. Balzani, A. Credi and M. Venturi, *ChemPhysChem*, 2008, **9**, 202.
16 E. Coronado, P. Gavina and S. Tatay, *Chem. Soc. Rev.*, 2009, **38**, 1674.
17 S. Silvi, M. Venturi and A. Credi, *J. Mater. Chem.*, 2009, **19**, 2279.
18 V. Balzani, A. Credi and M. Venturi, *Molecular devices and machines*, Wiley-VCH, Weinheim, 2008.
19 *Photochromism*, ed. G. H. Brown, Wiley-Interscience, New York, 1971.
20 *Molecular Switches*, ed. B. L. Feringa, Wiley-VCH, Weinheim, Germany, 2001.
21 N. Tamai and H. Miyasaka, *Chem. Rev.*, 2000, **100**, 1875.
22 K. Uchida, Y. Nakayama and M. Irie, *Bull. Chem. Soc. Jpn.*, 1990, **63**, 1311.
23 M. Hanazawa, R. Sumiya, Y. Horikawa and M. Irie, *Chem. Commun.*, 1992, 206.
24 M. Irie, *Chem. Rev.*, 2000, **100**, 1685.
25 S. Nakamura, S. Yokojima, K. Uchida, T. Tsujioka, A. Goldberg, A. Murakami, K. Shinoda, M. Mikami, T. Kobayashi, S. Kobatake, K. Matsuda and M. Irie, *J. Photochem. Photobiol., A*, 2008, **200**, 10.
26 M. Fialkowski, K. J. M. Bishop, R. Klajn, S. K. Smoukov, C. J. Campbell and B. A. Grzybowski, *J. Phys. Chem. B*, 2006, **110**, 2482.
27 G. Zimmerman, L. Y. Chow and U. J. Paik, *J. Am. Chem. Soc.*, 1958, **80**, 3528.
28 T. Schultz, J. Quenneville, B. Levine, A. Toniolo, T. J. Martinez, S. Lochbrunner, M. Schmitt, J. P. Shaffer, M. Z. Zgierski and A. Stolow, *J. Am. Chem. Soc.*, 2003, **125**, 8098.
29 G. Berkovic, V. Krongauz and V. Weiss, *Chem. Rev.*, 2000, **100**, 1741.
30 V. I. Minkin, *Chem. Rev.*, 2004, **104**, 2751.
31 P. L. Anelli, P. R. Ashton, N. Spencer, A. M. Z. Slawin, J. F. Stoddart and D. J. Williams, *Angew. Chem., Int. Ed. Engl.*, 1991, **30**, 1036.
32 P. R. Ashton, D. Philp, M. V. Reddington, A. M. Z. Slawin, N. Spencer, J. F. Stoddart and D. J. Williams, *Chem. Commun.*, 1991, 1680.
33 P. R. Ashton, D. Philp, N. Spencer and J. F. Stoddart, *Chem. Commun.*, 1991, 1677.
34 P. R. Ashton, P. T. Glink, M. V. Martinez-Diaz, J. F. Stoddart, A. J. P. White and D. J. Williams, *Angew. Chem., Int. Ed. Engl.*, 1996, **35**, 1930.
35 B. H. Northrop, S. J. Khan and J. F. Stoddart, *Org. Lett.*, 2006, **8**, 2159.
36 P. Bortolus and S. Monti, *J. Phys. Chem.*, 1987, **91**, 5046.
37 T. Fujimoto, A. Nakamura, Y. Inoue, Y. Sakata and T. Kaneda, *Tetrahedron Lett.*, 2001, **42**, 7987.
38 M. Asakawa, P. R. Ashton, V. Balzani, A. Credi, G. Mattersteig, O. A. Matthews, M. Montalti, N. Spencer, J. F. Stoddart and M. Venturi, *Chem.–Eur. J.*, 1997, **3**, 1992.
39 V. Balzani, A. Credi, G. Mattersteig, O. A. Matthews, F. M. Raymo, J. F. Stoddart, M. Venturi, A. J. P. White and D. J. Williams, *J. Org. Chem.*, 2000, **65**, 1924.
40 P. R. Ashton, R. Ballardini, V. Balzani, M. Gomez-Lopez, S. E. Lawrence, M. V. Martinez-Diaz, M. Montalti, A. Piersanti, L. Prodi, J. F. Stoddart and D. J. Williams, *J. Am. Chem. Soc.*, 1997, **119**, 10641.
41 V. Sindelar, S. Silvi and A. E. Kaifer, *Chem. Commun.*, 2006, 2185.
42 M. Ueda, N. Fukushima, K. Kudo and K. Ichimura, *J. Mater. Chem.*, 1997, **7**, 641.
43 K. M. Yeo, C. J. Gao, K. H. Ahn and I. S. Lee, *Chem. Commun.*, 2008, 4622.
44 R. Wang, T. Iyoda, L. Jiang, D. A. Tryk, K. Hashimoto and A. Fujishima, *J. Electroanal. Chem.*, 1997, **438**, 213.
45 K. Tamada, J. Nagasawa, F. Nakanishi, K. Abe, T. Ishida, M. Hara and W. Knoll, *Langmuir*, 1998, **14**, 3264.
46 S. D. Evans, S. R. Johnson, H. Ringsdorf, L. M. Williams and H. Wolf, *Langmuir*, 1998, **14**, 6436.
47 J. Hu, J. Zhang, F. Liu, K. Kittredge, J. K. Whitesell and M. A. Fox, *J. Am. Chem. Soc.*, 2001, **123**, 1464.
48 K. H. Shin and E. J. Shin, *Bull. Korean Chem. Soc.*, 2008, **29**, 1259.
49 R. Klajn, K. J. M. Bishop and B. A. Grzybowski, *Proc. Natl. Acad. Sci. U. S. A.*, 2007, **104**, 10305.
50 F. L. Callari and S. Sortino, *J. Mater. Chem.*, 2007, **17**, 4184.
51 S. Sortino, S. Petralia, S. Conoci and S. Di Bella, *J. Mater. Chem.*, 2004, **14**, 811.
52 T. Weidner, F. Bretthauer, N. Ballav, H. Motschmann, H. Orendi, C. Bruhn, U. Siemeling and M. Zharnikov, *Langmuir*, 2008, **24**, 11691.

View Article Online

Published on 21 April 2010. Downloaded by Pennsylvania State University on 06/03/2016 20:02:52.

53 K. Tamada, H. Akiyama and T. X. Wei, *Langmuir*, 2002, **18**, 5239.
54 H. Akiyama, K. Tamada, J. Nagasawa, K. Abe and T. Tamaki, *J. Phys. Chem. B*, 2003, **107**, 130.
55 P. B. Wan, Y. G. Jiang, Y. P. Wang, Z. Q. Wang and X. Zhang, *Chem. Commun*., 2008, 5710.
56 A. M. Kalsin, B. Kowalczyk, P. Wesson, M. Paszewski and B. A. Grzybowski, *J. Am. Chem. Soc*., 2007, **129**, 6664.
57 Y. S. Shon, C. Mazzitelli and R. W. Murray, *Langmuir*, 2001, **17**, 7735.
58 H. Choo, E. Cutler and Y. S. Shon, *Langmuir*, 2003, **19**, 8555.
59 C. J. Campbell, S. Soh and B. A. Grzybowski, *Langmuir*, 2008, **24**, 11600.
60 P. E. Laibinis, R. G. Nuzzo and G. M. Whitesides, *J. Phys. Chem*., 1992, **96**, 5097.
61 J. P. Folkers, P. E. Laibinis, G. M. Whitesides and J. Deutch, *J. Phys. Chem*., 1994, **98**, 563.
62 P. E. Laibinis, C. D. Bain, R. G. Nuzzo and G. M. Whitesides, *J. Phys. Chem*., 1995, **99**, 7663.
63 A. M. Kalsin and B. A. Grzybowski, *Nano Lett*., 2007, **7**, 1018.
64 F. Callari, S. Petralia and S. Sortino, *Chem. Commun*., 2006, 1009.
65 D. Witt, R. Klajn, P. Barski and B. A. Grzybowski, *Curr. Org. Chem*., 2004, **8**, 1763.
66 A. Manna, P. L. Chen, H. Akiyama, T. X. Wei, K. Tamada and W. Knoll, *Chem. Mater*., 2003, **15**, 20.
67 K. Tamada, H. Akiyama, T. X. Wei and S. A. Kim, *Langmuir*, 2003, **19**, 2306.
68 R. Klajn, M. A. Olson, P. J. Wesson, L. Fang, A. Coskun, A. Trabolsi, S. Soh, J. F. Stoddart and B. A. Grzybowski, *Nat. Chem*., 2009, **1**, 733.
69 R. Klajn, L. Fang, A. Coskun, M. A. Olson, P. J. Wesson, J. F. Stoddart and B. A. Grzybowski, *J. Am. Chem. Soc*., 2009, **131**, 4233.
70 M. A. Olson, A. Coskun, R. Klajn, S. K. Dey, K. P. Browne, B. A. Grzybowski and J. F. Stoddart, *Nano Lett*., 2009, **9**, 3185.
71 N. Koumura, R. W. J. Zijlstra, R. A. van Delden, N. Harada and B. L. Feringa, *Nature*, 1999, **401**, 152.
72 N. Koumura, E. M. Geertsema, M. B. van Gelder, A. Meetsma and B. L. Feringa, *J. Am. Chem. Soc*., 2002, **124**, 5037.
73 R. A. van Delden, M. K. J. ter Wiel, M. M. Pollard, J. Vicario, N. Koumura and B. L. Feringa, *Nature*, 2005, **437**, 1337.
74 M. M. Pollard, M. K. J. ter Wiel, R. A. van Delden, J. Vicario, N. Koumura, C. R. van den Brom, A. Meetsma and B. L. Feringa, *Chem.–Eur. J*., 2008, **14**, 11610.
75 B. Long, K. Nikitin and D. Fitzmaurice, *J. Am. Chem. Soc*., 2003, **125**, 5152.
76 B. Long, K. Nikitin and D. Fitzmaurice, *J. Am. Chem. Soc*., 2003, **125**, 15490.
77 K. Nikitin, E. Lestini, M. Lazzari, S. Altobello and D. Fitzmaurice, *Langmuir*, 2007, **23**, 12147.
78 S. Wagner, F. Leyssner, C. Kordel, S. Zarwell, R. Schmidt, M. Weinelt, K. Ruck-Braun, M. Wolf and P. Tegeder, *Phys. Chem. Chem. Phys*., 2009, **11**, 6242.
79 K. Nikitin, B. Long and D. Fitzmaurice, *Chem. Commun*., 2003, 282.
80 W. Geuder, S. Hunig and A. Suchy, *Tetrahedron*, 1986, **42**, 1665.
81 M. Ito, H. Sasaki and M. Takahashi, *J. Phys. Chem*., 1987, **91**, 3932.
82 J. W. Park, N. H. Choi and J. H. Kim, *J. Phys. Chem*., 1996, **100**, 769.
83 M. Felderhoff, S. Heinen, N. Molisho, S. Webersinn and L. Walder, *Helv. Chim. Acta*, 2000, **83**, 181.
84 K. G. Thomas and P. V. Kamat, *Acc. Chem. Res*., 2003, **36**, 888.
85 T. X. Wang, D. Q. Zhang, W. Xu, J. L. Yang, R. Han and D. B. Zhu, *Langmuir*, 2002, **18**, 1840.
86 E. Dulkeith, A. C. Morteani, T. Niedereichholz, T. A. Klar, J. Feldmann, S. A. Levi, F. van Veggel, D. N. Reinhoudt, M. Moller and D. I. Gittins, *Phys. Rev. Lett*., 2002, **89**, 203002.
87 H. Yamaguchi, K. Matsuda and M. Irie, *J. Phys. Chem. C*, 2007, **111**, 3853.
88 J. Zhang, J. K. Whitesell and M. A. Fox, *Chem. Mater*., 2001, **13**, 2323.
89 K. Matsuda, M. Ikeda and M. Irie, *Chem. Lett*., 2004, **33**, 456.
90 H. Yamaguchi, M. Ikeda, K. Matsuda and A. Irie, *Bull. Chem. Soc. Jpn*., 2006, **79**, 1413.
91 H. Miyasaka, T. Nobuto, A. Itaya, N. Tamai and M. Irie, *Chem.Phys. Lett*., 1997, **269**, 281.
92 H. Nishi and S. Kobatake, *Macromolecules*, 2008, **41**, 3995.
93 S. Perrier, C. Barner-Kowollik, J. F. Quinn, P. Vana and T. P. Davis, *Macromolecules*, 2002, **35**, 8300.
94 T. Kudernac, S. J. van der Molen, B. J. van Wees and B. L. Feringa, *Chem. Commun*., 2006, 3597.
95 D. Dulic, S. J. van der Molen, T. Kudernac, H. T. Jonkman, J. J. D. de Jong, T. N. Bowden, J. van Esch, B. L. Feringa and B. J. van Wees, *Phys. Rev. Lett*., 2003, **91**, 207402.
96 P. R. Hania, R. Telesca, L. N. Lucas, A. Pugzlys, J. van Esch, B. L. Feringa, J. G. Snijders and K. Duppen, *J. Phys. Chem. A*, 2002, **106**, 8498.
97 J. Li, G. Speyer and O. F. Sankey, *Phys. Rev. Lett*., 2004, **93**, 248302.
98 A. Perrier, F. Maurel and J. Aubard, *J. Phys. Chem. A*, 2007, **111**, 9688.
99 T. R. Evans, A. F. Toth and P. A. Leermakers, *J. Am. Chem. Soc*., 1967, **89**, 5060.
100 D. Levy and D. Avnir, *J. Phys. Chem*., 1988, **92**, 4734.
101 H. Kawai and T. Nagamura, *J. Photochem. Photobiol., A*, 1995, **92**, 105.
102 R. Heiligmanrim, Y. Hirshberg and E. Fischer, *J. Phys. Chem*., 1962, **66**, 2470.
103 E. Berman, R. E. Fox and F. D. Thomson, *J. Am. Chem. Soc*., 1959, **81**, 5605.
104 H. Gorner, *Phys. Chem. Chem. Phys*., 2001, **3**, 416.
105 M. Tomasulo, I. Yildiz and F. M. Raymo, *Inorg. Chim. Acta*, 2007, **360**, 938.
106 M. Ueda, H. B. Kim and K. Ichimura, *J. Mater. Chem*., 1994, **4**, 883.
107 P. Calero, E. Aznar, J. M. Lloris, M. D. Marcos, R. Martinez-Manez, J. V. Ros-Lis, J. Soto and F. Sancenon, *Chem. Commun*., 2008, 1668.
108 M. Ueda, K. Kudo and K. Ichimura, *J. Mater. Chem*., 1995, **5**, 1007.
109 V. A. Krongauz and A. Parshutkin, *Photochem. Photobiol*., 1972, **15**, 503.
110 V. A. Krongauz, S. N. Fishman and E. S. Goldburt, *J. Phys. Chem*., 1978, **82**, 2469.
111 V. A. Krongauz and E. S. Goldburt, *Nature*, 1978, **271**, 43.
112 D. V. Bavykin, E. N. Savinov and V. N. Parmon, *Langmuir*, 1999, **15**, 4722.
113 A. Coskun, P. J. Wesson, R. Klajn, A. Trabolsi, L. Fang, M. A. Olson, S. K. Dey, B. A. Grzybowski and J. F. Stoddart, *J. Am. Chem. Soc*., 2010, **132**, 4310.
114 U. Kreibig and M. Vollmer, *Optical properties of metal clusters*, Springer-Verlag, Berlin, 1995.
115 P. V. Kamat, *J. Phys. Chem. B*, 2002, **106**, 7729.
116 R. C. Jin, Y. W. Cao, C. A. Mirkin, K. L. Kelly, G. C. Schatz and J. G. Zheng, *Science*, 2001, **294**, 1901.
117 Y. N. Xia, P. D. Yang, Y. G. Sun, Y. Y. Wu, B. Mayers, B. Gates, Y. D. Yin, F. Kim and Y. Q. Yan, *Adv. Mater*., 2003, **15**, 353.
118 S. Underwood and P. Mulvaney, *Langmuir*, 1994, **10**, 3427.
119 M. D. Malinsky, K. L. Kelly, G. C. Schatz and R. P. Van Duyne, *J. Am. Chem. Soc*., 2001, **123**, 1471.
120 Y. G. Sun and Y. N. Xia, *Anal. Chem*., 2002, **74**, 5297.
121 A. J. Haes, S. L. Zou, J. Zhao, G. C. Schatz and R. P. Van Duyne, *J. Am. Chem. Soc*., 2006, **128**, 10905.
122 Y. Sugawara, T. A. Kelf, J. J. Baumberg, M. E. Abdelsalam and P. N. Bartlett, *Phys. Rev. Lett*., 2006, **97**, 266808.
123 N. T. Fofang, T. H. Park, O. Neumann, N. A. Mirin, P. Nordlander and N. J. Halas, *Nano Lett*., 2008, **8**, 3481.
124 V. K. S. Hsiao, Y. B. Zheng, B. K. Juluri and T. J. Huang, *Adv. Mater*., 2008, **20**, 3528.
125 Y. B. Zheng, B. K. Juluri, X. L. Mao, T. R. Walker and T. J. Huang, *J. Appl. Phys*., 2008, **103**, 9.
126 Y. B. Zheng, Y. W. Yang, L. Jensen, L. Fang, B. K. Juluri, A. H. Flood, P. S. Weiss, J. F. Stoddart and T. J. Huang, *Nano Lett*., 2009, **9**, 819.

 This journal is © The Royal Society of Chemistry 2010

View Article Online

Published on 21 April 2010. Downloaded by Pennsylvania State University on 06/03/2016 20:02:52.

127 S. J. van der Molen, J. H. Liao, T. Kudernac, J. S. Agustsson, L. Bernard, M. Calame, B. J. van Wees, B. L. Feringa and C. Schonenberger, *Nano Lett.*, 2009, **9**, 76.
128 M. C. T. Fyfe, P. T. Glink, S. Menzer, J. F. Stoddart, A. J. P. White and D. J. Williams, *Angew. Chem., Int. Ed. Engl.*, 1997, **36**, 2068.
129 T. Yoshida, K. Arishima, F. Ebisawa, M. Hoshino, K. Sukegawa, A. Ishikawa, T. Kobayashi, M. Hanazawa and Y. Horikawa, *J. Photochem. Photobiol., A*, 1996, **95**, 265.
130 E. Kim, Y. K. Choi and M. H. Lee, *Macromolecules*, 1999, **32**, 4855.
131 M. S. Kim, H. Maruyama, T. Kawai and M. Irie, *Chem. Mater.*, 2003, **15**, 4539.
132 G. Callierotti, A. Bianco, C. Castiglioni, C. Bertarelli and G. Zerbi, *J. Phys. Chem. A*, 2008, **112**, 7473.
133 D. S. Sidhaye, S. Kashyap, M. Sastry, S. Hotha and B. L. V. Prasad, *Langmuir*, 2005, **21**, 7979.
134 C. A. Stowell and B. A. Korgel, *Nano Lett.*, 2005, **5**, 1203.
135 P. Ahonen, D. J. Schiffrin, J. Paprotny and K. Kontturi, *Phys. Chem. Chem. Phys.*, 2007, **9**, 651.
136 P. Alivisatos, *Nat. Biotechnol.*, 2004, **22**, 47.
137 A. M. Derfus, W. C. W. Chan and S. N. Bhatia, *Nano Lett.*, 2004, **4**, 11.
138 I. L. Medintz, H. T. Uyeda, E. R. Goldman and H. Mattoussi, *Nat. Mater.*, 2005, **4**, 435.
139 J. Park, K. J. An, Y. S. Hwang, J. G. Park, H. J. Noh, J. Y. Kim, J. H. Park, N. M. Hwang and T. Hyeon, *Nat. Mater.*, 2004, **3**, 891.
140 Y. C. Jeong, S. I. Yang, K. H. Ahn and E. Kim, *Chem. Commun.*, 2005, 2503.
141 Y. C. Jeong, J. P. Han, Y. Kim, E. Kim, S. I. Yang and K. H. Ahn, *Tetrahedron*, 2007, **63**, 3173.
142 Y. C. Jeong, D. G. Park, I. S. Lee, S. I. Yang and K. H. Ahn, *J. Mater. Chem.*, 2009, **19**, 97.
143 J. H. Gao, W. Zhang, P. B. Huang, B. Zhang, X. X. Zhang and B. Xu, *J. Am. Chem. Soc.*, 2008, **130**, 3710.
144 R. Koole, M. M. van Schooneveld, J. Hilhorst, K. Castermans, D. P. Cormode, G. J. Strijkers, C. D. Donega, D. Vanmaekelbergh, A. W. Griffioen, K. Nicolay, Z. A. Fayad, A. Meijerink and W. J. M. Mulder, *Bioconjugate Chem.*, 2008, **19**, 2471.
145 J. H. Gao, H. W. Gu and B. Xu, *Acc. Chem. Res.*, 2009, **42**, 1097.
146 P. Tseng, D. Di Carlo and J. W. Judy, *Nano Lett.*, 2009, **9**, 3053.
147 E. A. Jares-Erijman and T. M. Jovin, *Nat. Biotechnol.*, 2003, **21**, 1387.
148 I. L. Medintz, A. R. Clapp, H. Mattoussi, E. R. Goldman, B. Fisher and J. M. Mauro, *Nat. Mater.*, 2003, **2**, 630.
149 A. R. Clapp, I. L. Medintz, J. M. Mauro, B. R. Fisher, M. G. Bawendi and H. Mattoussi, *J. Am. Chem. Soc.*, 2004, **126**, 301.
150 B. N. G. Giepmans, S. R. Adams, M. H. Ellisman and R. Y. Tsien, *Science*, 2006, **312**, 217.
151 E. Jares-Erijman, L. Giordano, C. Spagnuolo, K. Lidke and T. M. Jovin, *Mol. Cryst. Liq. Cryst.*, 2005, **430**, 257.
152 J. Folling, S. Polyakova, V. Belov, A. van Blaaderen, M. L. Bossi and S. W. Hell, *Small*, 2008, **4**, 134.
153 W. H. Binder, R. Sachsenhofer, C. J. Straif and R. Zirbs, *J. Mater. Chem.*, 2007, **17**, 2125.
154 J. Cusido, E. Deniz and F. M. Raymo, *Eur. J. Org. Chem.*, 2009, 2031.
155 I. L. Medintz, S. A. Trammell, H. Mattoussi and J. M. Mauro, *J. Am. Chem. Soc.*, 2004, **126**, 30.
156 M. Tomasulo, I. Yildiz, S. L. Kaanumalle and F. M. Raymo, *Langmuir*, 2006, **22**, 10284.
157 M. Tomasulo, I. Yildiz and F. M. Raymo, *Aust. J. Chem.*, 2006, **59**, 175.
158 M. Tomasulo, I. Yildiz and F. M. Raymo, *J. Phys. Chem. B*, 2006, **110**, 3853.
159 I. Yildiz, E. Deniz and F. M. Raymo, *Chem. Soc. Rev.*, 2009, **38**, 1859.
160 I. Yildiz, M. Tomasulo and F. M. Raymo, *J. Mater. Chem.*, 2008, **18**, 5577.
161 L. Y. Zhu, M. Q. Zhu, J. K. Hurst and A. D. Q. Li, *J. Am. Chem. Soc.*, 2005, **127**, 8968.
162 B. O. Dabbousi, J. Rodriguez-Viejo, F. V. Mikulec, J. R. Heine, H. Mattoussi, R. Ober, K. F. Jensen and M. G. Bawendi, *J. Phys. Chem. B*, 1997, **101**, 9463.
163 D. Gerion, F. Pinaud, S. C. Williams, W. J. Parak, D. Zanchet, S. Weiss and A. P. Alivisatos, *J. Phys. Chem. B*, 2001, **105**, 8861.
164 A. D. Yoffe, *Adv. Phys.*, 2001, **50**, 1.
165 M. Tomasulo, S. Sortino and F. M. Raymo, *Org. Lett.*, 2005, **7**, 1109.
166 M. Tomasulo, S. Sortino, A. J. P. White and F. M. Raymo, *J. Org. Chem.*, 2005, **70**, 8180.
167 E. Deniz, M. Tomasulo, S. Sortino and F. M. Raymo, *J. Phys. Chem. C*, 2009, **113**, 8491.
168 J. M. Tour, *Acc. Chem. Res.*, 2000, **33**, 791.
169 A. R. Pease, J. O. Jeppesen, J. F. Stoddart, Y. Luo, C. P. Collier and J. R. Heath, *Acc. Chem. Res.*, 2001, **34**, 433.
170 J. Reichert, R. Ochs, D. Beckmann, H. B. Weber, M. Mayor and H. von Lohneysen, *Phys. Rev. Lett.*, 2002, **88**, 176804.
171 B. Q. Xu and N. J. J. Tao, *Science*, 2003, **301**, 1221.
172 X. Y. Xiao, B. Q. Xu and N. J. Tao, *Nano Lett.*, 2004, **4**, 267.
173 F. Chen, X. L. Li, J. Hihath, Z. F. Huang and N. J. Tao, *J. Am. Chem. Soc.*, 2006, **128**, 15874.
174 X. L. Li, J. He, J. Hihath, B. Q. Xu, S. M. Lindsay and N. J. Tao, *J. Am. Chem. Soc.*, 2006, **128**, 2135.
175 J. M. Mativetsky, G. Pace, M. Elbing, M. A. Rampi, M. Mayor and P. Samori, *J. Am. Chem. Soc.*, 2008, **130**, 9192.
176 A. C. Whalley, M. L. Steigerwald, X. Guo and C. Nuckolls, *J. Am. Chem. Soc.*, 2007, **129**, 12590.
177 A. J. Kronemeijer, H. B. Akkerman, T. Kudernac, B. J. van Wees, B. L. Feringa, P. W. M. Blom and B. de Boer, *Adv. Mater.*, 2008, **20**, 1467.
178 C. Kergueris, J. P. Bourgoin, S. Palacin, D. Esteve, C. Urbina, M. Magoga and C. Joachim, *Phys. Rev. B: Condens. Matter*, 1999, **59**, 12505.
179 M. A. Rampi and G. M. Whitesides, *Chem. Phys.*, 2002, **281**, 373.
180 L. D. Qin, S. Park, L. Huang and C. A. Mirkin, *Science*, 2005, **309**, 113.
181 L. D. Qin, J. W. Jang, L. Huang and C. A. Mirkin, *Small*, 2007, **3**, 86.
182 X. D. Chen, A. B. Braunschweig, M. J. Wiester, S. Yeganeh, M. A. Ratner and C. A. Mirkin, *Angew. Chem., Int. Ed.*, 2009, **48**, 5178.
183 H. Shiigi, S. Tokonami, H. Yakabe and T. Nagaoka, *J. Am. Chem. Soc.*, 2005, **127**, 3280.
184 S. I. Taniguchi, M. Minamoto, M. M. Matsushita, T. Sugawara, Y. Kawada and D. Bethell, *J. Mater. Chem.*, 2006, **16**, 3459.
185 L. Bernard, Y. Kamdzhilov, M. Calame, S. J. van der Molen, J. H. Liao and C. Schonenberger, *J. Phys. Chem. C*, 2007, **111**, 18445.
186 M. Ikeda, N. Tanifuji, H. Yamaguchi, M. Irie and K. Matsuda, *Chem. Commun.*, 2007, 1355.
187 K. Matsuda, H. Yamaguchi, T. Sakano, M. Ikeda, N. Tanifuji and M. Irie, *J. Phys. Chem. C*, 2008, **112**, 17005.
188 T. Sakano, H. Yamaguchi, N. Tanifuji, M. Irie and K. Matsuda, *Chem. Lett.*, 2008, **37**, 634.
189 H. Nakanishi, K. J. M. Bishop, B. Kowalczyk, A. Nitzan, E. A. Weiss, K. V. Tretiakov, M. M. Apodaca, R. Klajn, J. F. Stoddart and B. A. Grzybowski, *Nature*, 2009, **460**, 371.
190 M. A. Mangold, C. Weiss, M. Calame and A. W. Holleitner, *Appl. Phys. Lett.*, 2009, **94**, 161104.
191 M. Irie, K. Sakemura, M. Okinaka and K. Uchida, *J. Org. Chem.*, 1995, **60**, 8305.
192 K. Uchida, E. Tsuchida, Y. Aoi, S. Nakamura and M. Irie, *Chem. Lett.*, 1999, 63.
193 K. Matsuda, M. Matsuo, S. Mizoguti, K. Higashiguchi and M. Irie, *J. Phys. Chem. B*, 2002, **106**, 11218.
194 N. Katsonis, T. Kudernac, M. Walko, S. J. van der Molen, B. J. van Wees and B. L. Feringa, *Adv. Mater.*, 2006, **18**, 1397.
195 S. Kirkpatrick, *Rev. Mod. Phys.*, 1973, **45**, 574.
196 J. J. Wu and D. S. McLachlan, *Phys. Rev. B: Condens. Matter*, 1997, **56**, 1236.
197 M. Eikerling, A. A. Kornyshev and U. Stimming, *J. Phys. Chem. B*, 1997, **101**, 10807.
198 J. G. Zhu, Y. F. Zheng and G. A. Prinz, *J. Appl. Phys.*, 2000, **87**, 6668.
199 W. Kuch, *Nat. Mater.*, 2003, **2**, 505.

View Article Online

Published on 21 April 2010. Downloaded by Pennsylvania State University on 06/03/2016 20:02:52.

200 N. Hur, S. Park, P. A. Sharma, J. S. Ahn, S. Guha and S. W. Cheong, *Nature*, 2004, **429**, 392.
201 N. A. Frey, S. Peng, K. Cheng and S. Sun, *Chem. Soc. Rev.*, 2009, **38**, 2532.
202 S. Decurtins, P. Gutlich, C. P. Kohler, H. Spiering and A. Hauser, *Chem. Phys. Lett.*, 1984, **105**, 1.
203 S. Haneda, H. Munekata, Y. Takatani and S. Koshihara, *J. Appl. Phys.*, 2000, **87**, 6445.
204 S. Hayami, Z. Z. Gu, M. Shiro, Y. Einaga, A. Fujishima and O. Sato, *J. Am. Chem. Soc.*, 2000, **122**, 7126.
205 S. Koshihara, A. Oiwa, M. Hirasawa, S. Katsumoto, Y. Iye, C. Urano, H. Takagi and H. Munekata, *Phys. Rev. Lett.*, 1997, **78**, 4617.
206 K. Matsuda, A. Machida, Y. Moritomo and A. Nakamura, *Phys. Rev. B: Condens. Matter*, 1998, **58**, R4203.
207 S. Ohkoshi, S. Yorozu, O. Sato, T. Iyoda, A. Fujishima and K. Hashimoto, *Appl. Phys. Lett.*, 1997, **70**, 1040.
208 F. Renz, H. Oshio, V. Ksenofontov, M. Waldeck, H. Spiering and P. Gutlich, *Angew. Chem., Int. Ed.*, 2000, **39**, 3699.
209 O. Sato, T. Iyoda, A. Fujishima and K. Hashimoto, *Science*, 1996, **272**, 704.
210 T. Yamamoto, Y. Umemura, O. Sato and Y. Einaga, *J. Am. Chem. Soc.*, 2005, **127**, 16065.
211 R. Mikami, M. Taguchi, K. Yamada, K. Suzuki, O. Sato and Y. Einaga, *Angew. Chem., Int. Ed.*, 2004, **43**, 6135.
212 Y. Einaga, *Bull. Chem. Soc. Jpn.*, 2006, **79**, 361.
213 Y. Einaga, *J. Photochem. Photobiol., C*, 2006, **7**, 69.
214 M. Suda, M. Nakagawa, T. Iyoda and Y. Einaga, *J. Am. Chem. Soc.*, 2007, **129**, 5538.
215 I. Carmeli, G. Leitus, R. Naaman, S. Reich and Z. Vager, *J. Chem. Phys.*, 2003, **118**, 10372.
216 M. S. Seehra, P. Dutta, S. Neeleshwar, Y. Y. Chen, C. L. Chen, S. W. Chou, C. C. Chen, C. L. Dong and C. L. Chang, *Adv. Mater.*, 2008, **20**, 1656.
217 M. Suda, N. Kameyama, A. Ikegami, M. Suzuki, N. Kawamura and Y. Einaga, *Polyhedron*, 2009, **28**, 1868.
218 M. Suda, N. Kameyama, M. Suzuki, N. Kawamura and Y. Einaga, *Angew. Chem., Int. Ed.*, 2008, **47**, 160.
219 C. Liu, B. S. Zou, A. J. Rondinone and J. Zhang, *J. Am. Chem. Soc.*, 2000, **122**, 6263.
220 G. Kataby, Y. Koltypin, A. Ulman, I. Felner and A. Gedanken, *Appl. Surf. Sci.*, 2002, **201**, 191.
221 C. R. Vestal and Z. J. Zhang, *J. Am. Chem. Soc.*, 2003, **125**, 9828.
222 S. H. Sun, C. B. Murray, D. Weller, L. Folks and A. Moser, *Science*, 2000, **287**, 1989.
223 S. H. Sun, *Adv. Mater.*, 2006, **18**, 393.
224 H. G. Bagaria, E. T. Ada, M. Shamsuzzoha, D. E. Nikles and D. T. Johnson, *Langmuir*, 2006, **22**, 7732.
225 P. Crespo, R. Litran, T. C. Rojas, M. Multigner, J. M. de la Fuente, J. C. Sanchez-Lopez, M. A. Garcia, A. Hernando, S. Penades and A. Fernandez, *Phys. Rev. Lett.*, 2004, **93**, 087204.
226 P. Dutta, S. Pal, M. S. Seehra, M. Anand and C. B. Roberts, *Appl. Phys. Lett.*, 2007, **90**, 213102.
227 A. Hernando, P. Crespo and M. A. Garcia, *Phys. Rev. Lett.*, 2006, **96**, 057206.
228 Y. Yamamoto, T. Miura, M. Suzuki, N. Kawamura, H. Miyagawa, T. Nakamura, K. Kobayashi, T. Teranishi and H. Hori, *Phys. Rev. Lett.*, 2004, **93**, 116801.
229 I. H. Campbell, S. Rubin, T. A. Zawodzinski, J. D. Kress, R. L. Martin, D. L. Smith, N. N. Barashkov and J. P. Ferraris, *Phys. Rev. B: Condens. Matter*, 1996, **54**, 14321.
230 H. Ishii, K. Sugiyama, E. Ito and K. Seki, *Adv. Mater.*, 1999, **11**, 605.
231 Y. F. Lu, H. Y. Fan, A. Stump, T. L. Ward, T. Rieker and C. J. Brinker, *Nature*, 1999, **398**, 223.
232 C. T. Kresge, M. E. Leonowicz, W. J. Roth, J. C. Vartuli and J. S. Beck, *Nature*, 1992, **359**, 710.
233 S. Huh, J. W. Wiench, J. C. Yoo, M. Pruski and V. S. Y. Lin, *Chem. Mater.*, 2003, **15**, 4247.
234 T. H. Chung, S. H. Wu, M. Yao, C. W. Lu, Y. S. Lin, Y. Hung, C. Y. Mou, Y. C. Chen and D. M. Huang, *Biomaterials*, 2007, **28**, 2959.
235 C. Y. Lai, B. G. Trewyn, D. M. Jeftinija, K. Jeftinija, S. Xu, S. Jeftinija and V. S. Y. Lin, *J. Am. Chem. Soc.*, 2003, **125**, 4451.
236 J. Lu, M. Liong, J. I. Zink and F. Tamanoi, *Small*, 2007, **3**, 1341.
237 I. I. Slowing, J. L. Vivero-Escoto, C. W. Wu and V. S. Y. Lin, *Adv. Drug Delivery Rev.*, 2008, **60**, 1278.
238 F. Torney, B. G. Trewyn, V. S. Y. Lin and K. Wang, *Nat. Nanotechnol.*, 2007, **2**, 295.
239 P. Sierocki, H. Maas, P. Dragut, G. Richardt, F. Vogtle, L. Cola, F. A. M. Brouwer and J. I. Zink, *J. Phys. Chem. B*, 2006, **110**, 24390.
240 S. Angelos, E. Choi, F. Vogtle, L. De Cola and J. I. Zink, *J. Phys. Chem. C*, 2007, **111**, 6589.
241 J. Lu, E. Choi, F. Tamanoi and J. I. Zink, *Small*, 2008, **4**, 421.
242 S. Angelos, E. Johansson, J. F. Stoddart and J. I. Zink, *Adv. Funct. Mater.*, 2007, **17**, 2261.
243 E. Johansson, E. Choi, S. Angelos, M. Liong and J. I. Zink, *J. Sol-Gel Sci. Technol.*, 2008, **46**, 313.
244 Y. Klichko, M. Liong, E. Choi, S. Angelos, A. E. Nel, J. F. Stoddart, F. Tamanoi and J. I. Zink, *J. Am. Ceram. Soc.*, 2009, **92**, S2.
245 S. Angelos, Y. W. Yang, N. M. Khashab, J. F. Stoddart and J. I. Zink, *J. Am. Chem. Soc.*, 2009, **131**, 11344.
246 S. Angelos, Y. W. Yang, K. Patel, J. F. Stoddart and J. I. Zink, *Angew. Chem., Int. Ed.*, 2008, **47**, 2222.
247 D. P. Ferris, Y. L. Zhao, N. M. Khashab, H. A. Khatib, J. F. Stoddart and J. I. Zink, *J. Am. Chem. Soc.*, 2009, **131**, 1686.
248 N. M. Khashab, A. Trabolsi, Y. A. Lau, M. W. Ambrogio, D. C. Friedman, H. A. Khatib, J. I. Zink and J. F. Stoddart, *Eur. J. Org. Chem.*, 2009, 1669.
249 K. C. F. Leung, T. D. Nguyen, J. F. Stoddart and J. I. Zink, *Chem. Mater.*, 2006, **18**, 5919.
250 T. D. Nguyen, K. C. F. Leung, M. Liong, C. D. Pentecost, J. F. Stoddart and J. I. Zink, *Org. Lett.*, 2006, **8**, 3363.
251 T. D. Nguyen, Y. Liu, S. Saha, K. C. F. Leung, J. F. Stoddart and J. I. Zink, *J. Am. Chem. Soc.*, 2007, **129**, 626.
252 T. D. Nguyen, H. R. Tseng, P. C. Celestre, A. H. Flood, Y. Liu, J. F. Stoddart and J. I. Zink, *Proc. Natl. Acad. Sci. U. S. A.*, 2005, **102**, 10029.
253 C. Park, K. Oh, S. C. Lee and C. Kim, *Angew. Chem., Int. Ed.*, 2007, **46**, 1455.
254 S. Saha, K. C. F. Leung, T. D. Nguyen, J. F. Stoddart and J. I. Zink, *Adv. Funct. Mater.*, 2007, **17**, 685.
255 R. Hernandez, H. R. Tseng, J. W. Wong, J. F. Stoddart and J. I. Zink, *J. Am. Chem. Soc.*, 2004, **126**, 3370.
256 T. D. Nguyen, K. C. F. Leung, M. Liong, Y. Liu, J. F. Stoddart and J. I. Zink, *Adv. Funct. Mater.*, 2007, **17**, 2101.
257 S. M. Grayson and J. M. J. Frechet, *Chem. Rev.*, 2001, **101**, 3819.
258 R. Rosario, D. Gust, M. Hayes, F. Jahnke, J. Springer and A. A. Garcia, *Langmuir*, 2002, **18**, 8062.
259 R. Rosario, D. Gust, A. A. Garcia, M. Hayes, J. L. Taraci, T. Clement, J. W. Dailey and S. T. Picraux, *J. Phys. Chem. B*, 2004, **108**, 12640.
260 B. I. Ipe, S. Mahima and K. G. Thomas, *J. Am. Chem. Soc.*, 2003, **125**, 7174.
261 R. Byrne and D. Diamond, *Nat. Mater.*, 2006, **5**, 421.
262 J. Sunamoto, K. Iwamoto, Y. Mohri and T. Kominato, *J. Am. Chem. Soc.*, 1982, **104**, 5502.
263 N. Shao, J. Y. Jin, S. M. Cheung, R. H. Yang, W. H. Chan and T. Mo, *Angew. Chem., Int. Ed.*, 2006, **45**, 4944.
264 A. Christopoulos, *Nat. Rev. Drug Discovery*, 2002, **1**, 198.
265 D. Fitzmaurice, S. N. Rao, J. A. Preece, J. F. Stoddart, S. Wenger and N. Zaccheroni, *Angew. Chem., Int. Ed.*, 1999, **38**, 1147.
266 D. Philp, A. M. Z. Slawin, N. Spencer, J. F. Stoddart and D. J. Williams, *Chem. Commun.*, 1991, 1584.
267 A. K. Boal, F. Ilhan, J. E. DeRouchey, T. Thurn-Albrecht, T. P. Russell and V. M. Rotello, *Nature*, 2000, **404**, 746.
268 R. Shenhar, T. B. Norsten and V. M. Rotello, *Adv. Mater.*, 2005, **17**, 657.
269 B. L. Frankamp, O. Uzun, F. Ilhan, A. K. Boal and V. M. Rotello, *J. Am. Chem. Soc.*, 2002, **124**, 892.
270 S. H. Sun, S. Anders, H. F. Hamann, J. U. Thiele, J. E. E. Baglin, T. Thomson, E. E. Fullerton, C. B. Murray and B. D. Terris, *J. Am. Chem. Soc.*, 2002, **124**, 2884.
271 M. M. Maye, I. I. S. Lim, J. Luo, Z. Rab, D. Rabinovich, T. B. Liu and C. J. Zhong, *J. Am. Chem. Soc.*, 2005, **127**, 1519.
272 D. Ryan, S. N. Rao, H. Rensmo, D. Fitzmaurice, J. A. Preece, S. Wenger, J. F. Stoddart and N. Zaccheroni, *J. Am. Chem. Soc.*, 2000, **122**, 6252.

 This journal is © The Royal Society of Chemistry 2010

View Article Online

Published on 21 April 2010. Downloaded by Pennsylvania State University on 06/03/2016 20:02:52.

273 M. A. Olson, A. B. Braunschweig, L. Fang, T. Ikeda, R. Klajn, A. Trabolsi, P. J. Wesson, D. Benitez, C. A. Mirkin, B. A. Grzybowski and J. F. Stoddart, *Angew. Chem., Int. Ed.*, 2009, **48**, 1792.
274 These "monofunctional" NPs are obtained inevitably in a mixture with an excess of non-functionalised NPs (that is, NPs covered entirely by "background" ligands).
275 M. Ueda, H. B. Kim and K. Ichimura, *Mater. Lett.*, 1994, **20**, 245.
276 R. Klajn, K. J. M. Bishop, M. Fialkowski, M. Paszewski, C. J. Campbell, T. P. Gray and B. A. Grzybowski, *Science*, 2007, **316**, 261.
277 R. Klajn, P. J. Wesson, K. J. M. Bishop and B. A. Grzybowski, *Angew. Chem., Int. Ed.*, 2009, **48**, 7035.
278 T. Kawai, S. Nakamura, A. Sumi and T. Kondo, *Thin Solid Films*, 2008, **516**, 8926.
279 N. S. Bell and M. Piech, *Langmuir*, 2006, **22**, 1420.
280 E. Goldburt, F. Shvartsman, S. Fishman and V. Krongauz, *Macromolecules*, 1984, **17**, 1225.
281 I. Cabrera and V. Krongauz, *Macromolecules*, 1987, **20**, 2713.
282 K. Matyjaszewski and J. H. Xia, *Chem. Rev.*, 2001, **101**, 2921.
283 K. Matyjaszewski, P. J. Miller, N. Shukla, B. Immaraporn, A. Gelman, B. B. Luokala, T. M. Siclovan, G. Kickelbick, T. Vallant, H. Hoffmann and T. Pakula, *Macromolecules*, 1999, **32**, 8716.
284 M. Piech, M. C. George, N. S. Bell and P. V. Braun, *Langmuir*, 2006, **22**, 1379.
285 M. C. George, A. Mohroz, M. Piech, N. S. Bell, J. A. Lewis and P. V. Braun, *Adv. Mater.*, 2009, **21**, 66.
286 F. X. Redl, K. S. Cho, C. B. Murray and S. O'Brien, *Nature*, 2003, **423**, 968.
287 J. J. Urban, D. V. Talapin, E. V. Shevchenko, C. R. Kagan and C. B. Murray, *Nat. Mater.*, 2007, **6**, 115.
288 V. F. Puntes, P. Gorostiza, D. M. Aruguete, N. G. Bastus and A. P. Alivisatos, *Nat. Mater.*, 2004, **3**, 263.
289 A. Courty, A. Mermet, P. A. Albouy, E. Duval and M. P. Pileni, *Nat. Mater.*, 2005, **4**, 395.
290 X. Tong, G. Wang, A. Soldera and Y. Zhao, *J. Phys. Chem. B*, 2005, **109**, 20281.
291 R. Klajn, T. P. Gray, P. J. Wesson, B. D. Myers, V. P. Dravid, S. K. Smoukov and B. A. Grzybowski, *Adv. Funct. Mater.*, 2008, **18**, 2763.
292 R. Klajn, A. O. Pinchuk, G. C. Schatz and B. A. Grzybowski, *Angew. Chem., Int. Ed.*, 2007, **46**, 8363.
293 K. P. Browne, R. Klajn, J. A. Villa and B. A. Grzybowski, *Small*, 2009, **5**, 2656.
294 B. A. Grzybowski and C. J. Campbell, *Chem. Eng. Sci.*, 2004, **59**, 1667.
295 B. A. Grzybowski, H. A. Stone and G. M. Whitesides, *Proc. Natl. Acad. Sci. U. S. A.*, 2002, **99**, 4147.
296 B. A. Grzybowski and G. M. Whitesides, *Science*, 2002, **296**, 718.
297 G. M. Whitesides and B. Grzybowski, *Science*, 2002, **295**, 2418.
298 K. V. Tretiakov, K. J. M. Bishop and B. A. Grzybowski, *Soft Matter*, 2009, **5**, 1279.
299 B. A. Grzybowski, H. A. Stone and G. M. Whitesides, *Nature*, 2000, **405**, 1033.
300 B. A. Grzybowski and G. M. Whitesides, *J. Phys. Chem. B*, 2002, **106**, 1188.
301 Z. L. Wang, X. Y. Kong, Y. Ding, P. X. Gao, W. L. Hughes, R. S. Yang and Y. Zhang, *Adv. Funct. Mater.*, 2004, **14**, 943.
302 A. I. Boukai, Y. Bunimovich, J. Tahir-Kheli, J. K. Yu, W. A. Goddard and J. R. Heath, *Nature*, 2008, **451**, 168.
303 T. E. Humphrey and H. Linke, *Phys. Rev. Lett.*, 2005, **94**, 096601.
304 Y. M. Lin, X. Z. Sun and M. S. Dresselhaus, *Phys. Rev. B: Condens. Matter*, 2000, **62**, 4610.
305 Y. Li and M. A. El-Sayed, *J. Phys. Chem. B*, 2001, **105**, 8938.
306 R. Narayanan and M. A. El-Sayed, *Nano Lett.*, 2004, **4**, 1343.
307 R. M. Rioux, H. Song, M. Grass, S. Habas, K. Niesz, J. D. Hoefelmeyer, P. Yang and G. A. Somorjai, *Top. Catal.*, 2006, **39**, 167.
308 M. Xie, H. H. Liu, P. Chen, Z. L. Zhang, X. H. Wang, Z. X. Xie, Y. M. Du, B. Q. Pan and D. W. Pang, *Chem. Commun.*, 2005, 5518.